(U)
Y CLASSIFICATION OF THIS PAGE

REPORT DOCUMENTATION PAGE

1a. REPORT SECURITY CLASSIFICATION: (U)	1b. RESTRICTIVE MARKINGS: N/A
2a SECURITY CLASSIFICATION AUTHORITY: N/A	3. DISTRIBUTION/AVAILABILITY OF REPORT: Distribution unlimited
2b DECLASSIFICATION/DOWNGRADING SCHEDULE: N/A	
4 PERFORMING ORGANIZATION REPORT NUMBER(S): N/A	5. MONITORING ORGANIZATION REPORT NUMBER(S): N/A
NAME OF PERFORMING ORGANIZATION: University of Ottawa, Canada	6b OFFICE SYMBOL (If applicable): N/A
7a. NAME OF MONITORING ORGANIZATION: Office of Naval Research	
ADDRESS (City, State, and ZIP Code): Dept. of Electrical Engg. University of Ottawa, 770 King Edward Ave. Ottawa, Ontario K1N 6N5 Canada	7b ADDRESS (City, State, and ZIP Code): 800 North Quincy Street, Arlington, VA 22217-5000
NAME OF FUNDING/SPONSORING ORGANIZATION: Office of Naval Research	8b. OFFICE SYMBOL (If applicable): ONR
9 PROCUREMENT INSTRUMENT IDENTIFICATION NUMBER: N00014-82-G-0011	
ADDRESS (City, State, and ZIP Code): 800 North Quincy Street, Arlington, VA 22217-5000	10 SOURCE OF FUNDING NUMBERS: PROGRAM ELEMENT NO 61153N; PROJECT NO. RR04108; TASK NO NR or 441; WORK UNIT ACCESSION NO

AD-A163 156

DTIC ELECTE JAN 16 1986 D

TITLE (Include Security Classification)

(U) Studies of the Electric Field Distribution in Biological Bodies - Experimental Dosimetry at Radiofrequencies

12 PERSONAL AUTHOR(S): Dr. Stanislaw S. Stuchly and Dr. Maria A. Stuchly

13a TYPE OF REPORT	13b TIME COVERED	14. DATE OF REPORT (Year, Month, Day)	15. PAGE COUNT
FINAL	FROM Dec.1981 TO Sept'85	1985 12 05	12

16 SUPPLEMENTARY NOTATION: N/A

17 COSATI CODES			18 SUBJECT TERMS (Continue on reverse if necessary and identify by block number)
FIELD	GROUP	SUB-GROUP	
08			

19. ABSTRACT (Continue on reverse if necessary and identify by block number)

The objective of the project was to develop and evaluate a computer-controlled system for measurements of the spatial distribution of the specific absorption rate (SAR) in biological bodies and to perform measurements on a model of the human body, with particular emphasis on exposures in the near-field of antennas.

In this report we provide only a summary of findings, as detailed information can be found in our publications and the four earlier reports.

Findings: Far-Field Exposures-

At frequencies above 160 MHz, in spite of large gradients, local values of the SAR are only about 20 times higher than the whole-body average SAR for homogeneous models of human body. However, an additional increase by a factor of 4-5 can be anticipated at interfaces of high water content tissues with air (gas) pockets and low water content tissues. The latter is

(see reverse)

20 DISTRIBUTION/AVAILABILITY OF ABSTRACT	21 ABSTRACT SECURITY CLASSIFICATION
☒ UNCLASSIFIED/UNLIMITED ☐ SAME AS RPT ☐ DTIC USERS	(U)
22a NAME OF RESPONSIBLE INDIVIDUAL: Dr. T.C. Rozzell	22b TELEPHONE (Include Area Code): (202)696-4053 / 22c OFFICE SYMBOL: ONR

DD FORM 1473, 84 MAR — 83 APR edition may be used until exhausted. All other editions are obsolete.

SECURITY CLASSIFICATION OF THIS PAGE

DTIC FILE COPY

based on investigations of simple heteregeneous models. The existence of large gradients and high local SARs, as confirmed by our results, further supports an accepted view that biological effects at relatively low average SARs are due to thermal interactions. This is particularly important at frequencies at and near the resonance frequency for a given species.

For humans, high SARs occur in the neck, and the ratio of the SAR in the neck to the whole-body average increases with frequency. Our investigations suggest that below 160 MHz, high ratios may occur. Presently, available theory offers little guidance in this respect, as the block model calculations have been shown to be unreliable for determining SARs in relatively small volumes.

Findings: Near-field Exposures

Based on the experimental findings we believe that because of the spatial pattern of energy deposition, the whole-body average SAR is not an adequate dosimetric measure for near-field exposures. For assessment of potential hazards and derivation of exposure limits a quantity such as the SAR averaged over 10% of the total volume or mass is suggested as a more adequate quantity. Furthermore, because the peak to average SARs are of the order of hundreds, if only the whole-body-average SAR is considered in establishing safety limits, potential problems may arise from high SARs in crucial locations, e.g. the eye. For instance, the ANSI standard exempts all portable transmitters having output power of 7W or less below 1 GHz, but a dipole antenna with a reflector deposits about 15 W/kg close to the body surface for the output power of 7W.

Similarly as for the far-field, presently available theories do not provide reliable data on peak SARs or SARs averaged over limited size volumes.

DISCLAIMER NOTICE

THIS DOCUMENT IS BEST QUALITY PRACTICABLE. THE COPY FURNISHED TO DTIC CONTAINED A SIGNIFICANT NUMBER OF PAGES WHICH DO NOT REPRODUCE LEGIBLY.

FINAL SCIENTIFIC REPORT

STUDIES OF THE ELECTRIC FIELD DISTRIBUTION IN BIOLOGICAL BODIES - EXPERIMENTAL DOSIMETRY AT RADIO FREQUENCIES

Research Grant No. N00014-82-G-0011

Office of Naval Research, Division of Biological Sciences

Department of the Navy, Arlington, VA 22217

Stanislaw S. Stuchly, Ph.D.

and

Maria A. Stuchly, Ph.D.

Department of Electrical Engineering

University of Ottawa

Ottawa, Ontario

Canada K1N 6N5

November 1985

INTRODUCTION

This research project was carried out from December 1, 1981 till September 31, 1985. Four scientific reports have been submitted earlier.

The objective of the project was to develop and evaluate a computer-controlled system for measurements of the spatial distribution of the specific absorption rate (SAR) in biological bodies and to perform measurements on a model of the human body, with particular emphasis on exposures in the near-field of antennas.

In this report we provide only a summary of findings, as detailed information can be found in our publications enclosed in the Appendix and the four earlier reports (see list of reports submitted).

EXPERIMENTAL SYSTEM AND MATERIALS

A computer-controlled scanning system is capable of positioning electric field probes within a volume of 2 x 0.5 x 0.5 m with an uncertainty of 0.05 mm. The system also provides for data acquisition, processing, display and recording (Stuchly et al, 1983). The system can acquire, and record the data on the SAR in over 650 locations within a full-scale model of the human body in approx. 1.5h. The specific absorption rate is calculated from the measured electric field intensity. The electric field intensity is measured with implantable triaxial electric-field probes. The probes have been fully characterized and calibrated at various frequencies. Their calibration accuracy is ±1 dB, while the repeatability in the SAR measurements is better than ±0.5 dB (Stuchly et al 1984). At the latter part of the project, performance of the probes was investigated at interfaces of

regions with different dielectric properties. This investigation was done in non-homogeneous spheres consisting of an inner air pocket surrounded by muscle material. A fully satisfactory behaviour of the probes was observed, when corrections for different calibration factors were applied. Differences between the calculated and measured values of the SAR at interfaces did not exceed ± 1 dB.

Special electronic circuitry was built to interface the electric field probes with the computer. During the course of the project three versions of the circuitry were built (Stuchly et al 1986c), with the latest one providing an improvement in the signal-to-noise ratio of about 7 dB. The electronic systems built allowed us to measure relatively weak electric fields in tissue, and to obtain a wide dynamic range of over 30 dB (Stuchly et al 1986c).

To simulate the electrical properties of tissues new tissue-equivalent materials have been developed. They are characterized by a long life time of over one year, in contrast to the previously developed materials which cannot be stored for longer than one month as their electrical and mechanical properties deteriorate rapidly (Hartsgrove and Kraszewski, 1984). The tissue-equivalent materials simulating muscle, average tissue, brain, bone and lung suitable in the frequency range from 100 MHz to 1 GHz are presently available (Hartsgrove et al, 1986).

Computer programs which have been developed provide not only control of the experiment and data acquisition, but data normalization and averaging, variety of SAR calculations (e.g. various average SARs), data extrapolation, comparisons with theory, where applicable, and plotting. Plotting can be done in various formats: standard x-y plots

3-D plots, and cross-sectional plots showing lines of a constant parameter (e.g. SAR = 1 W/kg)

ENERGY DEPOSITION IN THE FAR-FIELD

The far-field measurements were performed at three frequencies, 160, 350 and 915 MHz, for two polarizations (E and H) and at one frequency (350 MHz) for three (E,H & k) polarizations. Local values of the SAR were determined in approx. 650 points within a half of a homogeneous model, with the test-point grid denser in the head and torso than in the limbs. Average SARs for the body parts and the whole-body were calculated from the measured local SARs.

The spatial distribution of the SAR is highly non-uniform, with the SAR typically varying within three or more orders of magnitude. Very large gradients occur along the direction of wave propagation, and much higher SARs than the whole body average are produced in the nack for the E polarization at 160 and 350 MHz (Kraszewski et al 1984a, Stuchly et al, 1985a, 1986b).

At all frequencies an exponential decay of the SAR in the torso in the direction of wave propagation was observed. The attenuation coefficient was equal to that of a plane wave propagating in a semi-infinite slab having the same electrical properties. This finding is important as it indicates that the principles of geometrical optics can be applied to easily calculate the SAR distribution in the torso at frequencies lower than previously expected. Therefore, simple calculations can account for tissue layering in the torso, i.e. the skin, fat, bone, muscle, etc. at frequencies above 160 MHz. At frequencies

above 900 MHz such calculations apply also to the head and legs (Stuchly et al 1986b).

The neck-head region has a complex geometry and because of it SAR distributions are highly non-uniform and frequency dependent. For instance, at 160 MHz SAR ≈ 1000 mW/kg in a tissue slab across the neck 4 cm thick, compared to the whole-body average SAR ≈ 100 mW/kg for 1 mW/cm^2 incident power density in the E polarization. At 350 MHz SAR ≈ 400 mW/kg in the center of the neck, while the whole-body average SAR ≈ 40 mW/kg for 1 mW/cm^2 incident power density in the E polarization. Between 160 MHz and 350 MHz about 2 to 3 times greater rates of energy deposition occur in the head than the whole-body averages (Stuchly et al 1986b).

A comparison of the results of our measurements with theoretically predicted SAR distribution in a block model of man consisting of about 340 cells (details in the previous report - May 1984) shows that the block model does not provide adequate data on the SAR distribution, even approximately, at frequencies equal or greater than 350 MHz. Differences by a factor of 10 to 20 are typical. Such general features as for instance an exponential decay in the torso is not predicted by the block model. On the other hand a relatively good agreement between the theory (block model) and our measurements was observed for the whole-body average SARs. However, such agreement cannot be claimed for the averages calculated using spheroidal models for the H polarization. The measured average SARs are higher, likely because of a large part of energy being absorbed in the legs and therefore spheroidal model approximation having apparent limitations (Stuchly et al 1986b).

ENERGY DEPOSITION IN THE NEAR-FIELD

Measurements were performed at 160, 350 and 915 MHz for typical representative antennas (simulating portable transmitters and leakage fields), such as resonant dipoles, resonant dipoles with reflectors and resonant slots, and at about 150 MHz for a monopole antenna monitored on a box simulating hand-held transmitter.

All antennas were designed to be well matched in free space and with the human model in close proximity. The antennas were placed at distances of about one tenth of the wavelengths, either close to the neck-head for exposures simulating leaky transmitter cabinets (slot antennas).

At all frequencies and for all configurations investigated energy deposition was concentrated within a limited volume of approximately one tenth of the total body volume. The spatial distribution of the SAR was highly non-uniform, even more than for far-field exposures. The maximum local SAR were between 30 to 250 times greater than the whole-body average SARs depending on frequency and antenna configuration (Stuchly et al 1985a, 1986b, 1986b).

Similarly as in the far-field, the SAR on the antenna axis decays exponentially in the direction of propagation with an attenuation coefficient very close to that of a plane wave in a homogeneous half space. This conclusion does not apply to locations off the antenna axis and for antennas closer than about one tenth of the wavelength from the body surface.

For the E-polarization there is a tendency for the maximum SAR to shift toward the neck region, if the antenna is nearby that region,

otherwise maximum SARs are produced at the antenna axis (for homogeneous models).

The SAR pattern depends mainly on the antenna type, position and polarization, the whole-body SAR is basically determined by the antenna gain and its distance from the body (Stuchly et al 1985b).

A comparison with the theoretical predictions for the block model of man consisting of 180 cells was made for a dipole in the E polarization at 350 MHz. The average whole-body SARs were found within less than 2%. Large differences were found in the SAR distribution, similarly as in the far-field, the exponential decay of the SAR was not predicted by the theory. Relatively large differences, of an order of 5 to 10, were found between the SAR averaged over various body volumes. This comparison again underscored the inherent limitations of the theoretial analysis (Stuchly et al 1986a).

IMPLICATIONS OF THE FINDINGS

Far-field Exposures

At frequencies above 160 MHz, in spite of large SAR gradients, local values of the SAR are only about 20 times higher than the whole-body average SAR for homogeneous models of human body. However, an additional incrase by a factor of 4-5 can be anticipated at interfaces of high water content tissues with air (gas) pockets and low water content tissues. The latter is based on investigations of simple heteregeneous models. The existence of large gradients and high local SARs, as confirmed by our results, further supports an accepted view that biological effects at relatively low average SARs are due to

thermal interactions. This is particularly important at frequencies at and near the resonance frequency for a given species.

For humans, high SARs occur in the neck, and the ratio of the SAR in the neck to the whole-body average increases with frequency. Our investigations suggest that below 160 MHz, high ratios may occur. Presently, available theory offers little guidance in this respect, as the block model calculations have been shown to be unreliable for determining SARs in relatively small volumes (Stuchly et al 1986b).

Near-field Exposures

Based on the experimental findings we believe that because of the spatial pattern of energy deposition, the whole-body average SAR is not an adequate dosimetric measure for near-field exposures. For assessment of potential hazards and derivation of exposure limits a quantity such as the SAR averaged over 10% of the total volume or mass is suggested as a more adequate quantity. Furthermore, because the peak to average SARs are of the order of hundreds, if only the whole-body-average SAR is considered in establishing safety limits, potential problems may arise from high SARs in crucial locations, e.g. the eye. For instance, the ANSI standard exempts all portable transmitters having output power of 7W or less below 1 GHz, but a dipole antenna with a reflector deposits about 15 W/kg close to the body surface for the output power of 7W (Stuchly et al 1986b).

Similarly for the far-field, presently available theories do not provide reliable data on peak SARs or SARs averaged over limited size volumes (Stuchly et al 1986a).

REMARKS

1. The greatest difficulty in the project was due to the poor quality of implantable electric field probes that are available commercially. The probes are expensive and of limited capabilities, e.g. low sensitivity at lower RF frequencies for a reasonable size (diameter not greater than 1 cm). Some probes, such as Narda 2608 are extremely fragile and susceptible to mechanical breakage and deterioration due to high ion concentration in the tissue material in which the probes are immersed during the measurements.

In the later stages of the project the situation became particularly critical, as all available EIT probes broke due to aging of the high resistance lines. Our poor experience with available probes has led us to development of a new design. The new probe has been manufactured and is presently undergoing complete characterization. The probe operates in the frequency range 20-500 MHz, and has a diameter of 1 cm.

2. A unique experimental facility has been established, which is suitable for mapping electric fields inside and outside dielectric bodies. This facility is likely to remain fully utilized for further studies of RF energy deposition in models of biological bodies. In particular, studies of heterogeneous models of man and practical portable transmitters are under way. The facility is also suitable for electromagnetic compatibility (EMC) studies. The electronic circuitry is suitable for measurements of weak electric fields (1 V/m).

3. A computer controlled scanning system developed provides a viable method of measurements of the electric field strength or the specific absorption rate (SAR) in models of biological bodies. The

method can be used in both the far-and the near field of RF radiation sources at any frequency for which suitable probes are available. This method has several advantages when compared with other experimental methods as thermography, although it is not devoid of limitations as analyzed elsewhere (Stuchly et al 1986b). Experimental methods provide viable alternatives to assess the spatial pattern of the rate of energy deposition in biological bodies in those cases where theoretical calculations are not available. Unfortunately at the present time, accurate methods of SAR computation are not available for most of the practical exposure situations at radio frequencies.

Publications, Thesis and Presentations

1. G.W. Hartsgrove and A. Kraszewski (1984), "Improved Tissue-Equivalent Materials for Electromagnetic Absorption Studies", Proc. BEMS Meeting, Atlanta, GA, July 15-19.

2. G. Hartsgrove, A. Kraszewski, A. Surowiec, "Simulated Biological Materials for Electromagnetic Absorption Studies", submission to J. Bioelectromagnetics.

3. A. Kraszewski, M.A. Stuchly, S.S. Stuchly, G. Hartsgrove and D. Adamski (1984a), "Specific Absorption Rate Distribution in a Full-Scale Model of Man at 350 MHz", IEEE Trans. Microwave Theory and Tech., Vol. MTT-32, pp. 779-783, 1984.

4. A. Kraszewski, M.A. Stuchly, S.S. Stuchly and G. Hartsgrove (1984b) "Specific Absorption Rate Distribution in a Model of Man at Various Polarizations", Proc. 1984 International Microwave Symposium Digest, San Francisco, May 30-June 1, 1984.

5. A. Kraszewski, M.A. Stuchly, S.S. Stuchly and G. Hartsgrove (1984c), "Specific Absorption Rate Distribution in a Model of Man at 350 MHz", Proc. 1984 BEMS Meeting, Atlanta, GA, July 15-19.

6. A. Kraszewski, S.S. Stuchly, M.A. Stuchly, G. Hartsgrove and D. Adamski (1984d), "Specific Absorption Rate Distribution in a Model of Man Exposed in the Near Field", URSI/BEMS Symposium, Florence, Italy, August 26-29.

7. A. Kraszewski, S.S. Stuchly, M.A. Stuchly, G. Hartsgrove and D. Adamski (1984e), "Specific Absorption Rate Distribution in a Model of Man Exposed in the Near Field", BEMS Meeting, Atlanta, GA, July 15-19, (Abstract).

8. A. Kraszewski (1985a) "Electromagnetic Dosimetry in Full-Scale Models of Human Body", Proc. 1985 Intern. Symp. Microwave Technology in Industrial Development, Campinos, Brazil, July 22-25, pp. 377-380.

9. A. Kraszewski (1985b), "Mapping the Internal Electric Field in Models of Biological Objects", Proc. XV Europ. Microwave Conf. Paris, France, Sept. 9-13, pp. 649-654.

10. A. Kraszewski, S.S. Stuchly, M.A. Stuchly and G. Hartsgrove (1985c), "Energy Deposition in a Model of Man; Frequency Effects in the Near Field", BEMS Meeting, San Francisco, CA, June 16-20. (Abstract)

11. S.S. Stuchly, M. Barski, B. Tam, G. Hartsgrove and S. Symons, (1983) "Computer Based Scanning System for Electromagnetic Dosimetry", Rev. Sci. Instrum., 54 (11), pp. 1547-1550.

12. S.S. Stuchly, A. Kraszewski, M.A. Stuchly, G. Hartsgrove and G.H. Wong (1984a) "System for Measuring the Distribution of the Internal Electric Field in Models of Animals and Humans", Proc. 1984 IEEE EMC-S Symposium, Tokyo, Japan, October 16-18, pp. 380-382.

13. M.A. Stuchly, A. Kraszewski, S.S. Stuchly, G. Hartsgrove and D. Adamski (1984b) "Dosimetry in a Full Scale Model of the Human Body", Proc. 1984 IEEE-EMC-S Symposium, Tokyo, Japan, October 16-18, pp. 383-387.

14. M.A. Stuchly, A. Kraszewski and S.S. Stuchly (1984c), "Implantable Electric-Field Probes - Some Performance Characteristics", IEEE Trans. Biomed. Engn. Vol. BME-31, pp. 526-531.

15. M.A. Stuchly, A. Kraszewski, S.S. Stuchly and G. Hartsgrove (1984d), Distribution of Radiofrequency Energy in a Model of Man-Experimental Results for a Model of Man", Proc. URSI/BEMS Symposium, Florence, Italy, August 26-29.

16. M.A. Stuchly, A. Kraszewski and S.S. Stuchly (1985a), "Exposure of Human Models in the Near and Far-Field- A Comparison, IEEE, Trans. Biomed. Eng., Vol. BME-32, pp. 609-616.

17. S.S. Stuchly, A. Kraszewski, M.A. Stuchly, G. Hartsgrove and D. Adamski (1985b), "Energy Deposition in a Model of Man in the Near Field", Bioelectromagnetics, Vol. 6, pp. 115-129.

18. M.A. Stuchly, S.S. Stuchly, A. Kraszewski and G. Hartsgrove (1985c), "Energy Deposition in the Human Body from Radiofrequency Radiation in the Near-Field", Innov. Tech. Bio. Med., Vol. 6, pp. 555-566.

19. M.A. Stuchly, A. Kraszewski, S.S. Stuchly and G. Hartsgrove (1985d), "Energy Deposition in a Model of Man; Frequency Effects in the Far Field", 1985 BEMS Meeting, San Francisco, CA, June 16-20. (Abstract).

20. M.A. Stuchly, R.J. Spiegel, S.S. Stuchly, and A. Kraszewski (1986a), "Exposure of Man in the Near-Field of a Resonant Dipole: Comparison Between Theory and Measurements", IEEE Trans. Microwave Theory Tech., Vol. MTT-34, Jan. 1986 (in press - accepted).

21. S.S. Stuchly, M.A. Stuchly, A. Kraszewski and G. Hartsgrove (1986b), "Energy Deposition in a Model of Man; Frequency Effects", IEEE Trans. Biomed. Eng., Vol. BME-33, (in press- accepted).

22. M.A. Stuchly, S.S. Stuchly, G.W. Hartsgrove, J. Markowski and A. Kraszewski (1986c),"Instrumentation for Measurements of Electric Fields at Radio Frequencies", Proc. IEEE/IMTC'86, Boulder, CO, March 25-27.

23. G.H. Wong (1983), "Specific Absorption Rate Distribution in Simple Geometrical Bodies at Radio Frequencies", M.A.Sc. Thesis, University of Ottawa.

24. G.H. Wong, S.S. Stuchly, A. Kraszewski and M.A. Stuchly (1984) "Probing Electromagnetic Fields in Lossy Spheres and Cylinders", IEEE Trans. Microwave Theory and Techn., Vol. MTT-32, pp. 824-828.

REPORTS SUBMITTED

RESEARCH GRANT No. N00014-82-G-0011

1. Progress report: period December 1, 1981 - May 31, 1982

2. Annual report : period December 1, 1981 - November 30, 1982

3. Progress report: period December 1, 1982 - May 31, 1983

4. Annual report : period June 1, 1983 - May 31, 1984

SIXTH ANNUAL MEETING OF THE BIOELECTROMAGNETICS SOCIETY
ATLANTA, GEORGIA, JULY 15-19, 1984

ABSTRACT SUBMISSION FORM

Bf [1]

FIRST AUTHOR'S MAILING ADDRESS:

Name Mr. George Hartsgrove,
Address University of Ottawa, Electrical Eng. Dept.
City Ottawa, Ontario State Canada Zip K1N 6N5

First author's signature G. W. Hartsgrove

Please check preference for method of presentation:

Platform ..... ☐
Poster ..... ☒
No preference ..... ☐

Sponsored by _____ (a BEMS member).
Type abstract in space outlined below. Follow instructions (see opposite side).

IMPROVED TISSUE EQUIVALENT MATERIALS FOR ELECTROMAGNETIC ABSORPTION STUDIES.

George W. Hartsgrove, A. Kraszewski, Department of Electrical Engineering, University of Ottawa, Ottawa, Ontario, Canada K1N 6N5.

Material having dielectric properties equivalent to that of the human body are used in electromagnetic absorption studies. The formulas presently used are not stable over an extended period of time. A new gelling agent in conjunction with a bactericide has been found to greatly improve the stability of these mixtures thus extending their research lifetime to several months. It has also been found that sugar can be used instead of polyethylene powder (PEP) if a liquid form of the phantom material is preferable.

To assist in program scheduling, please underline the category below which best characterizes the subject matter of your paper.

Effects:
- Behavioral
- Cellular
- Developmental
- ELF
- Endocrine
- Genetic
- Hematopoietic
- Immunological
- Neurological
- Physiological
- Sensory
- Ultra-structural

Diagnostic applications
Dielectric properties of biological materials
Dosimetry
Exposure systems
Field perturbation
Hyperthermia
Instrumentation
Therapeutic applications

Other: _____

Authors are requested to send abstract and three (3) copies by March 1, 1984 to

Don Justesen
Research Service (151)
USVA Medical Center
Kansas City, MO 64030

Ref. [3] A79

Specific Absorption Rate Distribution in a Full-Scale Model of Man at 350 MHz

ANDRZEJ KRASZEWSKI, MARIA A. STUCHLY, SENIOR MEMBER, IEEE, STANISLAW S. STUCHLY, SENIOR MEMBER, IEEE, GEORGE HARTSGROVE, AND DANIEL ADAMSKI

Abstract—A computer-controlled scanning system and an implantable triaxial electric-field probe have been used to obtain maps of the specific absorption rate (SAR) in various cross sections of a full-scale model of man. The model was exposed to a 350-MHz plane wave that provided various orientations of the electric-field vector with respect to the body. The results obtained are in general agreement with previously published theoretical and experimental data. The SAR distributions in the torso and head were in relatively good agreement with cylindrical and spherical models, respectively. Enhanced absorption in the neck and the limbs, as previously found by the thermographic method, was observed. This study provides much more detailed information than previously available, with an absolute accuracy of ±1 db.

I. Introduction

THE AVERAGE specific absorption rate (SAR) has been extensively used in quantifying interactions of electromagnetic fields in the radio and microwave frequency range with biological systems. The importance of the distribution of SAR's within the exposed system is well recognized as an essential factor in quantifying biological effects. In recent years, numerous theoretical methods have been developed for dosimetry, as reviewed elsewhere [1]–[3]. Analyses of the so-called block model of man appear to be most promising in providing the SAR distribution [4]–[7]. Results of such analyses have recently been also utilized in calculating the thermal response of a man exposed to radio waves [8].

In view of the importance of SAR distribution, it is essential that theoretical data are quantitatively verified experimentally. Furthermore, as the capabilities of analytical methods are limited in treating such complex structures as biological bodies, experimental methods may offer the only viable means for studying the SAR distribution in models closely resembling the actual bodies under more complex exposure conditions (e.g., near-field exposure). There are three viable techniques for measuring SAR distributions. A thermographic method has been developed and successfully applied on scaled-down models [9]–[11]. The main limitations of this technique are a limited spatial resolution due to the small size of the models and a difficulty in incorporating the anatomical structure into such a small model. Conversely, if a full-scale model of man is analyzed by thermography, very high intensities of the exposure field are required. These limitations have led to the use of two other dosimetric techniques on full-scale models of man.

A nonperturbing temperature probe has been used to measure the SAR in a limited number of locations in a full-scale model of man exposed at frequencies of 1.29 and 2 GHz [12], [13], and models of other primates. An implantable electric-field probe offers an alternative tool for measuring the SAR distribution and has several advantages. In addition to being particularly suitable for measurements in full-scale models, the measurements are not dependent on the thermal properties of the model material. Not only the SAR, but also the direction of the electric field can be determined. Measurements can be performed in very low exposure fields, which do not cause any increase in the model temperature. Furthermore, the data can be conveniently obtained for a very large number of locations when an automatic probe positioning system is used.

In this paper, SAR distributions in a full-scale model of man exposed to a plane-wave at 350 MHz are presented. The data were obtained using a calibrated implantable electric-field probe and a computer-controlled scanning system. The exposure frequency of 350 MHz was selected because of the reported head resonance at this frequency [7] and the availability of SAR data for the block model of man [14].

II. Experimental Arrangement

A general view of the experimental arrangement is shown in Fig. 1. The system—except for the computer, the generator, and monitoring equipment—was placed in an anechoic chamber. An exposure field was produced by a resonant slot above the ground plane, having gain of 4.87 at 350 MHz. The antenna was located below the phantom model as illustrated in Fig. 1 for the E orientation (i.e., the electric-field vector parallel to the long axis of the body), or at the side of the phantom for the k orientation (i.e., the wave propagation from head to toe, the propagation vector parallel to the long axis of the body).

The scanning system was composed of a mechanical structure for supporting and positioning the probe and a

Manuscript received October 12, 1983, revised March 9, 1984. This work was supported by the Office of Naval Research, (USA), the Department of Health and Welfare Canada, and the Natural Sciences and Engineering Research Council of Canada.

A. Kraszewski, S. S. Stuchly, G. Hartsgrove, and D. Adamski are with the Department of Electrical Engineering, University of Ottawa, Ottawa, Ontario, Canada K1N 6N5.

M. A. Stuchly is with the Radiation Protection Bureau, Health and Welfare Canada, Ottawa, Ontario, Canada K1A 0L2.

0018-9480/84/0800-0779$01.00 ©1984 IEEE

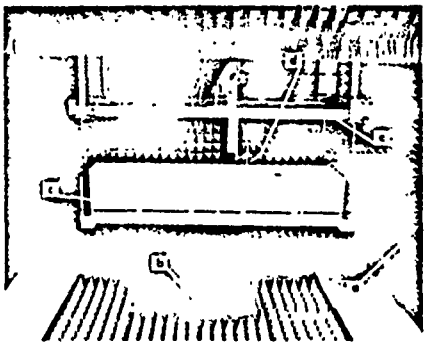

Fig. 1. Experimental arrangement (a) anechoic chamber, (b) antenna, (c) phantom model of the human body, (d) triaxial electric-field probe, and (e) mechanical structure for supporting and positioning the probe.

computer system for control of the experiment, data acquisition, storage, display, and recording. The probe could be placed at any location within a volume of $1.9 \times 0.5 \times 0.45$ m. The scanning resolution was 0.013 mm/step in each direction, and the position repeatability (uncertainty) was ± 0.05 mm. The probe could be moved at high speed with a velocity of approximately 12.5 mm/s, and at a low speed of 0.42 mm/s. The computer hardware and software are described elsewhere [15].

The full-scale plastic model shown in Fig. 2(a) had dimensions of a standard man. This plastic model was used to make a set of templates having exact dimensions of the plastic model in various cross sections (Figure 2(b)). These templates, in turn, were used to prepare 2.5-cm-thick styrofoam layers, which were glued together to obtain a hollow phantom of man (Fig. 2(c)). This phantom was filled with a mixture of water, sugar, and salt in such proportions that it had the following electrical properties: $\epsilon' = 38$ and $\sigma = 0.95$ S/m. These properties correspond to the tissue average properties at 350 MHz. The mixture had a relatively low viscosity, which facilitated penetration of the probe.

An implantable triaxial electric-field probe, model EIT 979,[1] was used to measure the electric-field intensity. This probe was previously fully characterized in terms of its sensitivity in tissue phantom material, noise, and modulation characteristics [16]. To improve the signal-to-noise ratio, and therefore the dynamic range of measurements, the radiofrequency signal was amplitude modulated at 516 Hz and a high-gain narrow-band amplifier was used at the output of the probe [16]. The probe sensitivity in the tissue phantom material was 2.1 $\mu V/(V^2/m^2)$, and the estimated calibration uncertainty was ± 1 dB. The minimum measurable electric-field intensity, with a signal-to-noise ratio of 10 and 1-Hz bandwidth amplifier, was 1.3 V/m (SAR = 1.6 mW/kg).

[1]Manufactured by Electronic Instrumentation and Technology Inc., Sterling, VA 22170, U.S.A.

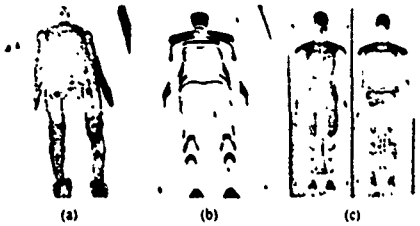

Fig. 2. Phantom model of man—design details, (a) plastic model of an average man, (b) set of templates, and (c) styrofoam mold

III. Results and Discussion

The SAR values at several locations within the body in three cross sections separated by 5 cm are shown in Fig. 3. Each data point is an average of at least five (5) separate measurements performed on various days and with various incident power levels within the linear range of the system operation. Fig. 4 shows the same data along two selected axes, as indicated, in the cross section close to the body center. The bars indicate one standard deviation. In all experiments, the SAR values were normalized to an incident power density of 1 mW/cm^2 at a plane corresponding to the body surface or point closest to the radiation source. When these data are compared with experimental data available in the literature for scaled-down models at 450 MHz [11], it is seen that, despite the difference in the exposure frequency, there is good agreement. "Hot spots" in our measurements are found in the neck region, with the SAR values ranging from 86 to 196 mW/kg in the plane $z = 10$ cm (corresponding approximately to the body center). These data can be compared with a maximum of 120 mW/kg in the center cross section for exposure at 450 MHz [11]. Similarly, in the legs, the maximum SAR values are 110 and 147 mW/kg in our measurements and at 450 MHz [11], respectively. It appears that the location of the maximum SAR in the legs is somewhat different at the two frequencies. A hot spot, of somewhat smaller intensity than at 450 MHz [11], was observed by us in the arms. This may be due to a difference in the arms articulation in the two phantom models.

A general qualitative agreement can be observed between our data and the theoretical calculations for the block model [14]. However, there is a significant difference in the quantitative SAR distribution, the locations of the hot spots, and the maximum values of the SAR. The most likely explanation for the observed differences is that the shapes of the block model and our phantom are significantly different and the torso of the block model consisted of a relatively small number of cells. In particular, there are

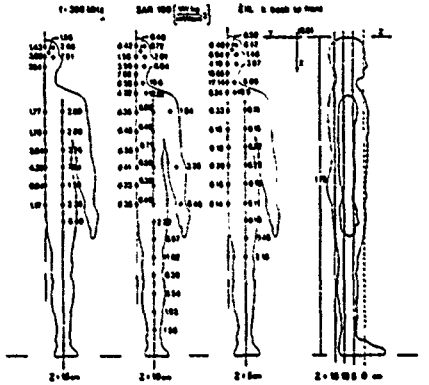

Fig. 3. Specific absorption rate (SAR) distribution (W/kg)•100 for a plane wave irradiation at a power density of 1 mW/cm² on the surface of the model, the electric field parallel to the long axis of the model $\vec{E} \parallel L$, the propagation k, from back to front, frequency 350 MHz.

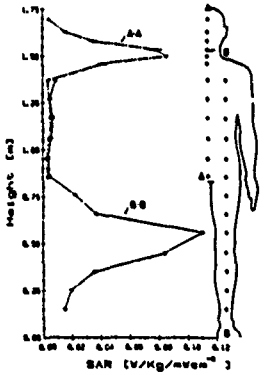

Fig. 4. Specific absorption rate (SAR) distribution along the man model height for two cross sections. 1 mW/cm² incident power density on the surface of the model, frequency 350 MHz $\vec{E} \parallel L$, k back to front, $z = 10$ cm (see Fig. 3, for z designation).

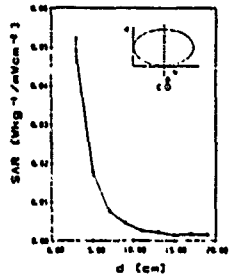

Fig. 5. Specific absorption rate (SAR) distribution in the upper torso (chest area −48 cm from the head top) along the axis as a function of the distance from the plane of the wave incidence: frequency 350 MHz, incident power density 1 mW/cm² in the plane tangent to the model $\vec{E} \parallel L$, k back to front.

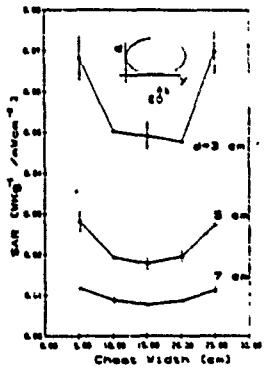

Fig. 6. Specific absorption rate (SAR) distribution in the upper torso (chest area−48 cm from the top of the head): frequency 350 MHz, incident power density 1 mW/cm² in the plane tangent to the model $\vec{E} \parallel L$, k back to front.

only two to three layers of cells in the block model, and our measurements indicate a rapid decrease of the SAR in the torso in the direction of the wave propagation (compare the SAR values at the same point for the three cross sections z in Fig. 3).

A rapid decrease in SAR values within the torso as a function of distance from the radiation source is further illustrated in Fig. 5. Since the SAR change is very rapid, values averaged over large size cells in the block model are obviously significantly different from those measured by the implantable probe, which provide averages for a relatively small volume. The deposition of energy at the body surface within the torso was also observed thermographically at 450 MHz [11].

A relatively good quantitative agreement between the calculated values for the block model [14] and our data was observed for the arms.

Fig. 6 shows the SAR distributions across the chest at various depths. Symmetry of the distribution within the uncertainty of measurements is observed for the center axis of the body. This is an expected result, confirming that measurements of the SAR within half of the body are sufficient.

The SAR distributions in the head of our model are shown in Fig. 7 for two orientations of the incident field with respect to the body. Corresponding calculated SAR distributions in a 16-cm-diameter sphere filled with the

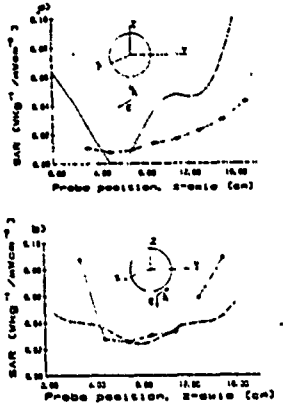

Fig. 7 Specific absorption rate (SAR) distribution in the head, frequency 350 MHz, incident power density 1 mW/cm², (a) $E \parallel L$, (b) $k \parallel L$. The dashed lines show the calculated SAR in a 16-cm-diameter sphere.

same phantom material are also shown for comparison. It can be noted that the overall shape of the curves is similar; however, the quantitative results are not surprisingly different, in view of the actual shape of the head. The SAR distribution in the head appears to be significantly different than that for the block model of man [14]. However a detailed analysis, which is outside of the scope of this paper, would be necessary to compare the results.

IV. Conclusions

Measurements of the specific absorption rate (SAR) distribution for a full-scale model of man filled with a phantom material having average tissue permittivity were performed at 350 MHz for a far-field exposure. Use of a computer-controlled mechanical scanning system and an implantable isotropic electric-field probe provided a good spatial resolution, an excellent reproducibility of results of ±0.5 dB, and a good absolute uncertainty of ±1 dB. The measurements were fully automated and, after proper calibrations and preparation, a large number of data points were conveniently obtained.

At a frequency of 350 MHz, a generally nonresonant behavior of the human body with maximum energy absorption at the surface on which the radiation is incident was confirmed. This conclusion did not, however, apply to the head, neck, and the limbs, where more complex distributions of the SAR were observed.

Our experimental data were in good agreement with reported experimental results at 450 MHz obtained by the thermographic technique [11]; however, only a few features of the distribution could be compared.

General qualitative agreement with theoretical data for the block model of man [14] appears to exist; however, our data are significantly different, particularly in the head–neck region [7]. Most likely, the differences are due to differences in shapes of the models and a limited number of cells for the block model, particularly in terms of layers (2 layers [7]).

Acknowledgment

Numerical calculations and helpful discussions with Drs. O. P. Gandhi and I. Chatterjee from the University of Utah, Salt Lake City, and stimulating discussions with Dr. D. Hill from the Canadian Department of Defence are greatfully acknowledged.

References

[1] C. H. Durney, "Electromagnetic dosimetry for models of humans and animals: A review of theoretical and numerical techniques," *Proc. IEEE*, vol. 68, pp. 33–40, 1980.

[2] O. P. Gandhi, "State of knowledge for electromagnetic absorbed dose in man and animals," *Proc. IEEE*, vol. 68, pp. 24–32, 1980.

[3] M. A. Stuchly, "Dosimetry of radio frequency and microwave radiation: Theoretical analyses," in *Biological Effects and Dosimetry of Nonionizing Radiation*, M. Grandolfo, S. M. Michaelson, Eds. New York: Plenum Publishing, 1983, pp. 163–177.

[4] K. M. Chen and B. S. Guru, "Induced EM fields inside human bodies irradiated by EM waves up to 500 MHz," *J. Microwave Power*, vol. 12, pp. 173–183, 1977.

[5] ——, "Internal EM fields and absorbed power density in human torso induced by 1–500 MHz EM waves," *IEEE Trans. Microwave Theory Tech.*, vol. MTT-25, pp. 746–756, 1977.

[6] M. J. Hagmann, O. P. Gandhi, and C. M. Durney, "Numerical calculation of electromagnetic energy deposition for a realistic model of man," *IEEE Trans. Microwave Theory Tech.*, vol. MTT-27, pp. 804–809, 1979.

[7] M. J. Hagmann, O. P. Gandhi, J. A. D'Andrea, and I. Chatterjee, "Head resonance: Numerical solutions and experimental results," *IEEE Trans. Microwave Theory Tech.*, vol. MTT-27, pp. 809–813, 1979.

[8] R. J. Spiegel, "The thermal response of a human in the near-zone of a resonant thin-wire antenna," *IEEE Trans. Microwave Theory Tech.*, vol. MTT-30, pp. 177–185, 1982.

[9] A. W. Guy, "Analysis of electromagnetic fields induced in biological tissues by thermographic studies in equivalent phantom models," *IEEE Trans. Microwave Theory Tech.*, vol. MTT-19, pp. 205–214, 1971.

[10] A. W. Guy, M. D. Webb, and C. C. Sorensen, "Determination of power absorption in man exposed to high frequency electromagnetic fields by thermographic measurements on real models," *IEEE Trans Biomed Eng.*, vol. BME-23, pp. 361–371, 1976.

[11] A. W. Guy, "Non-ionizing radiation. Dosimetry and interaction," in *Proc. ACGIH Topical Symp.*, Nov. 26–28, 1979, pp. 75–101.

[12] R. G. Olsen, "Preliminary studies. Far-field microwave dosimetric measurements of a full-scale model of man," *J. Microwave Power*, vol. 14, pp. 383–388, 1979.

[13] ——, "Far-field dosimetric measurements in a full-sized man model at 2.0 GHz," *Bioelectromagn.*, vol. 3, pp. 433–441, 1982.

[14] O. P. Gandhi and I. Chatterjee, private communication, 1983.

[15] S. S. Stuchly, M. Barski, B. Tam, G. Hartsgrove, and S. Symons, "Computer-based scanning system for electromagnetic dosimetry," *Rev. Sci. Instrum.*, vol. 54, no. 11, pp. 1547–1550, 1983.

[16] M. A. Stuchly, A. Kraszewski, and S. S. Stuchly, "Implantable electric field probes—Some performance characteristics," *IEEE Trans. Biomed. Eng.*, vol. BME-31, 1984, pp. 526–531, July 1984.

Andrzej Kraszewski was born in Poznan, Poland, on April 22, 1933. He received the M.Sc. degree in electrical engineering from the Technical University of Warsaw, Warsaw, Poland, in 1958, and the D.Sc. degree in technical sciences from the Polish Academy of Sciences, (PAN), Warsaw, in 1973.

Beginning in 1953, he was employed at the Telecommunication Institute, Warsaw, in the research and development of microwave components and systems. Beginning in 1963, he joined

UNIPAN Scientific Instruments, a subsidiary of the Polish Academy of Sciences, as the Head of the Microwave Laboratory. Starting in 1972, he was Manager of the Microwave Department of WILMER Instruments and Measurements, a subsidiary of the Polish Academy of Sciences in Warsaw, where he co-developed microwave instruments for moisture-content measurements and control. Since November 1980, as a Visiting Professor at the University of Ottawa, Canada, he has been engaged in research of interactions between dielectrics and electromagnetic fields. He is the author of several books on microwave theory and techniques, has published more than 80 technical papers on the subject, and holds 18 patents. He received several professional awards, among them the State Prize in Science in 1980.

Dr. Kraszewski is a member of the International Microwave Power Institute, the Polish Electricians Association, and is a member of the Editorial Board of the *Journal of Microwave Power*.

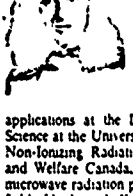

Maria A. Stuchly (M'71–SM'76) received the M.S. and Ph.D. degrees in electrical engineering from Warsaw Technical University and Polish Academy of Sciences in 1962 and 1970, respectively.

From 1962 to 1970, she was employed as a Senior R & D Engineer in a subsidiary of the Polish Academy of Sciences, in Warsaw, Poland. Between 1970 and 1976, she was engaged in research in the field of microwave instrumentation and measurements, and microwave power applications at the Departments of Electrical Engineering and Food Science at the University of Manitoba. Since 1976, she has been with the Non-Ionizing Radiation Section, Radiation Protection Bureau, Health and Welfare Canada, where she is responsible for the development of microwave radiation protection standards and carries out research in the field of biological effects of microwave radiation. She is also nonresident Professor of electrical engineering at the University of Ottawa.

Dr. Stuchly is a member of the Board of Directors of the Bioelectromagnetics Society and a member of the IEEE Technical Committee of Man and Radiation.

Stanislaw S. Stuchly (M'70–SM'72) was born in Lwow, Poland on November 20, 1931. He received the B.Sc. degree from the Technical University, Gliwice, Poland, and the M.Sc. degree from the Warsaw Technical University, both in electrical engineering, in 1953 and 1958, respectively, and the Ph.D. degree from the Polish Academy of Sciences, Warsaw, Poland in 1968.

From 1953 to 1959, he was a Research Engineer in the Industrial Institute for Telecommunications, Warsaw, Poland. From 1959 to 1963, he was with the Warsaw Technical University. In 1963, he joined UNIPAN–Scientific Instruments, subsidiary of the Polish Academy of Sciences. From 1970 to 1976, he was with the University of Manitoba, Winnipeg, Canada. Since 1977, he has been with the University of Ottawa, Canada, where he is presently a Professor of electrical engineering.

George Hartsgrove was born in Brantford, Ontario, Canada, on March 28, 1949. He graduated from Mohawk College, Hamilton, Ontario, in 1970.

Since 1976, he has been involved in bioelectromagnetic research at the National Research Council and, since 1981, at the University of Ottawa, Department of Electrical Engineering.

Daniel Adamski was born in Sudbury, Ontario, Canada, on November 22, 1960. He received the B.A.Sc. degree in electrical engineering from the University of Ottawa, Ontario, Canada.

From 1982–1983, he was a Research Engineer with the University of Ottawa, where he participated in the implementation of a dosimetry laboratory. He is currently pursuing the M.A.Sc. degree in Electrical Engineering at the University of Ottawa.

1984 MTT Conference Digest

Ref [4]

SPECIFIC ABSORPTION RATE DISTRIBUTION IN A MODEL OF MAN AT VARIOUS POLARIZATIONS

A. Kraszewski, M.A. Stuchly[1], S.S. Stuchly and G. Hartsgrove

Department of Electrical Engineering, University of Ottawa, Ottawa, Ontario, K1N 6N5, and [1] Radiation Protection Bureau, Health and Welfare Canada.

ABSTRACT

A computer-based scanning system and implantable electric field probes were used to obtain maps of the specific absorption rate (SAR) in various cross-sections of a full-scale model of the human body. The model was exposed to a plane-wave at 350 MHz at E and k polarizations with respect to the body. Enhanced absorption in the neck and the limbs, as previously found by the thermographic method, was observed. Significant differences between the SAR distribution and the SAR values calculated using the block model and those found in this work were observed.

Introduction

The average specific absorption rate (SAR) has been used in quantifying interactions of electromagnetic fields with biological systems at radio and microwave frequencies. The importance of the distribution of the SAR within the exposed system is well recognized as an essential factor in quantifying resulting biological responses. In recent years numerous theoretical methods have been developed for dosimetry, as reviewed elsewhere (1). The analysis of the so called block model of man appears to be most promising in providing the SAR distribution (2-5). In view of importance of the SAR distribution as well as the values of the local SAR, it is essential that the theoretical data is quantitatively verified experimentally. There are two viable techniques for measuring SAR distributions. A thermographic method has been developed and successfully applied to scaled down models (6,7). The main limitations of this technique are: a limited spatial resolution due to the size of the models and a difficulty in incorporating the anatomical structure into such models.

An implantable electric field probe offers an alternative for measuring the SAR distribution. This technique has several advantages. In addition to being particularly suitable for measurements in full-scale models, the measurements are not dependent on the thermal properties of the model material. Not only the SAR, but also the direction of the electric field can be determined. Measurements can be performed using very low exposure fields, which do not cause any increase in the model temperature. Furthermore, the data can be conveniently obtained for a very large number of locations when an automatic probe-positioning system is used.

In this paper we present the results of the SAR distribution measurements in a full-scale model of man exposed to a plane-wave at 350 MHz. The data was obtained using a calibrated implantable electric field probe and a computer-controlled scanning system. The exposure frequency of 350 MHz was selected because of the reported head resonance at this frequency (3) and the availability of the SAR data for the block model of man (8).

Experimental Arrangement

The experimental system, except for the computer, the generator and the monitoring equipment, was placed in an anechoic chamber. An exposure field was produced by a resonant dipole above the ground plane. The dipole was located below the model for the E polarization (i.e. the electric field vector parallel to the long axis of the body), or at the side of the model for the k polarization (i.e. the wave propagation from head to toe, the propagation vector parallel to the long axis of the body).

The scanning system composed of a mechanical structure for supporting and positioning of the probe and a computer-based system for control of the experiment, data acquisition, storage, display and recording are described elsewhere (9).

The full-scale styrofoam mold had the dimensions of a standard man. This mold was filled with a mixture of water, sugar and salt in such proportions that it had the following electrical properties: $\varepsilon' = 38$ and $\sigma = 0.95$ S/m. These properties correspond to the tissue "average" properties at 350 MHz (4,5).

Implantable triaxial electric field probes, model EIT 979 and Holaday HME-01 were used to measure the electric field intensity. These probes were previously fully characterized in terms of the sensitivity in the tissue phantom material, noise and modulation characteristics (10).

Results and Discussion

The specific absorption rates (SARs) in several locations within the body in three cross-sections separated by 5 cm are shown in Figure 1

fields by thermographic measurements on real models," IEEE Trans. Biomed. Eng., vol BME-23, pp 361-371, 1976.

(7) A.W. Guy, "Non-ionizing radiation: dosimetry and interactions," Proc. ACGIH Topical Symp. 1979, pp 75-101.

(8) O.P. Gandhi, and I. Chatterjee, Private communication, 1983.

(9) S.S. Stuchly, M. Saraki, S. Tam, G. Hartsgrove, and S. Symons, "A computer-based scanning system for electromagnetic dosimetry," Rev. Sci. Instrum., vol 54, No. 11, pp 1547-1550, 1983.

(10) M.A. Stuchly, A. Krzeszewski, and S.S. Stuchly, "Implantable electric field probes - some performance characteristics," IEEE Trans. Biomed. Eng., vol BME-31, 1984, to be published.

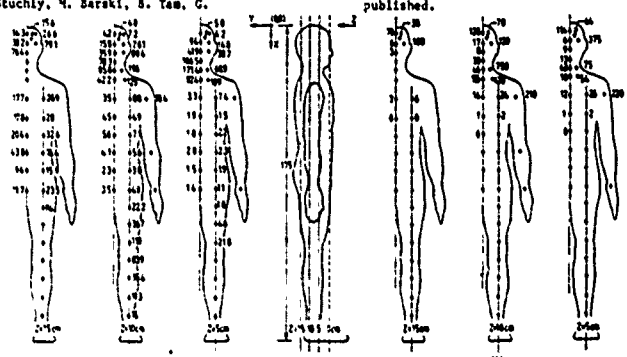

Figure 1. The specific absorption rate (SAR) in mW/kg for a plane-wave irradiation at 350 MHz and at a power density 1 mW/cm^2 on the surface of the model.

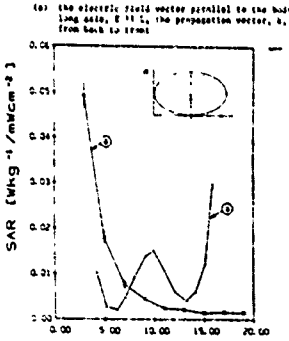

Figure 2. The specific absorption rate (SAR) distribution in the upper torso, for a plane-wave irradiation at a frequency of 350 MHz and a power density of 1 mW/cm^2.

(a) chest area - 45 cm from the top of the head. E || L & from back to front, scanning along the h.

(b) chest area - 38.5 cm from the top of the head. h || ⊥, the electric field shoulder-to-shoulder, propagation from head to toe, scanning perpendicular to h and E

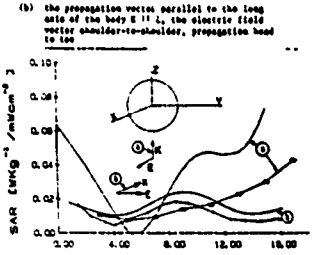

Figure 3. The specific absorption rate distribution in the head for a plane-wave irradiation at a frequency of 350 MHz and a power density of 1 mW/cm^2. Hashed lines are for a 16-cm lossy sphere - analytical results.

(a) and (b) for the E and k polarizations, respectively. Each data point is an average of at least five separate measurements. In all experiments the SARs were normalized to 1 mW/cm² of an incident power density at the plane corresponding to the body surface or the point closest to the radiation source.

Our data can be compared with the experimental results obtained by the thermographic technique (7). For the E polarization maxima of the SAR were found by us in the neck and the thigh regions, quite similar to the thermographic data at 450 MHz (7). Even quantitatively, the agreement is close in view of the frequency difference, e.g., in the neck we found SAR = 86 mW/kg, vs SAR = 120 mW/kg reported at 450 MHz.

Our experimental data were also compared with the theoretical values obtained for the block model of man (4,5,8). Significant differences between calculated values of the SAR and our results were observed. The comparison is confounded by the differences in the shape of the models and locations of the comparison sites (while our method provided the SAR values within a relatively small volume of about 1 cm^3, the cells in the block model are much larger, > 10 cm^3). However, the observed differences are of an order of magnitude or more, and are likely to be due to other factors. Particularly large differences occur in the SAR distribution both in the head and the torso for the k polarization. Our experimental data show a nearly exponential decay of the SAR with distance from the surface (see Figure 1(b), with extremely low SAR in the legs, while the theoretical calculations show appreciable SAR values in the legs (8).

A rapid decrease of the SAR values within the torso as a function of the distance away from the radiation source for the E polarization is illustrated in Figure 2. The deposition of the energy at the body surface within the torso was also observed thermographically at 450 MHz (7). For the k polarization the SAR distribution is qualitatively very similar to that of an elipsoidal cylinder which is not surprising in view of the similarities in shape.

The SAR distributions in the head are shown in Figure 3. Corresponding SAR distributions in a 16-cm diameter sphere filled with the same phantom material are also shown for comparison. It can be noted that the shape of the curves is very similar, however, the quantitative results are slightly different. The SAR distribution in the head appears to be different than that for the block model of man (8) as no significant resonances were found at 350 MHz.

Conclusions

Measurements of the specific absorption rate (SAR) distribution in a full-scale model of man filled with a phantom material having average tissue permittivity have been performed at 350 MHz for a far-field exposure and two polarizations. The use of a computer-controlled mechanical scanning system and implantable isotropic probes provided good spatial resolution, excellent reproductibility of results of ± 0.5dB, and a good absolute uncertainty of ± 1 dB. The measurements are fully automated and after proper calibrations and preparation, a large number of data points can be conveniently obtained without operator's assistance.

At 350 MHz a generally non-resonant behaviour of the human body, with maximum energy absorption at the surface on which the radiation is incident, was confirmed. This conclusion does not however apply to the head, neck and the limbs, where more complex distributions of the SAR were observed.

Our experimental data is in a relatively good agreement with the reported experimental results at 450 MHz obtained by the thermographic technique, (7), however, only a few features of the distribution could be compared.

The results of our experiments differ significantly from the values of the local SAR calculated for the block model of man (4,5,8). Particularly large differences occur in the head and torso for the k polarization. The distributions of the SAR in the head were found similar to that for a lossy sphere without any significant resonances at 350 MHz.

Our experimental results provide quantitative proof of serious limitations of the theoretical analysis of simplified models of man in terms of the distribution of energy. Our results also clearly indicate the significance of obtaining the SAR distribution in a reliable manner under realistic conditions.

Acknowledgements

Our thanks to Drs. O.P. Gandhi and I. Chatterjee for providing us with detailed results of the SAR calculations for the block of man. This research was supported by the Office of Naval Research (U.S.A.), Department of Health and Welfare Canada and the Natural Sciences and Engineering Research Council of Canada.

References

(1) C.H. Durney, "Electromagnetic dosimetry for models of humans and animals: A review of theoretical and numerical techniques," Proc. IEEE, vol 68, pp 3-40, 1980.

(2) K.M. Chen, and B.S. Guru, "Induced EM fields inside human bodies irradiated by EM waves up to 500 MHz," J. Microwave Power, vol 12, pp 173-183, 1977.

(3) K.M. Chen, and B.S. Guru, "Internal EM fields and absorbed power density in human torso induced by 1-500 MHz EM waves," IEEE Trans. Microwave Theory Tech., vol MTT-25, pp 746-756, 1977.

(4) M.J. Hagmann, O.P. Gandhi, and C.H. Durney, "Numerical calculation of electromagnetic energy deposition for a realistic model of man," IEEE Trans. Microwave Theory Techn., vol MTT-27, pp 804-809, 1979.

(5) M.J. Hagmann, O.P. Gandhi, J.A. D'Andrea, and I. Chatterjee, "Head resonance: Numerical solutions and experimental results," IEEE Trans. Microwave Theory Techn., vol MTT-27, pp 809-813, 1979.

(6) A.W. Guy, M.D. Webb, and C.C. Sorensen, "Determination of power absorption in man exposed to high frequency electromagnetic

SIXTH ANNUAL MEETING OF THE BIOELECTROMAGNETICS SOCIETY
ATLANTA, GEORGIA, JULY 15-19, 1984
ABSTRACT SUBMISSION FORM

FIRST AUTHOR'S MAILING ADDRESS:

Name Dr. Andrzej Kraszewski

Address Dept. of Electrical Engineering, University of Ottawa

City Ottawa Ont K1N 6N5 State CANADA Zip

First author's signature

Please check preference for method of presentation:

Platform ..... ☑

Poster ..... ☐

No preference..... ☐

Sponsored by Dr. Stanislaw S. Stuchly (a BEMS member).
Type abstract in space outlined below. Follow instructions (see opposite side).

SPECIFIC ABSORPTION RATE DISTRIBUTION IN A MODEL OF MAN AT 350 MHz.

Andrzej Kraszewski,* Maria A. Stuchly,† Stanislaw S. Stuchly, George Hartsgrove and Daniel Adamski* Department of Electrical Engineering, University of Ottawa. Ottawa, Ont., K1N 6N5, † also Radiation Bureau, Health and Welfare Canada.

A computer controlled system and an implantable isotropic electric field probe were used to obtain local values of the specific absorption rate (SAR) within a full scale homogeneous model of man. The model was exposed to a plane wave at 350 MHz and two polarizations, the electric field parallel to the axis and the propagation from-head-to-toe. For the electric field parallel to the model axis the SAR distribution is highly nonuniform with relatively narrow maxima in the neck (0.17 W/kg for 1 mW/cm^2) and just above the knee. In the torso the SAR decreases exponentially from the surface along the direction of the wave propagation. The distribution of the SAR in the head does not exhibit any significant maximum in the center as predicted by calculations for "the block model", but resembles the SAR distribution in a lossy sphere of the comparable diameter. For the wave propagation from head-to-toe the distribution of the SAR is also highly nonuniform with a maximum at the top of the head (close to the source) and with a smaller maximum in the neck region. The highest local SAR occurs in the shoulder region.

To assist in program scheduling, please underline the category below which best characterizes the subject matter of your paper.

Effects:
- Behavioral
- Cellular
- Developmental
- ELF
- Endocrine
- Genetic
- Hematopoietic
- Immunological
- Neurological
- Physiological
- Sensory
- Ultra-structural

Diagnostic applications
Dielectric properties of biological materials
Dosimetry
Exposure systems
Field perturbation
Hyperthermia
Instrumentation
Therapeutic applications

Other: _____

Authors are requested to send abstract and three (3) copies by March 1, 1984 to:

Don Justesen
Research Service (151)
USVA Medical Center
Kansas City, MO 64030

7.1 ENERGY ABSORPTION IN THE NEAR FIELD-EXPERIMENTAL RESULTS FOR A MODEL OF MAN

A. Kraszewski, S. Stuchly, M. Stuchly*
G. Hartsgrove and D. Adamski
Department of Electrical Engineering
University of Ottawa, Ottawa, Ontario,
KIN 6N5, Canada
*Radiation Protection Bureau, Health and Welfare Canada

Distributions of the electric field and the equivalent specific absorption rate (SAR) in full scale models of man exposed in the near-field of linear and slot antennas at a frequency of 350 MHz have been measured. A computer-controlled scanning system and a calibrated triaxial electric field probe were used. A full-scale styrofoam mold of the human body was filled with equivalent "average" tissue material and exposed in the near-field of an antenna located 8 cm from the back of the model with the feed point in the sternum region. For the E polarization and the dipole antenna the maximum equivalent SAR is located in the neck region above the feed point of the antenna. The distribution of the equivalent SAR along the direction of propagation at the feed point level exhibits an exponential decay with large values of the SAR on the surface (over 1W/kg/W). It has also been found that the maximum equivalent SAR on the axis of the model for the E polarization was twice as large as for the H polarization (110 mW/kg/W and 60 mW/kg/W, respectively). For the slot antenna and E polarization the maximum SAR occurs at the feed point of the antenna. We have found that the near-field distributions of the SAR are highly nonuniform with high values on the surface of the exposed model. It is evident, that in order to assess a potential health hazard from exposure in the near-field a detailed experimental mapping of the SAR distribution is necessary.

SIXTH ANNUAL MEETING OF THE BIOELECTROMAGNETICS SOCIETY
ATLANTA, GEORGIA, JULY 15-19, 1984
ABSTRACT SUBMISSION FORM

FIRST AUTHOR'S MAILING ADDRESS:

Name Dr. Andrzej Kraszewski

Address Dept. of Electrical Engineering, University of Ottawa

City Ottawa Ont K1N 6N5 State CANADA Zip

First author's signature

Please check preference for method of presentation:

Platform ☑

Poster ☐

No preference ☐

Sponsored by Dr. Maria A. Stuchly (a BEMS member).

Type abstract in space outlined below. Follow instructions (see opposite side).

SPECIFIC ABSORPTION RATE DISTRIBUTION IN A MODEL OF MAN EXPOSED IN THE NEAR FIELD. Andrzej Kraszewski,* Stanislaw S. Stuchly, Maria A. Stuchly[1)], George Hartsgrove and Daniel Adamski, Department of Electrical Engineering, University of Ottawa, Ottawa, Ont., K1N 6N5, [1)] also Radiation Protection Bureau, Health and Welfare Canada.

Since it is difficult to calculate exposure to a man from portable transmitters, the specific absorption rate (SAR) was measured in over 500 locations within a full scale model of the human body. The model was exposed to a resonant dipole radiating at 350 MHz, located 8 cm from the body surface parallel to the axis of the body with the feed point in the neck region. The SAR was measured within a tissue volume of less than 1 cm^3. The local values of the SAR exhibit an exponential decay with a maximum at the body surface, except in the neck and head regions. In the head the maximum is at the surface, but the changes inside the head are very slow. In the neck, after an initial exponential decay there is a small increase in the SAR. The maximum close to the neck surface is 0.6 W/kg for 1 W input power to the dipole. The SAR averaged along the direction perpendicular to the body axis shows large variations along the main axis of the body. A relatively broad maximum (0.18 W/kg for 1 W) is located in the neck-shoulder region. This is in qualitative agreement with the calculated data for 200 MHz (Spiegel, IEEE Trans., vol. MTT-30, 1982, p 177).

To assist in program scheduling, please underline the category below which best characterizes the subject matter of your paper.

Effects:	Neurological	Field perturbation
Behavioral	Physiological	Hyperthermia
Cellular	Sensory	Instrumentation
Developmental	Ultra-structural	Therapeutic applications
ELF	Diagnostic applications	
Endocrine	Dielectric properties	Other: _____
Genetic	of biological materials	
Hematopoietic	Dosimetry	_____
Immunological	Exposure systems	

Authors are requested to send abstract and three (3) copies by March 1, 1984 to:

Don Justesen
Research Service (151)
USVA Medical Center
Kansas City, MO 64030

ELECTROMAGNETIC DOSIMETRY IN FULL-SCALE MODELS OF THE HUMAN BODY Ref. [8]

A. Kraszewski
Dept. of Electrical Engineering, University of Ottawa
Ottawa, Ontario, CANADA K1N 6N5

Abstract. In investigations of biological effects of electromagnetic waves it is essential to identify spatial distributions of the electric fields induced inside exposed bodies. A computer-controlled system has been developed and an evaluation of the implantable electric-field probes has been performed which subsequently were used to obtain maps of the electric field induced in various cross-sections of a full-scale electrically-equivalent models of man. Some results from exposures in the near-field and the far-field of resonant dipoles and slots at frequencies from 160 MHz to 915 MHz are presented in the paper.

Introduction

Interactions of electromagnetic fields with biological tissues and bodies are complex function of numerous parameters. The intensity of the internal field induced inside biological bodies depends on the parameters of the external field, the frequency, the intensity, direction and polarization, as well as on the size, shape and the dielectric properties of the exposed body. As the magnetic permeability of tissue is practically equal to that of free space, all known and anticipated interactions occur through a mechanism involving the electric field. Therefore, the electric field vector or its distribution throughout the exposed body provides a full description of the exposure field-body interactions. The main objective of electromagnetic dosimetry is to quantify these interactions.

A dosimetric measure that has been widely adopted is the specific absorption rate (SAR) [1] defined as the time derivative of the incremental energy dW absorbed by an incremental mass of tissue (dm) contained in a volume element (dV) of a given density ρ. Thus,

$$SAR = \frac{d}{dt}\left(\frac{dW}{dm}\right) = \frac{d}{dt}\left(\frac{dW}{\rho\, dV}\right). \qquad (1)$$

Using the Poynting vector theorem for sinusoidally varying electromagnetic field, it may be written as

$$SAR = \frac{\sigma}{\rho} |E|^2 \qquad (2)$$

where σ is the tissue conductivity in S/m and $|E|$ is the rms value of the internal electric field in V/m. The SAR is expressed in W/kg or their derivatives. The whole-body average SAR is defined as a ratio of the total absorbed power in the exposed body to its mass. The local SAR refers to the value within a defined unit volume or unit mass, which can be arbitrarily small.

In bioelectromagnetic research dosimetry has been developing in two parallel, complimentary streams, theoretical and experimental. Theoretical dosimetry relies on the analysis of simplified models [2], while experimental dosimetry is concerned with the development of methods and instrumentation for measurements of the internal electric fields, SARs and related parameters.

This paper deals with the dosimetric experiments carried out at the University of Ottawa on full-scale models of an average man, at several frequencies and under various exposure conditions.

Experimental arrangement

Block diagram of the system employed in these experiments is shown in Fig.1. The whole system - except for the computer, the generator and monitoring equipment - is placed in an anechoic chamber. The scanning system [3] is composed of a mechanical structure for supporting and positioning the probe

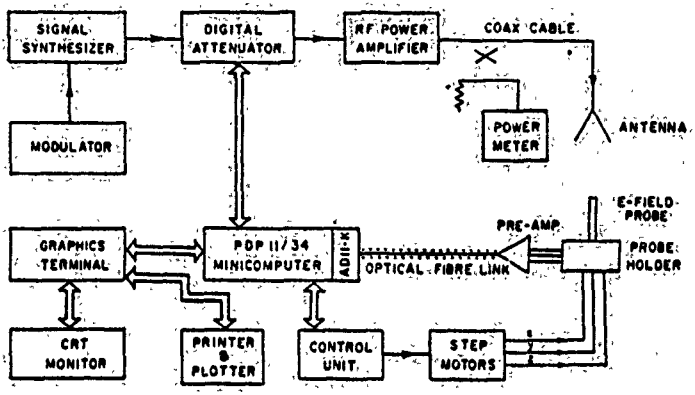

Fig.1. Block diagram of the measuring system

in any location within a volume of 1.9x0.5x0.45 m with accuracy of 0.1 cm, and a computer system for control of the experiment, data aquisition, storage, display and recording.

A mold closely approximating an anatomically correct average man of a height of 175 cm and a weight of 70 kg is filled with semiliquid phantom material whose electrical properties approximate those of the "average tissue", i.e. 2/3 of the muscle tissue. The model is placed horizontally with the antenna located below it. For E- and H-polarizations the electric-field vector is parallel or perpendicular to the long axis of body, respectively.

The electric field intensity is measured by the implantable

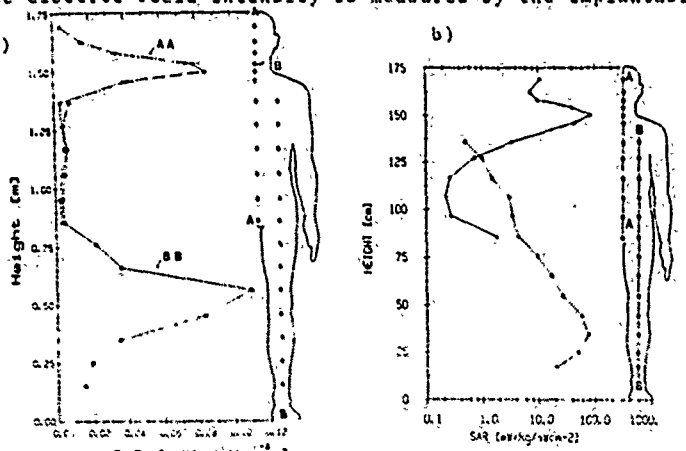

Fig.2. Distribution of the SAR local values in the mid-section. E-polarization at a) 350 MHz, b) 915 MHz.

triaxial electric field probe [4] - model EIT 979. The probe was fully characterized in terms of its sensitivity in tissue phantom material, noise and modulation characteristics [5] at every particular frequency and its calibration was spot-checked during the course of the experiments. The SAR is then calculated from the measured electric field intensity according to Eq.(2). The uncertainty in the SAR was estimated at ± 1 dB and was mostly due to the calibration uncertainty of the probe [6]. Reproducibility of the experiments conducted at different power levels and on various days was well within $\pm$ 0.5 dB range.

Experimental results

Far-field exposure. Distribution of the local SAR values in the mid-section of the body along two axis, for E polarization at 350 MHz and 915 MHz are shown in Fig.2. Maxima of the dissipated energy occur in the neck region at both frequencies. Large SARs also are produced in different locations in the legs. Similar distributions were obtained for the H polarization, with the SARs contribution from limbs varying versus frequency. Such increased the body-part absorption is sometimes referred to as the resonant absorption. The body-part increased SAR depends on polarization and for the homogeneous model of man on limb dimension - wavelength ratio. For instance, at 350 MHz and the E polarization [6] the SAR in the head-neck region is 2.5 times the whole-body average SAR.

Near-field exposure. Distributions of the SAR in cross-section of the homogeneous torso exposed to a near-field of resonant slots with reflectors, located in the distance of approx. 0.1 from the body surface, for E polarization at 350 MHz and 915 MHz are shown in Fig.3a. The similar distributions for resonant

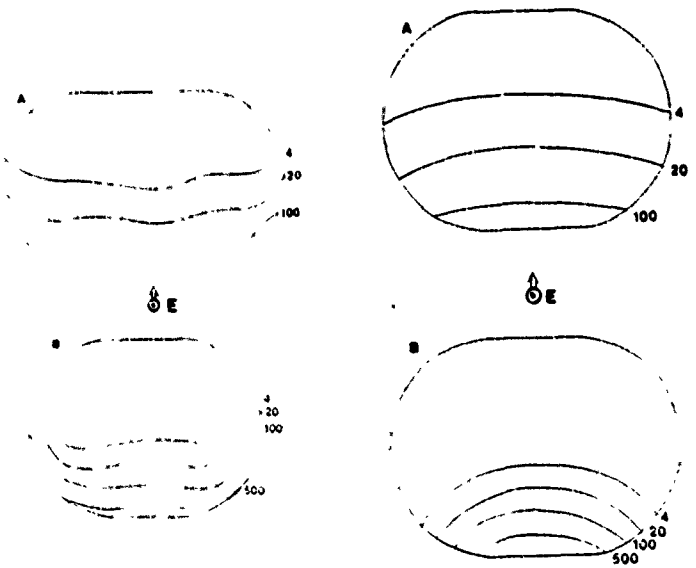

Fig.3. Distributions of the local SARs in the torso cross-sections for: a) slots with reflectors at A - 350 MHz; B- 915 MHz, b) resonant dipoles at A - 100 MHz; B - 915 MHz. Radiated power 1 W.

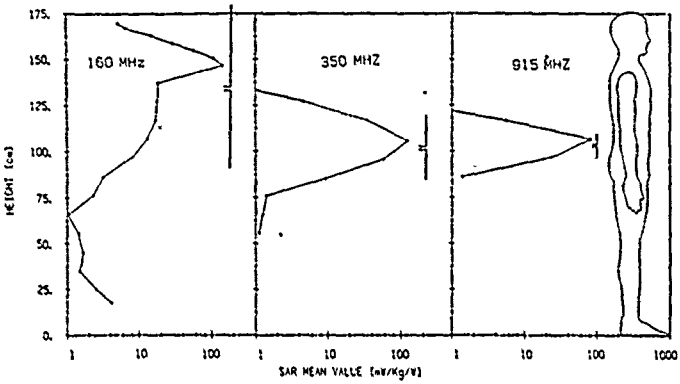

Fig.4. The specific absorption rates averaged over tissue layers perpendicular to the body axis for resonant dipoles with reflectors

dipoles with reflectors at 160 MHz and 915 MHz are shown in Fig.3b. It is evident that the maximum SAR occurs on the axis of the antenna and that the SAR decays exponentially inside the body along the direccion of propagation. More complex SAR distributions have been found in the head-neck region. At higher frequencies even though the average value of the SAR decreases (see Fig.4), the maximum values on the surface remain high. The energy absorption occurs over a smaller and smaller region of the body with increasing frequency.

Conclusions

Measurements of the specific absorption rate (SAR) spatial distribution in a full-scale models of man filled with a homogeneous phantom material having average tissue permittivity were performed at several frequencies from 160 MHz to 915 MHz. Various polarizations for far-field and near-field exposure were evaluated. A computer-controlled scanning system and an implantable isotropic electric-field probe provided a good spatial resolution, an excellent reproducibility ($\pm$0.5 dB) and uncertainty of measurement better than $\pm$ 1 dB. The measurements are fully automated and after a proper probe calibration, a large number of data points can be conveniently obtained for any radiating source -human body configuration.

The results on the spatial distribution of the SAR inside the human body under various exposure conditions are important in establishing protection standards against harmful exposures to RF energy as well as for producing more effective heating in cancer hyperthermia anf for design of better RF and microwave diathermy devices.

Acknowledgements

This work was supperted by grants from the U.S. Office of Naval Research, the Canadian Department of Health and Welfare and the Natural Sciences and Engineering Council of Canada.

References

[1] C.H.Durney et al., Radiofrequency Dosimetry Handbook, U.of Utah, 1978.
[2] M.J.Hagmann et al., IEEE Trans., vol MTT-27, 804-809, 1979.
[3] S.S.Stuchly et al., Rev.Sci.Instrum., vol.54 (11), 1547-1550, 1983.
[4] H.I.Bassen and G.S.Smith, IEEE Trans., vol.AP-31, 710-718, 1983.
[5] M.A.Stuchly et al., IEEE Trans., vol.BME-31, 526-531, 1984.
[6] A.Krazewski et al., IEEE Trans., vol.MTT-32, 774-783, 1984.

Conference Proceedings

RA.E97

15th EUROPEAN MICROWAVE CONFERENCE microwave 85

Monday 9th to Friday 13th September 1985

Palais Des Congrès, Paris, France

Supported by
SEE — SOCIÉTÉ DES ELECTRICIENS ET DES ELECTRONICIENS

In co-operation with

EUREL—The Convention of National Societies of Electrical Engineers of Western Europe
IMPI—The International Microwave Power Institute
URSI—The International Union for Radio Science
IEEE—The Region 8 and several Professional Groups
Antennas and Propagation
Electron Devices
Magnetics
Microwave Theory and Techniques

In association with

MICROWAVE EXHIBITIONS AND PUBLISHERS LTD.
Convex House, 43 Dudley Road, Tunbridge Wells, Kent TN1 1LE
Telephone: (0892) 44027 Telex: 95604 MEPNCL

MAPPING THE INTERNAL ELECTRIC FIELD IN MODELS OF BIOLOGICAL OBJECTS

A. Kraszewski*

ABSTRACT. A computer-controlled scanning system and triaxial electric field probes were used to measure spatial distribution of the electric field in a full-scale homogeneous model of the human body. Experimental results obtained at frequencies 160 MHz, 350 MHz and 915 MHz in the near-field of resonant dipoles and slots with reflectors are presented.

INTRODUCTION

In recent years advanced numerical techniques and modern computers have made the solution of many complex electromagnetic problems possible. However, theoretical analysis still remains very difficult and long computational time is required to solve some of the problems. For instance, in evaluating the potential hazards of the exposure of man to electromagnetic fields and in designing electromagnetically induced hyperthermia (for cancer therapy) it is essential to identify the spatial distribution of the electric field in the whole in the part of the human body. Due to the complexities in the shape and varying electrical properties of the body computations can not be accurately performed in many cases. Experimental methods in such cases can provide a viable alternative [1,2] .

This contribution describes an experimental system for the mapping of the spatial distributions of the electric fields inside models of the human body. The system operates at radio and microwave frequencies. Experimental results for near-field exposures of a model of man in the near-field of resonant dipoles and slots with reflectors at frequencies 160 MHz, 350 MHz and 915 MHz are discussed.

EXPERIMENTAL METHOD

To measure the electric field intensity inside the models miniature implantable triaxial probes were used [3] . A probe contains of three very short electric dipoles loaded with miniature Schottky-barrier diodes connected to the external circuitry by high resistance leads. The dipoles are arranged in Y- or I-beam configuration which allows for measurements of the electric field components. Thus, not only the magnitude but potentially also the direction of the electric field can be determined. Measurements are performrd at very low level exposure which do not cause measurable increase of the model temperature. The probes were calibrated prior to the experiments by measuring the electric field distributions in lossy dielectric spheres of various diameters. The probe output voltages for many locations in sphere were compared with the calculated values obtained from the Mie solution [4] , using the least-square technique. The results of calibration of the electric

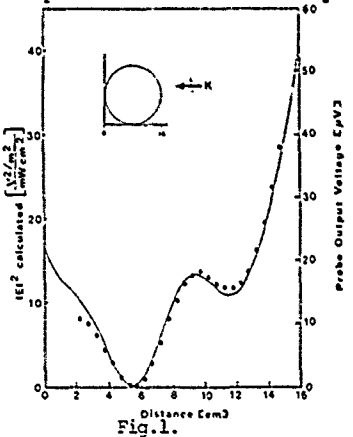

Fig.1.

* Dept. Electrical Engineering, University of Ottawa, Ottawa, Ont., Canada.

field probe (EIT model 979, OD. 9 mm) in a 16-cm diam. sphere filled with a lossy material at 475 MHz (AM 510 Hz) are shown in Fig.1. It may be seen that the probe output voltage (dots) follows the theoretical distribution (line) rather well and that even large gradients of the electric field can be finely reproduced by the probe. The uncertainty in the measurements of the electric field was estimated to be ± 0.5 dB. This is mostly due to the calibration uncertainty of the probe.

A calibrated probe may be positioned in any selected location in a model under computer control in a specially developed scanning system. A block diagram of the measuring system is shown in Fig.2. The system - except for

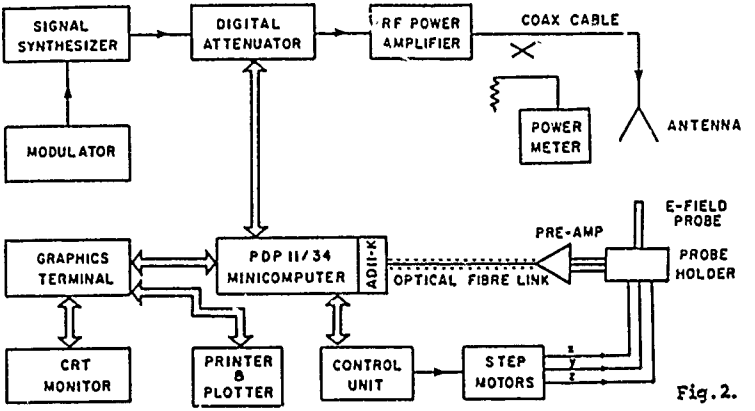

Fig.2.

the computer, generator and the monitoring equipment - is placed in an anechoic chamber. An optical fiber link connects the electric-field-probe amplifier with the remaining electronic circuitry located outside the chamber. The scanning system is composed of a mechanical structure for supporting and positioning the probe in any location within a volume of 1.9 m by 0.5 m by 0.45 m and a computer system for control of the experiment, data aquisition, storage, display and recording [5]. To increase the dynamic range of the measurements of the electric field intensity RF signals are amplitude modulated at about 500 Hz, which provides optimum signal to noise ratio [4]. The output signal from the probe is amplified, A/D converted and fed to the computer.

A plastic mold closly approximating an anatomically correct average man of a height of 175 cm and a weight of 70 kg was filled with semiliquid tissue-equivalent material whose dielectric properties approximate those of the "average tissue", i.e. 2/3 of the skeletal muscle properties. The model was placed horizontally on low-density styrofoam blocks. The antenna was located below the model for the E- and H-polarizations (i.e. the electric field vector being parallel or perpendicular to the long axis of the body), or at the side of the model for the k-polarization (i.e. the propagation vector parallel to the long axis of the body).

Resonant dipoles with reflectors operating at 160 MHz, 350 MHz and 915 MHz were employed as radiating antennas. Two resonant slots with reflectors placed close from the model torso (approx. 0.1λ) were also investigated. The dipoles simulated a potential situation of exposure to portable transmitters, while the slots that of leaky transmitter cabinets.

The primary advantages of the method presented here are that measurements in a large number of locations can be performed in a relatively short time, that the sensitivity of the measuring system can be spot-checked during the course of the experiments and that the local E-field intensity can be

measured at almost every point inside the model. This is possible because the scanning system allows probe movement with increments as small as 1 mm in all three directions.

EXPERIMENTAL RESULTS

Results of the experiments are presented in a form of the specific absorption rate (SAR) expressed in mW/kg, i.e. energy absorbed by an unit of volume of the tissue material. Note that

$$SAR = \frac{\sigma}{\rho} |E|^2$$

where σ is the conductivity of the tissue material in S/m, ρ is the material density in kg/m^3 (usually equals 1000 kg/m^3) and $|E|$ is the measured rms value of the electric field intensity in V/m. The conductivity of the material used in the experiments at 160 MHz, 350 MHz and 915 MHz, reported here, was equal to 0.8 S/m, 0.95 S/m and 1.17 S/m, respectively.

Distribution of the SAR (in mW/kg normalized to the radiated power of 1 W) along the antenna axis in the torso of the homogeneous model of full-scale man exposed to a near-field of resonant dipole with reflector is shown in Fig.3. The radiators were placed in such a way that the electric field vector was parallel to the main (vertical) body axis. In all cases investigated, for both types of radiators and at all frequencies, the SAR along the antenna axis decreases exponentially (notice the logarythmic scale) with distance from the body surface. Furthermore, the attenuation coefficients are very close to those estimated theoretically for the normal incidence of the plane-wave. That shows that the longer the wavelength, the greater the penetration depth in the tissue. The SAR close to the surface is much greater at 350 MHz and 915 MHz than at 160 MHz. For the slots the SAR close to the surface is less than that for the dipoles.

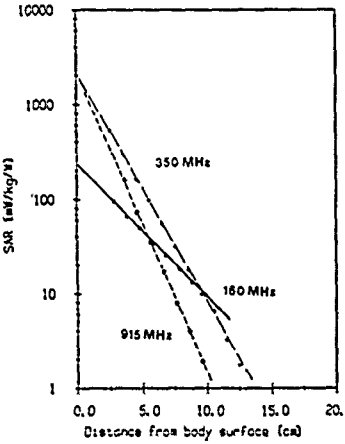

Fig.3. SAR in the torso on the axes of resonant dipoles vs. distance from the body surface.

Figures 4 and 5 illustrate the spatial distribution of the SAR in the cross-section of the torso on the radiator axes for dipoles and slots, respectively. The lines show the equi-SAR profiles in mW/kg per 1 W of the radiated output power. A difference in shape of the lines between the dipoles and the slots can be seen. The data presented can be be utilized in designing an array to obtain a desired heating contour.

Spatial distributions of the SAR averaged over tissue layers perpendicular to the body main axis for the dipoles and the slots are shown in Fig.6 and 7, respectively. The maximum SARs, except at 160 MHz, occur in the tissue layers on the radiators axes. At 160 MHz, as the dipole axis is close to the neck, the maximum shifts toward the neck, as also observed for far-field exposures [6]. It is evident, that for a homogeneous full-scale model of man exposed to near-field of resonant dipoles and slots with reflectors, the maximum of the electric field induced inside the body occurs most likely on the axis of the antenna and that it decays exponentially inside the body along the direction of propagation. At higher frequencies even though the average value of the SAR decreases sligthly (see Fig.6) [7] the maximum values on the surface remain high. With increasing frequency the energy absorption occurs in a smaller and smaller region of the model.

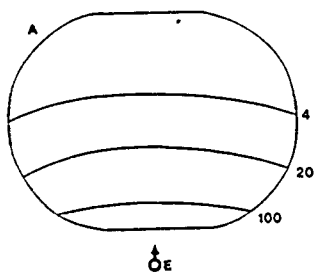

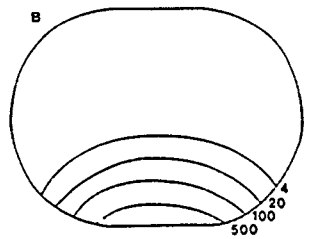

Fig.4. SAR (in mW/kg per 1 W) in the cross-section of the torso on the axis of the resonant dipoles with reflectors; A) 160 MHz, B) 915 MHz

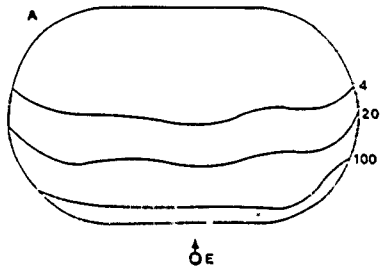

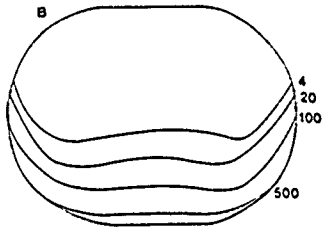

Fig.5. SAR (in mW/kg per 1 W) in the cross-section of the torso on the axis of the resonant slots with reflectors; A) 350 MHz, B) 915 MHz

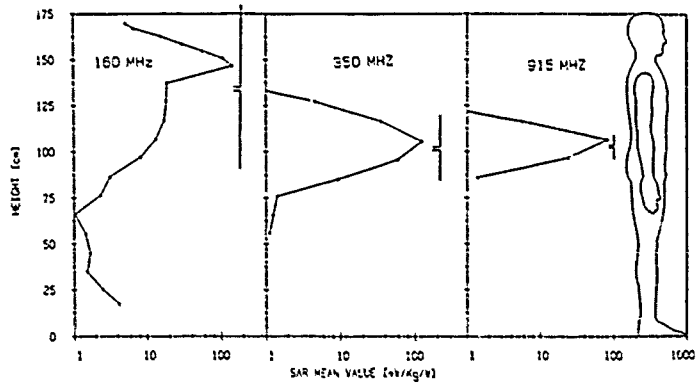

Fig.6. Specific absorption rate (SAR) averaged over tissue layers perpendicular to the body main axis for resonant dipoles with reflectors at three frequencies.

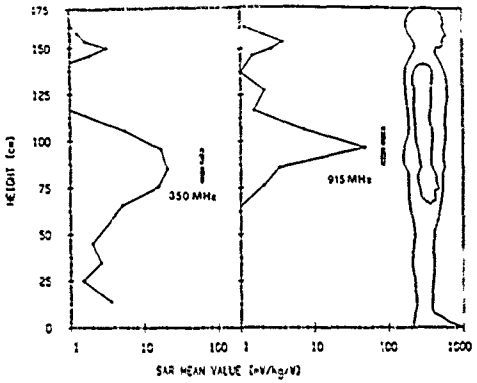

Fig.7. Specific absorption rate, SAR, averaged over tissue layers perpendicular to the body main axis for resonant slots with reflectors

CONCLUSIONS

Spatial distribution of the electric field intensity induced inside a full-scale model of man filled with a homogeneous tissue-equivalent material having average tissue permittivity were measured at frequencies of 160 MHz, 350 MHz and 915 MHz. Various polarizations for near-field exposure were evaluated. A comuter-controlled scanning system and an implantable isotropic electric-field probe provided good spatial resolution, excellent reproducibility of the results (± 0.5 dB) and acceptable uncertainty of the electric field measurement inside the model. The measurements are fully automated and after the proper probe calibration a large number of data can be conveniently collected at frequencies above 150 MHz (quality of the anechoic chamber available at the time is the limiting factor) for any radiating source - human body (model) configuration.

The results on spatial distribution of the electric field intensity induced inside the human body under various exposure conditions are important in establishing protection standards of exposure to RF energy. Furthermore, for the near-field exposures knowledge of the SAR distribution is essential in designing effective heating systems in hyperthermia for cancer therapy. This knowledge may also be utilized in designing new RF and microwave diathermy devices.

ACKNOWLEDGEMENTS

The author gratefully acknowledges grant support from the U.S.Office of Naval Research, the Health and Welfare Canada and the Natural Sciences and Engineering Research Council of Canada.

REFERENCES

[1] C.H.Durney et al., Radiofrequency Dosimetry Handbook, Rept.SAM-TR-78-22, USAF School of Aerospace Medicine, Brooks Air Force Base, TX, 1978.

[2] M.A.Stuchly and S.S.Stuchly, "Experimental Radio and Microwave Dosimetry", in: Handbook of Biological Effects of Electromagnetic Radiation, C.Polk and E.Postow (Eds), CRC Press Inc., 1985.

[3] H.I.Bassen and G.S.Smith, "Electric field probes - a review", IEEE Trans. Antennas and Prop., vol.AP-31, pp.710-718, 1983.

[4] M.A.Stuchly, A.Kraszewski and S.S.Stuchly, "Implantable electric-field probes - some performance characteristics", IEEE Trans. Biomed. Engng, vol.BME-31, pp.526-530, 1984.

[5] S.S.Stuchly, M.Barski, B.Tam, G.Hartsgrove and S.Symons, "Computer-based scanning system for electromagnetic dosimetry", Rev.Sci.Instrum., vol.54 (11), pp.1547-1550, 1983.
[6] A.Kraszewski, M.A.Stuchly, S.S.Stuchly, G.Hartsgrove and D.Adamski, "Specific absorption rate distribution in a full-scale model of man", IEEE Trans. Microwave Theory Techn., vol.MTT-32, pp.779-783, 1984.
[7] S.S.Stuchly, A.Kraszewski and M.A.Stuchly, "Energy deposition in a model of man in the near-field", Bioelectromagnetics, vol.6, pp.115-130, 1985.

SEVENTH ANNUAL MEETING OF THE BIOELECTROMAGNETICS SOCIETY
SAN FRANCISCO, CALIFORNIA, JUNE 16-20, 1985

ABSTRACT SUBMISSION FORM

~~FIRST~~ AUTHOR'S MAILING ADDRESS:

Name M.A. Stuchly, Health and Welfare Canada

Address Rm.233, EHC, Tunney's Pasture

City Ottawa, Canada State Ontario Zip K1A 0L2

First author's signature

Please check preference for method of presentation:

Platform ..... ☒

Poster ..... ☐

No preference ..... ☐

Sponsored by _____ (a full member of BEMS).

Please check if this is a student paper ..... ☐

Type abstract in space outlined below. Follow instructions (see opposite side).

ENERGY DEPOSITION IN A MODEL OF MAN; FREQUENCY EFFECTS IN THE NEAR FIELD.

A. Kraszewski, S.S. Stuchly, M.A. Stuchly[1] and G. Hartsgrove, Dept. of Electrical Engineering, University of Ottawa, Ottawa, Ont. K1N 5N6; 1) Radiation Protection Bureau, Health and Welfare Canada.

Spatial distributions of the specific absorption rate (SAR) were obtained in a full-scale model of man exposed in the near-field. The experiments were performed at 160, 350 and 915 MHz for resonant dipoles and slots with the electric field parallel and perpendicular to the main body axis. The antennas were matched and located about 0.1λ from the body surface in the shoulder area (dipoles) or in the abdomen area (slots). At all the frequencies investigated the SAR in the model on the antenna axis decreased exponentially with distance with the attenuation coefficient equal, within experimental error, to that of a plane wave propagating in a semi-infinite tissue layer. Large spatial gradients of the SAR were observed at all frequencies, the gradients were more pronounced for dipoles than for slots. At 160 and 315 MHz, but not at 915 MHz, the maximum SAR was located in the neck region for the E polarization. For the dipoles the shift was approximately 20 cm off the antenna axis. For resonant dipoles and dipoles with reflectors, the greatest whole-body average SAR per 1 W of antenna input power was at 350 MHz. The mean SAR averaged over a tissue layer 8 cm thick and perpendicular to the main body axis was from about 11 to 18 times greater than the whole-body average SAR. The SAR on the body surface was from about 120 to 240 times greater than the whole-body average. The mean for body-layers and surface SARs depend on frequency, polarization, antenna type and its distance from the body.

To assist in program scheduling, please underline the category below which best characterizes the subject matter of your paper:

Electric and Magnetic Properties	Instrumentation and Exposure Systems
Mechanism of Interaction	ELF Studies
Modulated Fields	*In Vivo* Studies
Dosimetry and Exposure Assessment	*In Vitro* Studies
Medical Application and Technique	Other: _____

Provide three (3) key words that characterize this work: 1. SAR distribution
2. Near-field 3. model of man

Authors are requested to send abstracts and three (3) copies by February 1, 1985, to:

Elliot Postow
Naval Medical R&D Command
Naval Medical Command National Capital Region
Bethesda, Maryland 20814-5044

Computer-based scanning system for electromagnetic dosimetry

Stanislaw S. Stuchly, Mariusz Barski, Benjamin Tam, George Hartsgrove, and Stephen Symons

Department of Electrical Engineering, University of Ottawa, Ottawa, Ontario K1N 6N5, Canada

(Received 29 November 1982; accepted for publication 15 July 1983)

This paper describes an experimental system developed for the purpose of studying the distribution of electric field in lossy bodies. Ultimately, a map of the internal electric field intensity in a phantom model of the human body exposed in the near field of radio and microwave radiators is obtained. The field is sampled by a nonperturbing probe in a number of points under computer control using a system consisting of a microcomputer and a minicomputer. A description is given of the hardware and software components of the scanning system and the results of experimental evaluation of the performance of the system. For illustration the electric field distributions in simple configurations obtained experimentally are presented and compared with analytical results.

PACS numbers: 41.10.Dq, 87.60.Mv, 41.10.Fs

INTRODUCTION

Experimental electromagnetic dosimetry is related to the studies of the physico-engineering aspects of the interaction between radio and microwave radiations and biological systems.[1] Specifically, it concerns the determination of the distribution of the internal electric field intensity in a phantom model of the human body exposed in the near field of radio and microwave radiators.[2] This objective is achieved using a computer-based scanning system capable of acquiring, storing, displaying, and recording the electric field intensity and its direction. Nonperturbing miniature implantable triaxial probes are used for measuring the electrical field.[3] The field distribution in human phantoms obtained through these studies, will be used in designing specific, pertinent to the near-field exposures, experiments with laboratory animals and in extrapolating the results to humans.

A general view of the experimental system for electromagnetic dosimetry is shown in Fig. 1. The system consists of the following subsystems: (a) an anechoic chamber; (b) an electromagnetic radiator fed from an appropriate power generator. A 350-MHz reflector-backed $\lambda/2$ dipole is shown for illustration; (c) a realistic full-scale phantom model of the human body; (d) a triaxial electric field probe; and (e) the scanning system composed of: a mechanical structure for supporting and positioning of the probe and a computer system for control of the experiment, data acquisition, storage, display, and recording (not shown in the photograph).

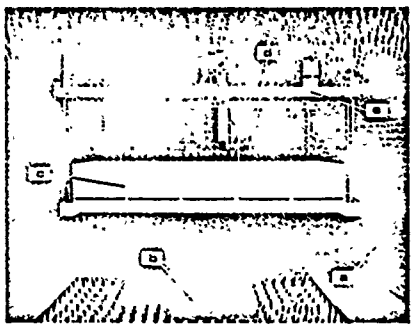

FIG. 1. General view of the system for experimental dosimetry; (a) anechoic chamber, (b) radio-frequency antenna, (c) phantom model of the human body, (d) triaxial electric field probe, (e) mechanical structure for supporting and positioning the probe.

Only the scanning system is described in this paper. The results of the electric field probes and the results of the electric field patterns in simple geometrical bodies are presented elsewhere.[4,5]

I. DESCRIPTION OF THE SYSTEM

A. Mechanical structure

The mechanical structure used for supporting and positioning of the electric field probe consists of three custom-made (Velmex, Inc.) independent guiding slides forming an *xyz*-coordinate system, see Fig. 1(e). The longest, fixed *x* slide is suspended from the concrete ceiling on four steel rods and moves the *y* slide. The *y* slide, in turn, drives the *z* slide which supports and positions the probe carriage. All slides use a lead-screw arrangement.

The probe can be placed at any location within a cube of $1.9 \times 0.5 \times 0.45$ m. The dimension of the cube can be altered by repositioning limit switches, at the ends of each slide.

Most of the metal parts of the system are covered by an absorbing material (ferrite) to minimize reflections.

B. Drives

The slides of the system are driven by three independent stepping motors (SLO–SYN model M092–FC09) each controlled by a separate translator module (STM103 SLO–SYN). The module provides sequencing and switching logic needed for the bidirectional control of the stepping motor. The speed, direction, and number of steps are directly con-

trolled by TTL pulse signals from the microprocessor-based control unit.

C. Modes of operation

The system can operate in a manual or a computer-supervised mode. In the manual mode the probe motion is controlled by switches on a portable, hand-operated unit. The motors can operate at fast and slow speed which is switch selectable. Selected coordinates of the probe can be stored in a file in the minicomputer memory, thus producing a map of measurement points.

In the computer supervised mode the probe scans automatically through all points of the previously selected map and the corresponding values of the electric field intensity for each position are recorded. After completing the data-acquisition phase the computer can display the results in graphical form on a CRT screen or they can be printed in tabular form on a line printer.

II. COMPUTER HARDWARE

Computing functions required for control of the scanning unit, data acquisition, display, and recording of the data have been divided between two devices, namely, a microprocessor-based control unit and a PDP11/34 minicomputer. Some details of the computer hardware are shown in Fig. 2.

The control unit is based on the 8085 microprocessor. A parallel interface links it with the portable hand-operated unit, the motor translators, and the limit switches. A serial link is provided for communication with the PDP/11 such that the control unit is seen by the PDP/11 as any other standard asynchronous terminal. In the manual mode, the control unit surveys all the control and limit switches and sends pulses to the translators as directed by the operator. Pulses sent to the translators are counted separately.

Actual states of the x, y, and z counters serve as probe coordinates and can be transmitted to the PDP/11 whenever the motors are not running. Then, if echoed back in an identical form, the control unit turns on the "data stored" light indicator on the hand-operated unit. This indicator is turned off again each time the probe moves to a new location. These coordinates are stored as a PDP/11 data file.

In the computer-supervised mode, the control unit causes the probe to move to a selected position, the coordinates of which are stored in the PDP/11 data file. After the probe reaches the desired position its new coordinates are transmitted back to the PDP11. This procedure serves a dual purpose, namely that of the continuous testing of the serial interface line and acknowledging that the control unit has finished its task. When the probe reaches its new position, the output signals from the electric field measurement system are converted into a digital form by an A/D converter (AD11-K) and stored in the computer memory as a data file. This information can be retrieved for tabular or graphical display using a DEC GIGI graphic terminal and a CRT monitor or a DECWRITER IV graphics printer.

To protect the electric field probe against accidental mechanical damage, the highest priority nonmaskable interrupt line of the 8085 microprocessor is activated by a switch mounted on the probe holder. "Go to manual mode" (Reset) and "Go to computer-supervised mode" are the two other interrupts used in the control unit.

III. SOFTWARE

The program for the control unit is written in the 8085 assembly language, while that for the PDP11 in FORTRAN.

The basic objectives of the control unit software are: (i) To provide reliable asynchronous serial communication between the 8085 microprocessor and the PDP/11 minicomputer. Serial input and output lines of the 8085 microprocessor are used as an asynchronous receiver and transmitter, respectively, with a baud rate of 1200. (ii) To move the carriage along the x and y axes simultaneously, provided that it remains in the retracted z position (home). For the carriage in any other z position (the probe possibly immersed in the phantom) horizontal motion is not possible. (iii) To stop the movements in any direction if the corresponding limit switch has been activated. (iv) To prevent multiple storage of a particular position of the carriage. The control unit can respond to the STORE button only once between changes in the carriage's position. (v) To protect the probe from mechanical damage.

The supervising computer (PDP11) software performs the following functions: experiment control, interactive communication with the operator, data acquisition, data storage, data processing, and data display.

During the execution of the program, the operator may

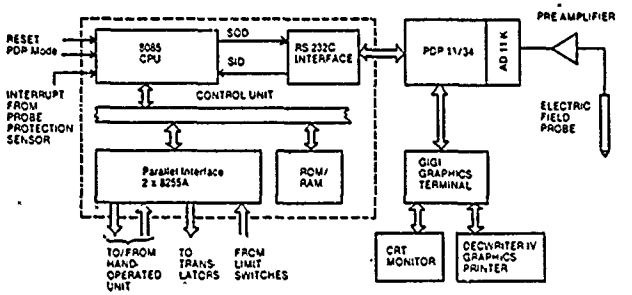

FIG. 2. Computer hardware used in the system for experimental dosimetry.

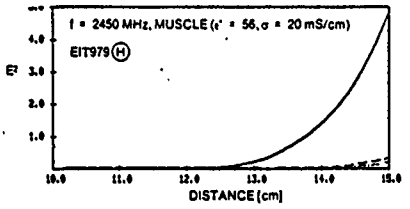

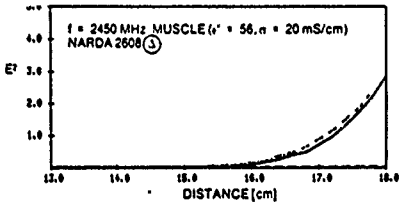

FIG. 3. Internal electric field intensity in a slab of a muscle-equivalent material vs distance *along* the direction of propagation of the wave at 2450 MHz. Different lines represent signals from the orthogonal dipoles (Ref. 4). The differences between the *H* and *A* dipole configurations are clearly visible (Ref. 4).

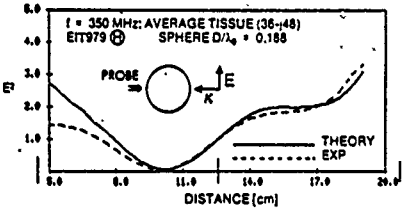

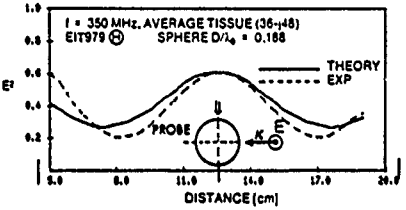

FIG. 5. Internal electric field intensity in a sphere filled with an "average tissue"—equivalent material at 350 MHz vs distance across the diameter in the direction *parallel* and *normal* to the direction of propagation of the wave. The vertical markers on the horizontal axis indicate the center and the walls of the sphere, respectively.

enter certain parameters which are recorded before the data are actually collected.

Parameters such as irradiating power, frequency, type of radiator, or type of the probe can be stored at the beginning of the data file.

Since both, creating the map and, even more so, acquiring data are highly time consuming, particular emphasis was placed on the development of the software which would help the operator to avoid errors. For example, the computer displays information on the current state of the experiment, and informs the operator of possible optional actions which can be undertaken. In case of an error, the experiment can be repeated starting from any point without the necessity of restarting.

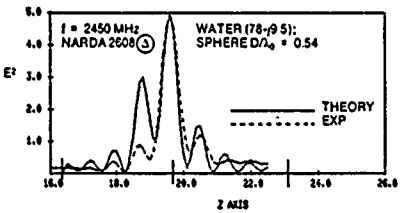

FIG. 4. Internal electric field intensity in a sphere filled with water at 2450 MHz vs distance across the diameter in the direction *parallel* to the direction of propagation of the wave. The vertical markers on the horizontal axis indicate the center and the walls of the sphere, respectively.

After the data have been acquired and stored the PDP11 is used to display the information in a graphical format.

For illustration the internal electric field distributions in simple geometrical configurations of lossy materials obtained experimentally are presented in Figs. 3–5 and compared with analytical results. Figure 3 depicts the square of the internal electric field intensity in a slab of a muscle-equivalent material versus distance along the direction of propagation of the wave at 2450 MHz. The well-known exponential character is clearly visible. Figure 4 presents the square of the internal electric field intensity in a sphere filled with water at a frequency of 2450 MHz vs distance across the diameter in the direction parallel to the direction of propagation of the wave. Very good spatial resolution of the probe is demonstrated in the main lobe of the characteristic. Finally, in Fig. 5 the internal electric field intensity in a sphere filled with an "average tissue"—equivalent material at 350 MHz is shown versus distance across the diameter in the direction parallel and normal to the direction of propagation of the wave. A relatively good agreement between the theoretical and experimental distributions is evident.

At the present time only the magnitude of the electric field is displayed and recorded. A program for display of both the magnitude and the direction of the measured electric field is being developed.

IV. SYSTEM PERFORMANCE

Salient characteristics of the system, such as the scanning volume, resolution, repeatability of finding a selected

TABLE I. Results of the experimental evaluation of the scanning system.

			Axis		
			x	y	z
Maximum linear displacement		cm	190	50	45
Scanning resolution		mm/step	0.013	0.013	0.013
Position repeatability (uncertainty)		mm	±0.05	±0.05	±0.05
Low speed	Simple motion	mm/s	0.42	0.42	0.42
	Composite motion		0.41	0.427	0.42
High speed	Simple motion	mm/s	12.3	12.5	12.6
	Composite motion		11.7	12.0	12.3

position, and the scanning speed were verified experimentally.

A. Scanning volume

With the limit switches at the far ends of the slides the measured scanning volume was 190×50×45 cm.

B. Resolution

A dial gauge with a resolution of 0.025 mm/div. (0.001 in./div.) was used to measure the displacement of the probe. In this experiment 100 steps of each motor were used. The summary of the results for the three axes is given in Table I.

C. Repeatability

For the z axis the same dial gauge was used. For 10 consecutive excursions from the home position to a specified position along the z axis the uncertainty in the probe position (repeatability) was found to be less than 0.05-mm s.d.

In the x–y plane a different technique was used. A simple map of a few points separated by several centimeters from each other was stored in the computer. The probe was replaced with a needle and a flat sheet of graph paper was placed under the scanning system. The map was scanned nine times under computer control, each time starting from the initial position in the corner of the scanning field. Each time the needle was lowered to punch a hole in the graph paper. The sheet was then shifted by a few centimeters and the scan was repeated. Using a microscope, the dimensions of the holes which were punched nine times were compared with those punched only once. The uncertainty of positioning along both x and y axes were found to be less than 0.05 mm.

D. Speed

Finally, both the low- and high-speed motions were examined for a simple motion (only one coordinate changing at a time) and for a composite motion (both x and y coordinates changing simultaneously). The measurement results are given in Table I.

ACKNOWLEDGMENTS

This research was supported by grants from the Office of Naval Research, U. S. A. Dept. of the Navy and by Health and Welfare Canada. The authors gratefully acknowledge valuable discussions with Dr. M. A. Stuchly from Health and Welfare Canada and Dr. A. Kraszewski from the University of Ottawa. Assistance of D. Adamski and G. Wong from the University of Ottawa is very much appreciated.

[1] O. P. Gandhi, Proc. IEEE 68, 24 (1982).
[2] C. H. Durney, M. F. Iskander, H. Massoudi, S. J. Allen, and J. C. Mitchell, U. S. A. F. School of Aerospace Medicine Report No. SAM-TR-80-32, 1980.
[3] G. S. Smith, IEEE Trans. Microwave Theory Tech. MTT-29, 1213 (1981).
[4] M. A. Stuchly, A. Kraszewski, S. S. Stuchly, and G. Hartsgrove, presented at the Vth Annual Meeting of the Bioelectromagnetics Society, Boulder, CO, 12–16 June, 1983 (abstract).
[5] S. S. Stuchly, M. Barski, B. Tam, G. Hartsgrove, and S. Symons, presented at the Vth Annual Meeting of the Bioelectromagnetics society, Boulder, CO, 12–16 June, 1983 (abstract).

Ref. D12

SYSTEM FOR MEASURING THE DISTRIBUTION OF THE INTERNAL ELECTRIC FIELD IN MODELS OF ANIMALS AND HUMANS

Stanislaw S. Stuchly, Andrzej Kraszewski, Maria A. Stuchly,*
George Hartsgrove and Gary H. Wong

Department of Electrical Engineering
University of Ottawa
Ottawa, Ont. Canada

*Radiation Protection Bureau
Health and Welfare Canada
Ottawa, Ont. Canada

stract

In investigations of biological effects of elec-
omagnetic waves it is essential to know spatial dis-
ributions of the electric field inside exposed bodies.
computer-controlled system has been developed for
is purpose, and a comprehensive evaluation of the
plantable electric field probes has been performed.
electric field intensity inside a model of the
imal or human body can be obtained at any frequency
thin the range of 100 MHz to 10 GHz, with an uncer-
inty of ±1 dB.

INTRODUCTION

Dosimetry of electromagnetic fields is concerned
th the determination of the rate of energy deposition
biological bodies and their electrical models. The
e of energy deposition is defined as the specific
sorption rate (SAR). The SAR is related to the in-
sity of the electric field in situ and the electric
operties of the tissue. Knowledge of the SAR is
ential in quantifying biological effects of the
ctromagnetic fields and developing exposure for
ctromagnetically induced hyperthermia in treatment
cancer.

In our investigations dosimetric data are obtained
ing non-perturbing implantable triaxial electric
ld probes [1,2] and a computer-controlled mechanical
nning system capable of acquiring, storing, display-
and recording the electric field intensities at
ious locations inside full-scale phantom models of
mal and human bodies. The field distributions ob-
ned using this system are used in designing speci-
, pertinent to the near and far-field exposures with
oratory animals and in extrapolating the results to
ans.

Considerable amount of the far-field experimental
simetric data has been obtained with phantom models
animals and scaled-down models of humans using the
rmographic technique [3]. This technique, although
ows a direct display of the local SAR values, re-
res very high power levels and suffers from limited
atial resolution particularly for scaled-down models.
o, the direction of the internal electric field
ot be retrieved from the experimental data.

The limitations of the thermographic technique
e led us to the development of a new system, which
vides accurate vector maps of the electric field in
l-scale phantom models of animal and human bodies
. The process of data acquisition is fully automa-
and is performed under computer control.

SCRIPTION OF THE SYSTEM

General

A block diagram of the system and a general view
the part located in the anechoic chamber are shown in Figures 1 and 2, respectively. The whole system consists of the following radiofrequency/microwave elements:

- a radio frequency (RF) and microwave (MW) anechoic chamber
- an antenna fed from an appropriate (RF/MW) power source
- a full-scale phantom model of the animal or human body
- a triaxial electric-field probe and associated electronic circuitry,

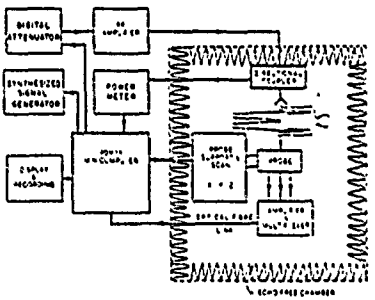

Fig. 1 Block diagram of the experimental system.

and the scanning system composed of:

- a mechanical structure for supporting and positioning of the probe together with the associated electronic circuitry, and
- a computer-based system for control of the experiment, data acquisition, storage, display and recording.

The details of the initial design and operation of the scanning system were presented elsewhere [4] and therefore only RF/MW elements and the recent modifications of the experimental system will be discussed here.

Radiofrequency/microwave elements

The anechoic chamber with the effective dimensions of 6 x 4 x 2.5 m is formed by the Advanced Absorber absorbing pyramids 30 cm and 45 cm long. The reflections from the walls of the chamber have been evaluated at several frequencies and were found to be below -20 dB for frequencies greater than 300 MHz and below -30 dB for frequencies above 2 GHz.

Various antennas such as resonant dipoles and reflector-backed resonant dipoles and resonant slots with reflectors were designed and tested at frequencies of 350, 950 and 2450 MHz. These antennas are well matched and provide well-defined near and far-field radiation pattern for dosimetric experiments. The intensity of the electric field in the absence of the phantom model was calculated and also verified experimentally using commercially available electric field probes.

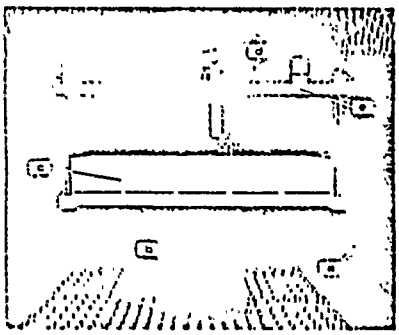

Fig. 2 Scanning system inside the anechoic chamber a) anechoic chamber; b) antenna; c) model of the human body; d) electric field probe; e) mechanical structure of the scanning system.

The antenna is fed from an RF/MW power amplifier (HCC Al 4CK) whose output power is monitored by a digital power meter (HP 436A) through a directional coupler (HP 7750). The power amplifier is driven from a synthesized signal generator (HP 8656A) through a computer-controlled digital attenuator (TEXCAN PA51).

Implantable triaxial electric-field probes, a Narda Model 2608, an ETT Model 979 and a Holaday Model HSM-01 were used to measure the electric field intensity. The calibration procedures and characteristics of these probes are described elsewhere [5]. The output voltages of the probes were fed to three independent battery-operated amplifiers, summed up and transmitted via an optical-fiber link to a second amplifier located outside the anechoic chamber. The output of this amplifier was connected to an A/D converter of a PDP 11/3. computer controlling the experiment. This arrangement significantly reduced the level of unwanted interfering signals.

The probe output signals proportional to the SAR values at various locations in the model, are stored in the digital format in the computer memory together with the corresponding coordinates of the probe positions. At the present time the SAR values are usually plotted as a function of probe coordinates and are easy to read and interpret.

Various molds of simple geometries [6] and that of the full-scale model of the human body [7] were made of an RF-transparent polystyrene foam. The molds were glued using an epoxy resin and sealed using various caulking mixtures. Recently, a new mold of the human body has been introduced. It is made from a thermoplastic material molded around a model of a standard man.

A semi-solid phantom material (mixture of water, sugar and salt) which simulates the electrical properties of the "average" tissue was used at 350 MHz [6]. At frequencies of 915 and 2450 MHz saline solutions can be used as phantom materials. The permittivities of different phantom materials were monitored using an automatic measurement system with an uncertainty better than 3%. Recently, improved tissue equivalent materials have been developed [8]. They are characterized by variable viscosity and significantly increased shelf life.

PERFORMANCE EVALUATION

The performance of the whole system was evaluated by measuring the distributions of the electric field in lossy spheres and infinite loss/ cylinders at 350, 920 and 2450 MHz. The results were compared with theory and used for calibration of the implantable probes [6].

The sum of three voltages (V_T) detected by the diode-loaded dipoles in the probe is related to the square of the total electric field intensity $|E_T|^2$ by the following expression:

$$V_T = B|E_T|^2,$$

where B is the sensitivity of the probe in the tissue phantom material.

The sensitivity of each probe was determined for each model from the following expression:

$$B = \frac{\sum_{i=1}^{N}(V_T)_i(|E_T|^2)_i}{\sum_{i=1}^{N}(|E_T|^2)_i^2},$$

where $(V_T)_i$ is the total voltage at the probe detector diodes (a sum of the three voltages of the three dipoles), measured at an experimental point i, $(|E_T|^2)_i$ is the theoretical value of the internal electric field intensity in the same point, and N is the number of points. The final value of the sensitivity was arrived at by an iterative process, in which only an unperturbed part of the distribution was included, i.e., that part for which the relative difference between the theoretical and experimental values was less than 10%.

There are several sources of errors in the system that may affect the accuracy of experimental results. Some of the errors can be limited to negligibly small through proper arrangements and care. These include reflections from the walls and the scanning system. In this work they have been eliminated by placing the whole system in an anechoic chamber and covering the frame of the scanning system with absorbing tiles. The incident electric field has to be well-defined in terms of its amplitude and direction. The field intensity in our tests was determined from the antenna gain calibration and measurements of the input power to the antenna. The uncertainty in the intensity was estimated at +/-.5 dB. The direction (alignment) of the antenna with respect to the probe was arranged within 2°. The intensity of the field was always adjusted so that the probes operated in the linear region.

The main accuracy limitations in this experiment are due to the probes themselves, namely to the cross-coupling of the dipoles, lack of a perfectly isotropic response (due to small differences between the three dipole-diode assemblies), remnant pick-up by their high resistance leads and the field perturbation by the leads.

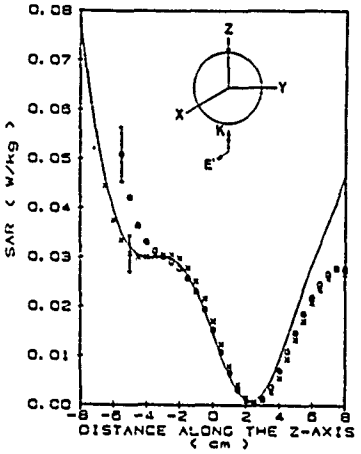

Fig. 3 Comparison of the calculated and measured SAR distribution along the z-axis of an average-tissue-phantom sphere; solid line indicates the calculated values, x x measured values with the EIT probe, □ □ measured values with the Holaday probe; $\varepsilon' = 38.9$, $\sigma = 1.04$ S/m, $f = 350$ MHz, Incident Power Density = 1 mW/cm^2, Diameter = 16 cm, Diameter/λ_0 = 0.19, Sensitivity B = 3.1±0.3 μV/(V^2/m^2) for the EIT probe and 12±2μV/(V^2/m^2) for the Holaday probe; the vertical bars show the estimated uncertainty of measurements; the double arrow indicates the direction of incidence of the wave and the single arrow shows the point where the probe is introduced into the phantom.

As an illustration a comparison of the theoretical d experimental results for a 16-cm diameter sphere at 0 MHz is shown in Fig. 3. The probe is introduced om the positive z direction, while the wave is inci-nt from the negative z direction. A very good agree-nt is evident for a small-diameter probe (EIT), 9 . For a large diameter probe (Holaday, 19 cm) sig-ficant deviations occur at one end of the distance anned. The differences between the theory and exper-nt close to the point of the probe entrance is most ely caused by formation of a neck through which the ntom material is flowing outside the mold.

The experiments were also performed using a full-ale phantom model of the human body at 350 MHz. The ults and discussion are presented in a companion er [9].

CONCLUSIONS

The experiments with simple geometrical bodies as well as with the full-scale phantom model of the human body indicate, that the implantable electric field probes combined with a computer-based scanning system constitute a powerful research tool in experimental dosimetry. Spatial resolution of a fraction of a millimeter and the uncertainty of the electric field intensity of ±1 dB obtained are fully satisfactory for the majority of electromagnetic dosimetry applications.

ACKNOWLEDGEMENTS

This work was supported by grants from the U.S. Office of Naval Research, Health and Welfare Canada and the Natural Sciences and Engineering Council of Canada.

REFERENCES

[1] H.I. Bassen and G.S. Smith, "Electric field probes - A review", IEEE Trans. Antennas and Prop., vol. AP-31, pp. 710-718, 1983.

[2] M.A. Stuchly and S.S. Stuchly, "Experimental Radio and Microwave Dosimetry in Handbook", Biological Effects of Electromagnetic Fields, C. Polk and E. Postow, Eds., CRC Press, in press, 1984.

[3] A.W. Guy, "Analysis of Electromagnetic Fields Induced in Biological Tissues by Thermographic Studies in Equivalent Phantom Models", IEEE Trans. Microwave Theory Tech., vol. MTT-19, pp. 205-214, 1971.

[4] S.S. Stuchly, M. Barski, B. Tam, G. Hartsgrove and S. Symons, "A Computer-Based Scanning System for Electromagnetic Dosimetry", Rev. Sci. Instrum., 54 (11), pp. 1547-1550, 1983.

[5] M.A. Stuchly, A. Kraszewski and S.S. Stuchly, "Implantable Electric Field Probes - Some Performance Characteristic", IEEE Trans. Biomed. Eng., vol. BME-31, in press, 1984.

[6] G.N. Wong, S.S. Stuchly, A. Kraszewski and M.A. Stuchly, "Probing Electromagnetic Fields in Lossy Spheres and Cylinders", IEEE Trans., Microwave Theory and Tech., vol. MTT-32, in press, 1984.

[7] A. Kraszewski, M.A. Stuchly, S.S. Stuchly, G. Hartsgrove and D. Adamski, "Specific Absorption Rate Distribution in a Full-size Model of Man at 350 MHz", IEEE Trans. Microwave Theory and Tech., vol. MTT-32, in press, 1984.

[8] G.W. Hartsgrove and A. Kraszewski, "Improved tissue-equivalent materials for electromagnetic absorption studies", 1984 BEMS Meeting, Atlanta, GA, July 15-19, 1984, (abstract).

[9] M.A. Stuchly, A. Kraszewski, S.S. Stuchly, G. Hartsgrove and D. Adamski, "Dosimetry in a full-scale model of the human body", EMC '84, Tokyo, October 14-18, 1984.

DOSIMETRY IN A FULL-SCALE MODEL OF THE HUMAN BODY

Maria A. Stuchly, Radiation Protection Bureau,
Health & Welfare Canada, Ottawa, Ont. K1A 0L2;
Andrzej Kraszewski, Stanislaw S. Stuchly, George Hartsgrove
and Daniel Adamski, Department of Electrical Engineering,
University of Ottawa, Ottawa, Ont. K1N 6N5, Canada.

Abstract

A computer controlled scanning system and implantable triaxial electric field probes were used to obtain maps of the specific absorption rate (SAR) in various cross-sections of a full-scale electrically-equivalent model of man. The data was obtained for exposures in the far-field, and the near-field of a resonant slot at 350 MHz. The results were found in a general agreement with previously published theoretical estimations of the average SAR and experimental results for scaled down models. However, significant quantitative differences were observed between the theory and experiment in the spatial distribution of the SAR.

Introduction

Knowledge of the spatial distribution of the specific absorption rate (SAR) is essential to quantify biological effects of radio frequency radiation (RF) and to extrapolate the results of experiments with animals for evaluation of a potential hazard to humans. The SAR is defined as the rate at which RF energy is imparted into a unit mass of the exposed body.

Considerable amount of data on the specific absorption rate have previously been obtained by theoretical analyses [1-3], and experiments with scaled down models [4]. However, only relatively simple models have been treated theoretically, and while the whole-body average SAR can be calculated for various exposure conditions in the far-field of radiation sources, the spatial distribution of the SAR has only been calculated for relatively large volumes. The calculations have been performed for the so called block model of man [5]. In this model the human body is divided into cubical cells of various volumes. Because of the symmetry of the human body, only half of it is analyzed, so half of the head is divided into about 170 cells [6] and the remaining parts of the body are also divided into 170 cells [5]. The limitations of such analysis are apparent in view of complexity of the human anatomy.

The SAR distribution has also been determined experimentally by the thermographic technique [4,7]. In this technique a scaled down model of the body is exposed for a few seconds to high power RF radiation, whose frequency is scaled proportionally to the model size. Immediately after the exposure thermographic scans of selected model surfaces are taken. From the measured temperature profiles, the SAR distribution is calculated. The main limitations of this technique are due to difficulties in incorporating anatomical and electrical differences of various tissues and organs of the body, and a need for high power of the radiation source. The last limitation is particularly serious when near-field exposures are considered.

The aforementioned reasons have led us into development of a measurement method and a system [8], which are capable of providing accurate maps of the SAR in full-scale models of the human body. The models can be made to resemble the human body closely both anatomically and electrically, and a good spatial resolution can be obtained.

In this paper we present the results of our measurements for an electrically-homogeneous model of man exposed to a plane-wave at 350 MHz in various polarizations, and exposed in the near field of a resonant slot. The frequency of 350 MHz was selected because of previously reported increased absorption and highly non-uniform SAR distribution in the head [6]. The resonant slot is a good representation of practical exposure situations resulting from leaky transmitter cabinets or other hardware.

Experimental System and Methods

A description of the experimental system is given in a companion paper [8].

Far-field exposure was created by placing a resonant slot at a sufficiently large distance from the surface of the model. A correction for the spheroidal wave-front was incorporated into the data processing program. Three polarizations of the incident field were investigated, namely, the electric field vector parallel to the long body axis, called the E polarization ($E \parallel L$), the magnetic vector parallel to the long body axis, called the H polarization ($H \parallel L$), and the propagation vector parallel to the long body axis, propagation from head-to-toe, called the k polarization ($k \parallel L$).

Near-field exposure was created by placing the resonant slot 8 cm away from the body surface. The electric field was parallel to the long body axis.

The electrical properties of the material filling the model of the human body were equal to the average tissue properties e.g. the dielectric constant $\varepsilon' = 35$ and the conductivity $\sigma = 0.55$ S/m.

An implantable triaxial electric field probe, EZT model 979, which was previously calibrated [8], had a sensitivity in the tissue material of 2.1 $\mu W/(V/m)^2$, with an estimated uncertainty of ± 1 dB. The minimum measurable field intensity was 1.3 V/m (SAR = 1.6 mW/kg) for a signal to noise ratio of 10, and an amplifier bandwidth of 1 Hz.

Exposure in the Far-Field

The specific absorption rate (SAR) in three cross-sections of the human body for the H polarization is shown in Figure 1. The cross-sections include the body centre (z = 10 cm) and two other planes 5 cm off-centre. Each data point is an average of at least five separate measurements performed at various incident power levels or on different days. A highly non-uniform distribution of the SAR can be noted. For instance, in the centre cross-section the SAR values range from 3.6 to 112 mW/kg for an incident power of 1 mW/cm^2.

For the E polarization similary non-uniform distribution occurs, with the maximum SAR located in the neck [9]. This is illustrated in Figure 2 showing the SAR along the two body axis at the center cross-section of the body. These results can be compared with the experimental data available in literature for scaled down models at ~50 MHz [7]. Despite the difference in the exposure frequency the

data is in good agreement. The maximum SAR in the neck in the center plane is approximately 90 mW/kg (Figure 2) as compared with 120 mW/kg measured at 350 MHz [7]. Similarly, in the legs the maximum SARs are 110 mW/kg and 147 mW/kg in our measurements at 350 MHz and at 450 MHz [7], respectively.

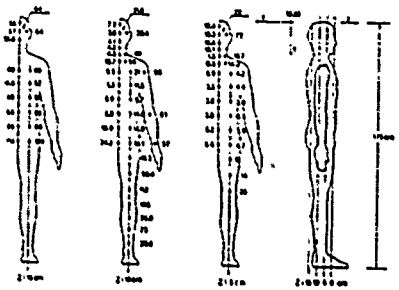

igure 1. The distribution of the SAR (mW/kg) in a oogeneous model of man exposed to a plane wave of 1 W/cm² at 350 MHz, the H polarization.

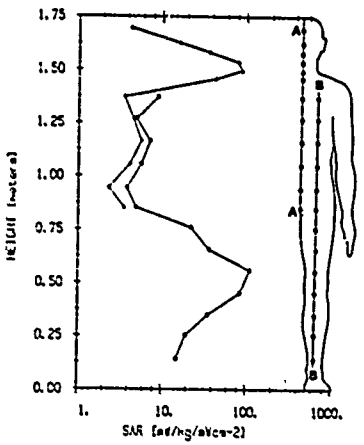

gure 2. The specific absorption rate (SAR) in the ter body cross-section (z = 10 cm) along the two lected axis, 350 MHz, 1 mW/cm², the E polarization.

The distribution of the SAR at 350 MHz is rticularly complex in the neck region as shown in gure 3. The maximum occurs on the axis of symmetry, t is shifted away from the plane of the wave cidence. At points off the axis of symmetry the SAR reases with the distance from the plane of wave cidence.

The distribution along two selected axis in the nter cross-section of the body for the H arization (the magnetic field parallel to the long s of the body) is shown in Figure 4. In this case re is a maximum in the neck region, but its nitude is small. A much more pronounced maximum of SAR is in the knee region, its magnitude is

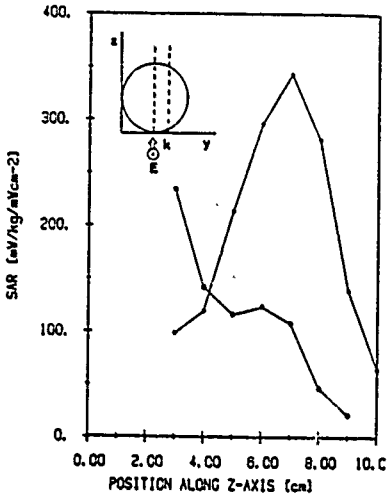

Figure 3. The specific absorption rate (SAR) in the neck vs. the position along z_0 axis (the direction of propagation), 350 MHz, 1 mW/cm², the E polarization; • on the axis, o 5 cm off the axis.

similar to that for the E polarization. In general, at 350 MHz there are many similarities between the data for the two polarizations. This is illustrated in Figure 5, which shows the changes in the mean SAR along the axis of the model for the E and H polarization. The mean SAR is calculated at each point as an average value in the horizontal tissue layer. The main difference is a significant increase of the SAR in the neck for the E polarization.

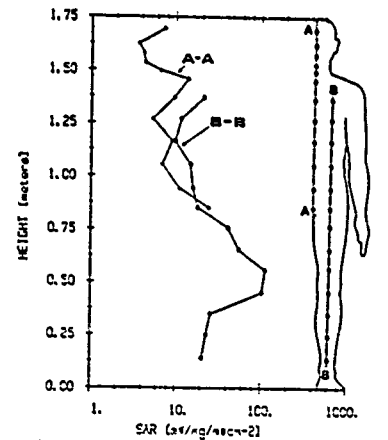

Figure 4. The specific absorption rate (SAR) in the center body cross-section (z = 10 cm) along two axis, 350 MHz, 1 mW/cm², the H polarization.

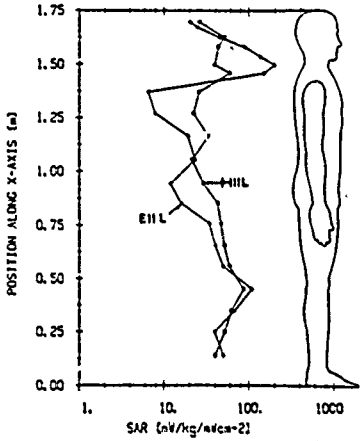

Figure 5. The specific absorption rate (SAR) averaged over horizontal layers of the body, comparison between the E_z(E||L) and the H (H||L) polarization, 350 MHz, 1 mW/cm^2.

The whole body average SARs for the two polarizations are fairly close, but significant differences occur between the rate of energy absorption in various body parts, e.g. head-neck, or arms. The data on the average SAR in various body parts is summarized in Table 1.

Body Part	SAR (mW/kg)	
	E||L	H||L
Head & neck	93.8	31.2
Upper torso	11.2	25.3
Lower torso	17.0	31.1
Arms	36.0	68.9
Legs	55.5	56.9
Whole Body	40.0	47.0

TABLE 1. Average specific absorption rates in various parts of a full-scale model of man exposed to a plane-wave of 1 mW/cm^2 at 350 MHz.

For wave propagation from head-to-toe, in the so called k polarization, the SAR decreases with the distance away from the plane of incidence, but again a small increase, of a lower magnitude occurs, in the neck region (Figure 6). In this case the maximum is relatively broad.

Comparison with Theory

Theoretical analysis has previously been performed using the method of moments to solve the tensor integral equation describing the fields inside a homogeneous (or inhomogeneous) block model of man [5,6]. A half of the body, which is sufficient to analyze, because of the body symmetry, has been divided into 340 cells, with 170 of them in the head-neck region. The comparison can only be done for the E polarization. The average SAR in the head and for the whole body as measured by us are very close to those calculated, 102 mW/kg and 40.2 mW/kg measured

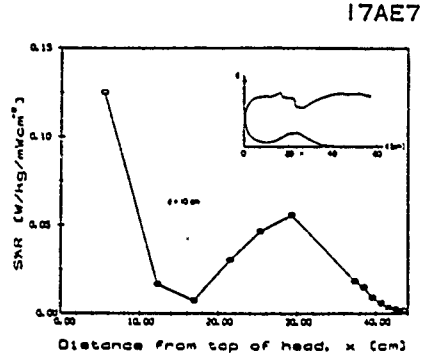

Figure 6. The specific absorption rate (SAR) along the center axis of the body, 350 MHz, 1 mW/cm^2, the k polarization.

for the head and the whole-body, as compared with calculated values of 108 mW/kg and 46.5 mW/kg, respectively.

Significant differences have been found in the SAR distributions. The best illustration is presented in Figure 7. This is a typical comparison of the experimental and theoretical SARs in the torso for the E polarization at 350 MHz. The SAR in the torso decreases exponentially within the first 5 cm or more.

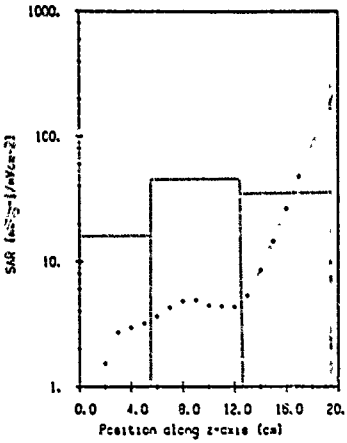

Figure 7. Comparison of the specific absorption rate (SAR) in the torso (17 cm from the feet) along the direction of wave propagation z. The wave is incident at the model wall shown by the vertical line at z = 19.5 cm, and propagates in the negative z direction. The points show the measured data, the dotted line blocks show the calculated data, f = 350 MHz, the E polarization. The slant line shows the least square-fit into the experimental points (more points are used for the fit than shown in the figure).

This has been our consistent finding for both the E and H polarizations. In about 8 cm from the surface upon which the wave is incident the SAR decreases more than 30 times (e.g. in Figure 7 it decreases from approximately 200 to 7 mW/kg). However, the theory predicts a different behaviour with comparable SARs within the first and second cell layer (z = 13 - 19.5 cm, and z = 5.5 - 13 cm) from the plane of incidence, respectively. It is apparent, that the averages of the experimental data for the corresponding layers would be significantly different, even in the first layer (notice the logarithmic scale).

The most likely reason for the observed differences is a relatively small number of cells within the torso of the block model. In particular, there are only two to three layers of cells in the block model. The cell size is comparable with the wavelength in the tissue material. The differences in the geometrical shape of the models may also contribute to the differences in the SAR spatial distribution.

Exposure in the Near-Field

The distribution of the SAR along two axis of the body exposed to a near-field of a resonant slot at 350 MHz is shown in Figure 8. The SAR values here are averaged within the body slices in the direction of the wave propagation. It is evident that the maximum SAR occurs on the axis of the slot. Furthermore, the maximum is broad in both directions, e.g. the SAR on the body axis (A-A) is the same as 10 cm off the axis (B-B). A small increase of the SAR in the neck region is visible, but the SAR value is about five times below that on the slot axis.

Figure 9 shows the variations of the SAR along the direction of propagation on the axis of the slot. It can be noticed that similarly to the far-field exposure, the SAR decreases exponentially with

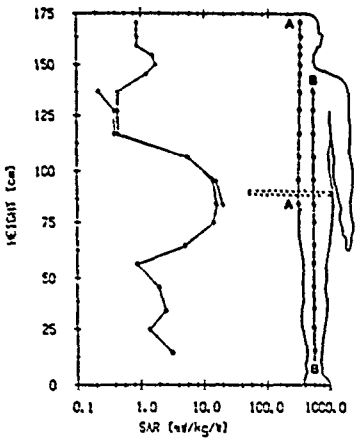

Figure 8. The specific absorption rate (SAR) averaged along the direction of wave propagation in various points on two selected body axis. Exposure to a resonant slot at 350 MHz, 1 W input power, the E polarization, the slot placed 9 cm from the body surface, 87 cm from the model base (bottom of feet).

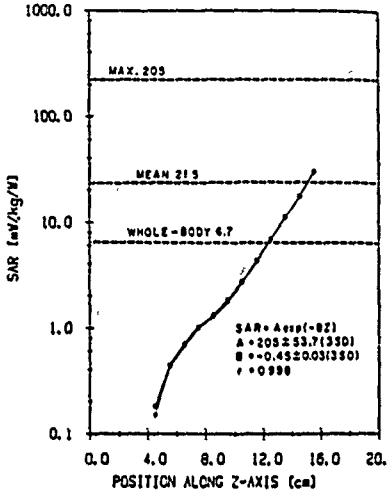

Figure 9. The specific absorption rate (SAR) along the direction of wave propagation in the torso on the axis of a resonant slot, 350 MHz, 1 W input power. The points show the measured values and the line is the least-square fit.

distance from the surface at which the wave is incident. It has been found that the attenuation coefficients are equal (within the measurement error) for the two cases (near and far field exposures), and very close to the attenuation coefficient calculated for a planar model with the electrical properties of the tissue phantom material.

The whole-body average SAR resulting from exposure to a resonant slot 9 cm away from the torso is 5.7 mW/kg for 1 W of the input power to the slot. When this is compared with the far-field exposure, one can evaluate that about 6 W of the input power to the slot are an equivalent of 1 mW/cm^2 for the far-field, in terms of the whole-body average SAR (see Table 1). A comparison of the SAR on the surface of the torso (Figures 7 and 9) indicates that on the axis of the slot it is 205 mW/kg (Figure 9) for 1 W of the input power and in the far-field approximately 200 mW/kg for 1 mW/cm^2 of the incident power density.

Conclusions

The spatial distribution of the SAR in a full-scale homogeneous model of man at 350 MHz is highly non-uniform for all three polarizations investigated. The SAR typically varies over at least three orders of magnitude. Large gradients of the SAR occur along the direction of propagation, and in the torso the decrease in SAR with the distance from the surface upon which the wave is incident is exponential.

The spatial distribution of the SAR is particularly complex in the head-neck region, with a maximum inside the neck for the E polarization.

The theoretical analysis of a block model of man having 340 cells [5,7] does not provide reliable

information on the spatial distribution of the SAR at 350 MHz.

For a resonant slot radiator at 350 MHz, which represents typical exposure from a leaky transmitter cabinet, the SAR is highly non-uniform with the maximum on the slot axis. The SAR along the slot axis decreases exponentially with distance from the body surface, when the slot is positioned close to the torso.

Acknowledgements

Financial support by the grants from the U.S. Office of Naval Research, Canadian Department of Health and Welfare and the Natural Sciences and Engineering Research Council of Canada is gratefully acknowledged. Assistance of Mrs. J. Smith and Mr. D.W. Lecuyer of Health and Welfare Canada in preparation of the manuscript is highly appreciated.

References

1. C.H. Durney, "Electromagnetic dosimetry for models of humans and animals: a review of theoretical and numerical techniques". Proc. IEEE, Vol.68, pp.3-40, 1980.

2. O.P. Gandhi, "State of knowledge for electromagnetic absorbed dose in man and animals". Proc. IEEE, Vol.68, pp.24-32, 1980.

3. O.P. Gandhi, "Biological effects and medical applications of RF electromagnetic fields". IEEE Trans. Microwave Theory Techn., Vol.MTT-30, pp.1831-1847, 1982.

4. A.W. Guy, M.D. Webb, and C.C. Sorensen, "Determination of power absorption in men exposed to high frequency electromagnetic fields by thermographic measurements on scale models". IEEE Trans. Biomed. Engr., Vol.BME-23, pp.361-371, 1976.

5. H.J. Hagmann, O.P. Gandhi and C.H. Durney, "Numerical calculation of electromagnetic energy deposition for a realistic model of man". IEEE Trans. Microwave Theory Techn., Vol.MTT-27, pp.804-809, 1979.

6. H.J. Hagmann, O.P. Gandhi, J.A. D'Andrea, and I. Chatterjee, "Head resonance: Numerical solutions and experimental results". IEEE Trans. Microwave Theory Techn., Vol.MTT-27, pp.809-813, 1979.

7. A.W. Guy, "Non-ionizing radiation: dosimetry and interactions". Proc. ACGIH Topical Symp., 1979, pp.75-101.

8. S.S. Stuchly, A. Krazewski, M.A. Stuchly, G. Hartsgrove and G. Wong, "System for measuring the distribution of the internal electric field in models of animals and humans". EMC '84 Tokyo, October 14-18, 1983.

9. A. Krazewski, M.A. Stuchly, S.S. Stuchly, G. Hartsgrove and D. Adamski, "Specific absorption rate distribution in a full-scale model of man at 350 MHz". IEEE Trans. Microwave Theory Techn., Vol.MTT-32, 1984, to be published.

Ref. [14]

Implantable Electric-Field Probes—Some Performance Characteristics

MARIA A. STUCHLY, SENIOR MEMBER, IEEE, ANDRZEJ KRASZEWSKI, AND STANISLAW S. STUCHLY, SENIOR MEMBER, IEEE

Abstract—Performance characteristics of three implantable triaxial field probes for measuring intensities of the internal electric fields in biological tissues at radio frequencies are given. The sensitivity in air between 100 MHz and 3 GHz, and in phantom materials at 350, 915, and 2450 MHz, are given for the Holaday model IME-01, EIT model 979, and Narda model 2608 implantable probes, as well as their noise and modulation characteristics.

Introduction

IMPLANTABLE field probes for measuring intensities of the internal electric fields in biological tissues at radio frequencies have been analyzed extensively [1]-[6]. Single- and triple-axis (isotropic) probes have been designed and are available commercially. These probes are used to measure the intensities of the electric field in live animals and in models of biological bodies [7], [8].

The performance of the probes, in terms of their input impedance and the electric field response as functions of the dielectric properties of the medium, has been analyzed [2]. The errors in the probe response resulting from the proximity of a material interface [3], and from direct coupling of the incident field to the lossy transmission line conductors, have also been evaluated [4]. The limitations imposed on the measurement of amplitude-modulated signals by the resistive line and the shunt capacitance of the diode, acting as a low-pass filter, have been examined theoretically [4].

The essential operating parameters of implantable probes are the directional response, dynamic range, sensitivity, noise voltage, response to modulated fields, field perturbation, and spatial response. Some of these parameters were previously determined for experimental single- and triple-axis probes [5], [6] and for a commercial single-axis probe [9]. In this paper, the sensitivity, noise, and modulation characteristics of three commercially available implantable isotropic triaxial probes are given. Information on the modulation and noise characteristics is essential for the selection of the modulation frequency in an experimental dosimetry system designed to measure the internal electric field in various models of biological bodies [10].

Experimental Materials and Methods

Description of the Probes

Three commercially available triaxial electric-field probes, namely, a Holaday IME-01, an EIT 979, and a Narda 2608, were tested. The dimensions of the probes and the dipole configurations are given in Table I. The length of the dipoles and models of the detector diodes are not available. A general description of implantable electric-field probes is presented in a recent review paper [11].

Manuscript received August 29, 1983; revised March 5, 1984. This work was supported in part by the U.S. Office of Naval Research and by the Department of Health and Welfare, Canada.

M. A. Stuchly is with the Department of Electrical Engineering, University of Ottawa, Ottawa, Ont., Canada K1N 6N5, and the Radiation Protection Bureau, Department of Health and Welfare, Ottawa, Ont., Canada K1A 0L2.

A. Kraszewski and S. S. Stuchly are with the Department of Electrical Engineering, University of Ottawa, Ottawa, Ont., Canada K1N 6N5.

0018-9294/84/0700-0526$01.00 © 1984 IEEE

TABLE I
DIMENSIONS OF THE PROBES AND DIPOLE CONFIGURATIONS

Probe Model	Effective Diameter[a] (mm)	Dipole Configuration[b]
Narda 2608	3	A
EIT 979	9	I
Holaday IME-01	17	A

[a]Refers to the sensing tip of the probe with encapsulation.
[b]Refers to the configuration of the dipoles [11]. The overall length of the probes is approximately 30 cm.

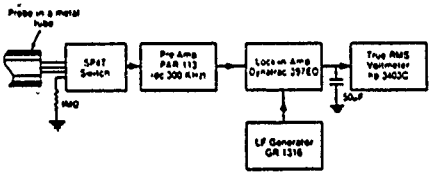

Fig. 1. Experimental arrangement for noise voltage determination.

Noise Characteristics

The noise voltage was measured in the experimental arrangement shown in Fig. 1.[1] The measurements were performed for the input of the amplifier (Pre-Amp) short circuited for a 1-MΩ resistor at the input and for three diodes of each of the probes. All the data were obtained for two bandwidth settings of the lock-in amplifier, namely, the effective noise bandwidth of 0.5 and 5.0 Hz. The test probe was placed in a metal tube to limit interference by stray electromagnetic fields.

The noise spectral density (in $\mu V/\sqrt{Hz}$) was calculated as a ratio of the rms voltage to the bandwidth.

Modulation Characteristics

The modulation characteristics were determined in the experimental arrangement shown in Fig. 2 for the EIT and Narda probes, and in that shown in Fig. 3 for the Holaday probe. In both cases, an electric field of known intensity was produced in the exposure cell. A low-frequency signal was applied to the radio frequency source as a modulation signal and as a reference signal to the lock-in amplifer. The input impedance of the preamplifier was 10 MΩ with a shunt capacitance of 15 pF. The amplitude of the modulation signal was adjusted to obtain 100 percent modulation, and the modulation frequency was varied point-by-point from 0 to 6 kHz. The output voltages (rms values) from all three dipole diodes were measured and their sums calculated. These sums were taken as measures of the square of the electric-field intensities. The measurements were repeated at three field intensities, low enough to ensure operation in the square-law range of the probe diodes; very little data variability was experienced.

Sensitivity and Linearity

The probe's sensitivity was determined in air at ten frequencies in a range from 100 MHz to 3 GHz, and in the tissue phantom materials at selected frequencies of 350, 915, and 2450 MHz. The sensitivity in air was determined by comparing the sum of voltages (rms values) from the three probe diodes to the known intensity of the electric field. Standard exposure electric fields were established in the TEM cell (Fig. 3) and in standard waveguides (WR 284 and WR 340) (Fig. 2). The TEM cell had dimensions 22.5 × 15 cm and a characteristic impedance of 50 Ω. All the sensitivity measurements were performed without amplitude modulation and with 560-Hz amplitude modulation.

Typically, the sensitivity in air was determined at various electric-field intensities ranging from 10 to 200 V/m (rms). Least-square analysis and curve fitting were then performed.

To determine the probe sensitivity in the tissue phantom material, a planar model, consisting of a slab of tissue-equivalent material having a permittivity as shown in Table II, of a cross section 0.5 × 0.5 m and a thickness of 10 cm, contained in a Styrofoam box, was used. The model was exposed to a plane wave of a known power density whose electric-field vector was parallel to the model interface. The electric-field intensity was measured with the test probe moving outside and inside the phantom material along the direction of the wave incidence. The field intensity at the air-phantom material interface was extrapolated from the measured points in free space and in the phantom. The electric-field intensity at the air-phantom interface also can be calculated from the measured incident field (without the model) as

$$E_0 = E_i \frac{2}{1 + \sqrt{\epsilon' - j\epsilon''}} \qquad (1)$$

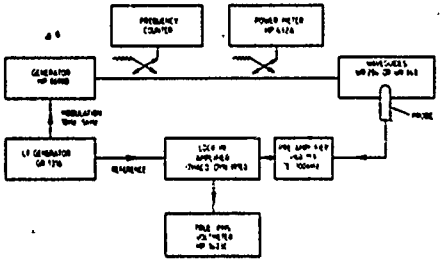

Fig. 2. Experimental arrangement for determination of the sensitivity in air and modulation characteristics at frequencies above 1000 MHz.

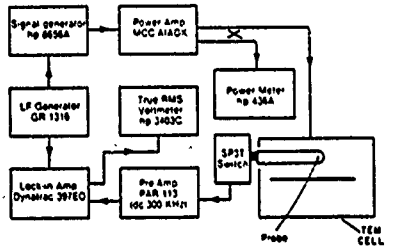

Fig. 3. Experimental arrangement for determination of the sensitivity in air and modulation characteristics at frequencies 100–1000 MHz.

[1]The Holaday IME-01 probe was used without its standard preamplifiers.

TABLE II
THE PERMITTIVITY OF THE PHANTOM MATERIAL USED IN SENSITIVITY MEASUREMENTS

Frequency (MHz)	Dielectric Constant	Conductivity (S/m)
350	53	1.4
915	52.5	1.5
2450	48	2.3

where E_0 is the electric-field intensity at the interface, E_i is the incident electric-field intensity, ϵ' is the relative dielectric constant, and ϵ'' is the loss factor of the phantom material ($\epsilon'' = \sigma/\omega\epsilon_0$).

The intensity of the electric field in the phantom material was measured by the probe at a few points along the direction of wave propagation and then extrapolated to the interface. If the voltages measured by the probe at the interface are U_M and U_A in the phantom material and air, respectively (see Fig. 7), the probe enhancement factor can be defined as

$$K = a_M/a_A \tag{2}$$

where

$$U_M = a_M E_0^2 \tag{3}$$

and

$$U_A = a_A E_0^2 \tag{4}$$

where E_0 is given by (1). The coefficients a_M and a_A are the probe sensitivities in the phantom material and air, respectively.

This calibration technique is essentially identical to that described previously by Hill [9].

EXPERIMENTAL RESULTS

Noise and Modulation Characteristics

The noise spectral density as a function of frequency for the three probes and short circuit is shown in Fig. 4. To obtain the total noise voltage, the noise for a given probe should be added to that of the short circuit (the short circuit noise was subtracted from the data shown in Fig. 4 to facilitate clear graphical presentation). The line-frequency (60 Hz) contributions, particularly the odd harmonics, are significant, and these frequencies should be avoided in selecting the modulation frequency. The noise voltage decreases with frequency particularly fast at frequencies above 1000 Hz.

Fig. 5 shows the relative probe sensitivity as a function of the modulation frequency for an amplitude-modulated electric field. This characteristic does not depend on the carrier radio frequency and is practically identical for any probe of the same model. The sensitivity changes little with the modulation frequency up to about 200 Hz, and decreases to about 0.1 at approximately 5 kHz for the EIT and Holaday probes and at 2 kHz for the Narda probe.

The modulation frequency response of the implantable electric-field probes is determined by the resistance of the leads and the shunt capacitance of the diode, as well as the shunt input capacitance of the amplifier [11]. The modulation characteristics of the three probes presented in Fig. 5 seem quite similar, suggesting that the roll-off frequency is, in each case, determined by the input amplifier rather than the

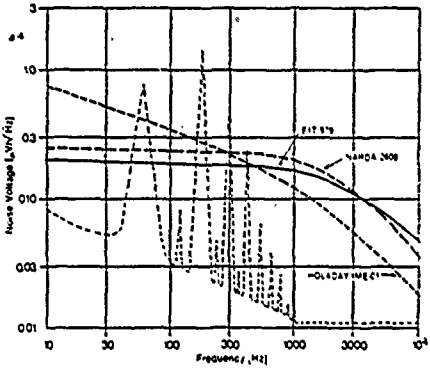

Fig. 4. Noise spectral density as a function of frequency for three probes. The fine-dashed line indicates the voltage at a power-line frequency of 60 Hz and its harmonics measured with system short-circuited; these values should be added to the values indicated for the three probes.

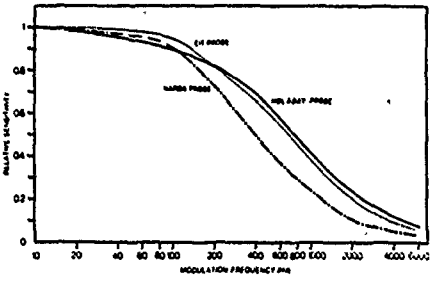

Fig. 5. Modulation characteristics—relative sensitivity as a function of amplitude modulation frequency.

properties of the probe itself. Since the electrical parameters of the high-resistance leads and the shunt capacitance of the diode are not available, this point cannot be fully clarified.

The data on the noise voltage (Fig. 4) and the modulation sensitivity can be used to select the optimum modulation frequency which offers a maximum signal-to-noise ratio. For all three probes, the optimum modulation frequency[2] lies between 400 and 800 Hz (excluding the power-line frequency harmonics). At these modulation frequencies, the signal-to-noise ratio is at least 10 dB higher (when the amplifier bandwidth is 1 Hz) than for an unmodulated RF signal.[3]

Further advantage of using amplitude-modulated radio frequency exposure fields in experimental dosimetry results from use of selective ac rather than dc amplifiers at the out-

[2]This may refer to the specific instrumentation system used (input preamplifier).

[3]The dc sensitivity of the probe was estimated by extrapolating the ac data at very low frequencies to dc, which seems to be the worst case. A dc-300 kHz preamplifier was used in both cases.

put of the probe. Not only can higher gains be realized, but troublesome zero offsets are eliminated [12].

Sensitivity in Air

Fig. 6 shows the probe sensitivity in air in μV_{rms}, normalized to 1 $(V/m)^2$, as a function of frequency for a CW electric field. The points are the averages of three to five measurements performed for various exposure fields ranging from 50 to 200 V/m (rms). Performance of the Narda probe below 200 MHz was found unsatisfactory due to the voltage induced in the high-resistance leads.

The sensitivity in air was measured in two different arrangements without an overlap. A significant and unexpected increase of the sensitivity above 1 GHz may appear to be caused by an artifact in the experimental system. However, the sensitivities at 915 MHz (in the TEM cell) are significantly higher than in the flat region (100–700 MHz). Also, the sensitivities at 2000 and 2450 MHz were determined in two different waveguides, WR 340 and WR 284, respectively, which would indicate a trend rather than an artifact.

Sensitivity in Tissue Materials

Typical data obtained in the process of the determination of the enhancement factor or the sensitivity in the tissue phantom are shown in Fig. 7 for the Holaday probe at 350 MHz. The points show the measured values and the lines the least-square fits using equations describing the electric field of the incident (short dash), reflected plus incident (long dash), and the transmitted (solid line) waves, respectively.[4] The electric-field intensity in air (the reflected plus the incident wave) E_A is described by the relationship [13]

$$E_A = E_I\left[1 + \Gamma e^{2\gamma(z-z_0)}\right] = E_I\left[1 + \frac{1-\sqrt{\epsilon'-j\epsilon''}}{1+\sqrt{\epsilon'-j\epsilon''}}\, e^{2\gamma(z-z_0)}\right] \quad (5)$$

where Γ is the reflection coefficient, γ is the propagation constant in air, z is the distance along the direction of propagation, and z_0 is the distance from the interface. The distances are measured from the point where E_I (the intensity of the incident field) is defined. The intensity of the electric field in the phantom material is equal to [13]

$$E_F = E_0 e^{-\gamma_t(z-z_0)} = E_I\,\frac{2}{1+\sqrt{\epsilon'-j\epsilon''}}\, e^{-\gamma_t(z-z_0)} \quad (6)$$

where γ_t is the propagation constant in the phantom material

$$\gamma_t = 2\pi f\sqrt{\epsilon_0\mu_0}\;\sqrt{\epsilon'-j\epsilon''}.$$

The ratio of the extrapolated values of the squares of the electric-field intensities in the phantom material and air, i.e., U_M/U_A, is the enhancement factor. The sensitivity in phantom material can be calculated then as [see (2)–(4)]

$$a_m = Ka_A'. \quad (7)$$

[4]These values were calculated from the measured incident power density and the calculated reflection coefficient at the air-phantom material interface.

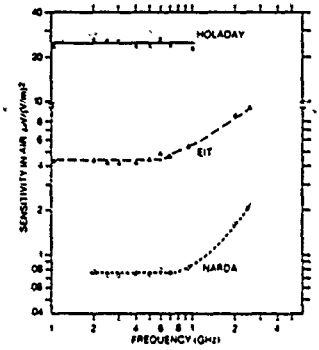

Fig. 6. Sensitivity of the probes in air in $\mu V_{rms}/(V/m)^2$ for CW radio frequency.

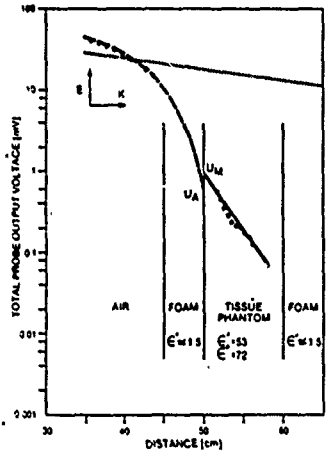

Fig. 7. An example of the experimental data obtained in the process of measuring the enhancement factor for the probe in the tissue phantom. Holaday IME-01 probe at 350 MHz. The points show the measured values. The solid line shows the least-squares fit (in the logarithmic scale) to the experimental data in the phantom. The long-dashed curve shows the fit of the curve described by (5) to the experimental data in air. The short-dashed curve shows the least-squares fit to the experimental data for the incident field (without the tissue phantom).

The enhancement factors and their standard deviations at 350, 915, and 2450 MHz are given in Table III. These results were obtained in the far-field of half-wavelength dipoles placed in the anechoic chamber. The electric field intensity at the interface was about 30 V/m (rms) at 350 and 915 MHz, and about 40 V/m (rms) at 2.45 GHz. These values were limited by the available power of the generators and the minimum distances required to obtain the far-field exposure condition.

The enhancement factor for the Narda probe is greater than for the remaining two probes, as this probe has its dipoles en-

TABLE III
THE ENHANCEMENT FACTOR (AN INCREASE IN SENSITIVITY) FOR PROBES IN THE TISSUE PHANTOM MATERIAL; SHOWN ARE THE AVERAGE AND STANDARD DEVIATIONS (SD)

Frequency	350 MHz	915 MHz	2.45 GHz
Holaday IME-01	6.1 ± 0.28	2.24 ± 0.04	–
EIT 979	7.2 ± 0.8	2.56 ± 0.07	1.56 ± 0.08
Narda 2608	9.9 ± 0.8	6.10 ± 0.31	5.22 ± 0.19

capsulated in a high-dielectric constant material. However, for all the probes studied, the enhancement factor is frequency dependent, and therefore, the calibration has to be performed at each frequency at which the probe is used. An extrapolation for closely spaced frequencies is possible, as the sensitivity variations are generally small.

Calibration of the implantable probes in tissue phantom materials is subject to several factors affecting its accuracy. These factors include the uncertainty in the intensity of the incident field, the reflections from the nearby objects resulting in standing waves, reflections from the Styrofoam box containing the phantom material, uncertainty in the dielectric properties of the phantom material, homogeneity of the phantom material, alignment of the incident electric field with the phantom material interface, the uncertainty in measuring the probe output voltage, the perturbation by the probe, and the uncertainty in the probe positioning. Some of these factors can be easily controlled, e.g., the reflections from the nearby objects have been practically eliminated as can be seen in Fig. 7 where the measured values in air very closely follow the theoretical relationship. Similarly, the reflections from the far surface of the model are very small. The dielectric properties of the tissue phantom material were measured with an uncertainty of less than 2 percent. Furthermore, they do not critically change the probe sensitivity, particularly for insulated probes [2]. The probes were positioned within ± 1 mm. The main sources of error that remained were due to the uncertainty of the incident electric field, the probe perturbation, and the uncertainty in the measured probe output. This last factor includes the directional response of the probe. Furthermore, when only limited power is available, the sensitivity of the probe only may be sufficient to obtain a few data points in the tissue material phantom. This limitation has affected the accuracy of measurements of the EIT and Narda probes at 350 MHz (Table III). The worst case calibration uncertainty was estimated to be within 10 percent (SD). The standard deviations in Table III show that the actual measurement results are well within these limits.

CONCLUSIONS

Three commercially available triaxial electric-field probes have been evaluated and calibrated for use in experimental dosimetry at frequencies of 350, 915, and 2450 MHz. On the basis of noise and amplitude modulation characteristics, we concluded that the signal-to-noise ratio increases compared to an unmodulated signal: about ten times when the radio frequency exposure field is amplitude modulated at frequencies between about 400 and 800 Hz. The power-line frequency and its harmonics should be avoided.

TABLE IV
THE APPROXIMATE MINIMUM INTENSITIES (WITH THE SIGNAL-TO-NOISE RATIO 10) OF THE ELECTRIC FIELD IN TISSUE PHANTOM MATERIAL MEASURABLE FOR 500 HZ MODULATION AND 1-HZ BANDWIDTH AMPLIFIER

Frequency	350 MHz	915 MHz	2.45 GHz
Holaday IME-01	0.25 V/m	0.45 V/m	–
EIT 979	1.3 V/m	2.1 V/m	1.7 V/m
Narda 2608	3.0 V/m	3.8 V/m	2.4 V/m

The sensitivity of the probes in air changes relatively little over a wide range of frequencies (100 MHz-1 GHz), and generally increases with frequency above 1 GHz. However, the sensitivity in the tissue phantom material depends on the exposure frequency, and the probes have to be calibrated at a specific frequency of operation. The estimated lowest intensities of the electric field in the tissue phantom material that can be measured with a signal-to-noise ratio of 10 using a 1-Hz bandwidth amplifier and 500-Hz amplitude modulation are given in Table IV. The sensitivity can be improved further by using an amplifier with a narrower bandwidth.

ACKNOWLEDGMENT

Assistance provided by G. Hartsgrove and S. Symons of the University of Ottawa is gratefully acknowledged.

REFERENCES

[1] G. S. Smith and R. W. P. King, "Electric-field probes in material media and their applications in EMC," *IEEE Trans. Electromagn. Compat.*, vol. EMC-17, pp. 206-211, 1975.
[2] G. S. Smith, "A comparison of electrically short bare and insulated probes for measuring the local radio frequency electric field in biological systems," *IEEE Trans. Biomed. Eng.*, vol. BME-22, pp. 477-483, 1975.
[3] —, "The electric-field probe near a material interface with application to the probing of fields in biological bodies," *IEEE Trans. Microwave Theory Tech.*, vol. MTT-27, pp. 270-278, 1979.
[4] —, "Analysis of miniature electric-field probes with resistive transmission lines," *IEEE Trans. Microwave Theory Tech.*, vol. MTT-29, pp. 1213-1224, 1981.
[5] H. Bassen, W. Herman, and R. Hoss, "EM probe with fiber optic telemetry system," *Microwave J.*, vol. 20, pp. 35, 38, 39, 47, 1977.
[6] H. Bassen, P. Herchenroeder, A. Cheung, and S. Neuder, "Evaluation of an implantable electric-field probe within finite simulated tissues," *Radio Sci.*, vol. 12, no. 6S, pp. 15-25, 1977.
[7] A. B. Carnie, D. A. Hill, and H. M. Assenheim, "Dosimetry for a study of effects of 2.45-GHz microwaves on mouse testis," *Bioelectromagn.*, vol. 1, pp. 325-336, 1980.
[8] T. W. Athey and R. F. Cleveland, "Power deposition in a head model exposed to hand-held UHF transceivers," presented at the 4th Annu. Meet. Bioelectromagn. Soc. (Abstract), Los Angeles, CA, June 28-July 2, 1982.
[9] D. A. Hill, "Waveguide technique for the calibration of miniature implantable electric-field probes for use in microwave-bioeffects studies," *IEEE Trans. Microwave Theory Tech.*, vol. MTT-30, pp. 92-99, 1982.
[10] S. S. Stuchly, M. Barski, B. Tam, G. Hartsgrove, and S. Symons, "A computer-based scanning system for electromagnetic dosimetry," *Rev. Sci. Instr.*, 1983, accepted for publication.
[11] H. I. Bassen and G. S. Smith, "Electrical field probes—A review," *IEEE Trans. Antennas Propagat.*, vol. AP-31, pp. 710-718, 1983.
[12] S. S. Stuchly, M. Barski, B. Tam, G. Hartsgrove, and S. Symons, "A computer-controlled experimental system for electromagnetic dosimetry," in *Proc. 5th Annu. Conf. Bioeng. Electron. Soc.* (abstract), June 12-17, 1983, Boulder, CO, p. 111.
[13] C. P. Paul and S. A. Nasar, *Introduction to Electromagnetic Fields*. New York: McGraw-Hill, 1982, 263 pp.

Maria A. Stuchly (M'71-SM'76) received the M.S.E.E. degree from the Warsaw Technical University, Warsaw, Poland, in 1962, and the Ph.D. degree from the Polish Academy of Sciences, in 1970.

Between 1962 and 1976 she was employed at the Warsaw Technical University, an Institute of the Polish Academy of Science, and at the University of Manitoba, Winnipeg, Canada. Since 1976 she has been with the Radiation Protection Bureau, Department of Health and Welfare, Canada. She is responsible for research and regulations in the area of health protection against electromagnetic fields. She is also an Adjunct Professor in the Department of Electrical Engineering, University of Ottawa, Ottawa, Ont., Canada.

Andrzej Kraszewski was born in Poznań, Poland, on April 22, 1933. He received the M.Sc. degree in electrical engineering from the Technical University of Warsaw, Warsaw, Poland, in 1958, and the D.Sc. degree in technical sciences from the Polish Academy of Sciences (PAN), Warsaw, in 1973.

In 1953 he joined the Telecommunication Institute, Warsaw, Poland, in the research and development of microwave components and systems. In 1963 he joined UNIPAN Scientific Instruments, a subsidiary of the Polish Academy of Sciences, as the Head of the Microwave Laboratory. In 1972 he became the Manager of the Microwave Department of WILMER Instruments and Measurements, a subsidiary of the Polish Academy of Sciences in Warsaw, where he co-developed microwave instruments for moisture content measurements and control. Since November 1980 he has been a Visiting Professor at the University of Ottawa, Ottawa, Ont. Canada, where he is engaged in the research of interactions between dielectric and electromagnetic fields. He is the author of several books on microwave theory and techniques, has published more than 80 technical papers on the subject, and holds 18 patents.

Dr. Kraszewski is a member of the International Microwave Power Institute, the Polish Electricians Association, and is on the Editorial Board of the *Journal of Microwave Power*. He received several professional awards, among them the State Prize in Science, in 1980.

Stanislaw S. Stuchly (M'70-SM'72) was born in Lwow, Poland, on November 20, 1931. He received the B.Sc. degree from the Technical University, Gliwice, Poland, the M.Sc. degree from Warsaw Technical University, both in electrical engineering, in 1953 and 1958, respectively, and the Ph.D. degree from the Polish Academy of Sciences, Warsaw, Poland, in 1968.

From 1953 to 1959 he was a Research Engineer at the Industrial Institute for Telecommunications, Warsaw, Poland, engaged in research in the field of radar and microwave theory and techniques. From 1959 to 1963 he was with the Warsaw Technical University as an Assistant Professor working in the field of microwave measurements. In 1963 he joined UNIPAN–Scientific Instruments, Subsidiary of the Polish Academy of Sciences–as a Manager of the Microwave Instruments Division. In 1970 he immigrated to Canada. From 1970 to 1976 he was with the University of Manitoba, Winnipeg, Canada, as an Associate Professor in the Departments of Agricultural Engineering and Electrical Engineering. Since 1977 he has been with the Department of Electrical Engineering, University of Ottawa, Ottawa, Ont., Canada, where he is presently a Professor and teaches courses and carries out research in the field of microwave theory and techniques, as well as digital instrumentation and applications of computers. He is also a nonresident Professor at Carleton University, Ottawa, Canada. He is the author of over 80 scientific papers in the field of microwave theory and techniques, as well as analog and digital instrumentation. He holds 18 patents.

URSI Florida Aug 27-30 1984

Rol(05)

7.2 DISTRIBUTION OF RADIOFREQUENCY ENERGY IN A MODEL OF MAN - EXPERIMENTAL RESULTS

M. Stuchly,* A. Kraszewski, S. Stuchly
G. Hartsgrove
Department of Electrical Engineering
University of Ottawa, Ottawa, Ontario,
K1N 6N5, Canada
*Radiation Protection Bureau, Health and Welfare Canada

Spatial distribution of the electric field inside bodies exposed to radiofrequency (RF) fields and the specific absorption rate (SAR) are important factors in quantifying biological responses. A computer-controlled system and implantable triaxial electric field probes were used to experimentally determine the SAR distribution inside a full scale model of man. The model having homogeneous electrical properties was exposed to a plane wave at 350 MHz with the electric field vector parallel to the body axis, and with the wave propagation vector parallel to the body axis - propagation from head to toe. The SAR was measured with an estimated uncertainty of ± 1 db. The reliability and accuracy of our experimental method was verified using simple geometrical bodies such a slabs, spheres and cylinders, for which theoretical SAR distributions are available. Our experimental data was compared with the values obtained numerically for a block model of man, and with the experimental values obtained thermographically at 450 MHz. Significant differences in the values of the local SAR were noted between our data and the theoretical values (block model) for both polarizations investigated. A good agreement with the thermographic results was observed.

Our results clearly indicate the significance of obtaining the SAR distribution in a reliable manner under realistic conditions. Furthermore, the method developed is also suitable for measuring the SAR distribution in anatomically realistic (bones, internal organs) models under practically any exposure conditions.

Exposure of Human Models in the Near and Far Field—A Comparison

MARIA A. STUCHLY, SENIOR MEMBER, IEEE, ANDRZEJ KRASZEWSKI, AND STANISLAW S. STUCHLY, SENIOR MEMBER, IEEE

Abstract—The specific absorption rate (SAR) was measured in over 650 locations in a full-scale model of man exposed in the far and near field of antennas at 350 and 915 MHz. The whole-body average, the body-parts average, and the distributions of the SAR's are compared for three wave polarizations for the far and the near-field exposures. Effects on the energy deposition of the antenna type, gain, and location in the near field are discussed.

I. Introduction

BIOLOGICAL effects and potential health hazards of radio-frequency (RF) electromagnetic waves have been the subject of continuing investigations since the Second World War and at times also a subject of controversies. To quantify the exposure conditions and the resulting responses for various biological species, the specific absorption rate (SAR) is used. The SAR is defined as the rate at which RF energy is imparted to the body [1]. It is well recognized that both the whole-body average SAR, as well as the spatial SAR distribution, are important parameters affecting biological responses [2].

In recent years there has been a widespread and growing use of portable and mobile RF devices. The user of these devices is exposed to RF radiation in the near field of the antenna. However, recommendations on RF exposure limits are based on the experimental data for the far-field exposures and are usually formulated in terms of the far-field parameters [3], [4]. Only general guidance regarding the SAR is given for the near-field exposures [3], [4]. Available data on the distribution of the SAR in humans or their models exposed in the near field are very limited [5]. Most of the analytical and experimental data reported deal with simple models such as a slab [6] or a spheroid [7]–[9]. A block model of man exposed to a dipole was also analyzed [10]. Comparisons of our experimental data to the calculated SAR values are the subject of separate publications in preparation. A considerable amount of data is available on average SAR's for both the far- and near-field conditions [11], [12].

In this paper we compare our experimental results of the SAR distribution in a full-scale model of man exposed in the far and the near field at frequencies of 350 and 915 MHz. The whole-body average and the body-part average SAR's are also compared, using as a term of reference the output power of the antenna which results in the same SAR as 1 mW/cm^2 in the far field. As three different types of antennas have been investigated, the data presented may be of assistance in determining exposure limits for portable transmitters. In particular, one of the antennas, namely a resonant dipole with a reflector, may be considered as representing the worst-cause conditions, as the energy couples very well to the body.

The exposure frequency of 350 MHz was selected because of the previously reported greater than the whole-body average SAR in the head in the far field [13]. The frequency of 915 MHz is frequently used in various industrial, scientific, and medical (ISM) applications. Both frequencies selected are close to frequencies employed in portable and mobile transmitters.

II. Measurement Method

A computer-controlled scanning system was used to position an electric field probe in a full-scale model of man. The system is described in detail elsewhere [14], so only a brief description is given here. The human model and the scanning system are placed in an anechoic chamber. An optical fiber link connects the electric field probe and the amplifier with the remaining electronic circuitry and a minicomputer located outside the chamber. The use of the optical link greatly reduces RF interference.

The model of man used at 350 MHz was made of low-density Styrofoam (dielectric constant approximately 1.05) filled with a semiliquid mixture of the following properties, the dielectric constant $\epsilon' = 38$ and the conductivity $\sigma = 0.95$ S/m. The geometrical shape of the model closely approximated an anatomically correct average man with a height of 175 cm and a weight of 70 kg. A plastic model used in ionizing radiation dosimetry (manufactured by Anderson Research Laboratories Inc., Stamford, CT) was employed to prepare our model. The method of the model preparation is illustrated elsewhere [5]. At 915 MHz a thin shell (1.5 mm) model made of thermoplastic (dielectric constant approximately 3) was used. This model was easier to prepare than the Styrofoam model and more durable. The mold was prepared by wrapping thermoplastic material around the plastic model using a heat gun. The RF model was filled with a semiliquid material with $\epsilon' = 37$ and $\sigma = 1.17$ S/m. The electrical properties of the phan-

Manuscript received September 12, 1984; revised March 7, 1985. This work was supported by the U.S. Office of Naval Research, the Department of Health and Welfare, Canada, and the Natural Sciences and Engineering Research Council of Canada.

M. A. Stuchly is with the Radiation Protection Bureau, Department of Health and Welfare, Ottawa, Ont., Canada K1A 0L2.

A. Kraszewski and S. S. Stuchly are with the Department of Electrical Engineering, University of Ottawa, Ottawa, Ont., Canada K1N 6N5.

0018-9294/85/0800-0609$01.00 © 1985 IEEE

tom material filling the models were selected to approximate those of the "average tissue," i.e., 2/3 of the muscle properties [11]. Both models were placed horizontally and were supported from the bottom on low-density Styrofoam blocks.

The electric field intensity was measured by an implantable triaxial electric field probe: an EIT, model 979. The probe was fully characterized and calibrated prior to the experiments [15], and its calibration was spot-checked during the course of the experiment. The SAR was calculated from the measured electric field strength (SAR = $E^2\,\sigma/\rho$, E is the rms value of the electric field strength σ is the tissue conductivity, σ is the tissue density, ρ = 1 g/cm^3). The uncertainty in the SAR was estimated at ± dB, and was mostly due in the calibration uncertainty of the probe [15]. The measurement repeatability was within ±0.5 dB. For each exposure condition investigated, the SAR was measured in over 650 locations within one-half of the model.

For exposures in the far field, the human model was placed at a distance sufficiently large to ensure the far-field conditions. The distances were greater than 1 and 0.5 m, 350 and 915 MHz, respectively. A complete map of the power density at the plane of the model of man facing the radiation source was obtained for a given placement of the source without the model in place. The correction for the nonplanar wave front (amplitude only) was incorporated in the computer program that normalized the measured SAR values to 1 mW/cm^2 of the incident power.

Antennas investigated in the near field included: a resonant (half-wavelength) dipole, a resonant dipole with a metal reflector, and a resonant slot. The antennas were matched to a 50 Ω transmission line at the test frequencies (with the model of man in the test position). The power reflected from the antennas did not exceed 5 percent of the incident power in the worse case. The slot antenna at 350 MHz was 42.8 cm long (half wavelength), 3.0 cm wide, and a metal reflector was at a distance of 16.2 cm.

At both frequencies for the E- and H-polarizations the antenna axis was parallel to the model long axis. At 350 MHz the antenna center was located at 103, 137, and 156.6 cm from the feet base for both dipoles, and at 85 cm for the slot. In the h-polarization the dipole was located along the body vertical axis, 14 cm above the head. At 915 MHz the antenna center was located 137 cm from the feet base. The various positions were selected either to represent typical practical exposure situations (137 cm for the dipoles—portable transmitters, 85 cm for the slot—a leaky cabinet) or test effects of the vertical antenna placement.

The model of the human body was exposed to RF radiation incident from the back for the far- and the near-field exposures. Since the model was homogeneous the geometrical differences between the front and the back were relatively small.

III. Average SAR

The whole-body average SAR was calculated by a summation of the locally measured values, incorporating the volume weighing factor following the prescribed rule [16]. The estimated uncertainty in the whole-body average SAR was ± 25 percent. Tables I and II show comparisons between the far- and the near-field exposures at 350 and 915 MHz, respectively. An input power to the antenna that results in the same whole-body average SAR as exposure to 1 mW/cm^2 in the far field at the same frequency is given for various antennas in the near field. At 350 MHz (Table I) the measured value of the SAR in the far-field for the E-polarization is very close to that given in the handbook [11], as well as that calculated for the block model [17]. However, for the H-polarization the difference between the experimentally determined SAR and the handbook [11] value is greater than the measurement uncertainty. Similarly, at 915 MHz (Table II) both values for the E-polarization are very close (within 10 percent), but a larger difference occurs for the H-polarization. An exact explanation of the existing discrepancies is not available at present. Two observations may explain this lack of agreement. Theoretical data given in the handbook [11] for frequencies above 200 MHz for the H-polarization are based on an analysis of a greatly simplified model, namely an infinite cylinder [18]. Despite the fact that these calculations correlate well with calculations for spheroidal models at frequencies below resonance [19], it appears that the differences in shapes between the model and the actual human body are important for the H-polarization at these frequencies. Previous measurements of the SAR of human subjects showed the differences of a factor from 2.7 to 3.9 from the calculated values for a spheroidal model (in that case for the E-polarization) [20]. Errors in the average SAR calculations from our measured data cannot be excluded, but do not appear likely to be greater than the estimated 25 percent, as the procedure was verified for lossy dielectric spheres and cylinders.

The whole-body average SAR depends on the antenna type (Table I), and for the same antenna type is nearly proportional to the antenna gain, as illustrated for the dipole and the dipole with a reflector. As the reflector doubles the gain, the input power is reduced by a factor of two. However, a slot, which has a gain of 4.9, is much less efficient in depositing the energy into the model. The range of the input power given in Table I for the dipole in the E-polarization results from variations in the vertical placement of the dipole. Because of the body curvature (e.g., neck) the distance between the antenna surface and the body varies, even though the antenna axis remains at a constant distance of 8 cm. For the dipole with a reflector at 350 MHz, practically all the power delivered to the antenna is absorbed in the model, which is not surprising in view of the good matching of the dipole, small distance from the model (d/λ = 0.09) and large size of the reflector. This configuration can be considered as the worst-case exposure condition, as in practical situations, e.g., for portable transmitters, the antennas are designed to radiate power out. The wave polarization does not seem to play a very significant role in terms of the equivalent input power in the near field for the exposure conditions used in our experiments.

TABLE I
THE INPUT POWER TO THE ANTENNA IN THE NEAR FIELD FOR THE WHOLE-BODY AVERAGE SAR EQUAL TO THAT FROM EXPOSURE TO A PLANE WAVE AT 350 MHz AND 1 mW/cm² (SHOWN IN BRACKETS)

[illegible]	[illegible]			[illegible]	
Antenna	Dipole	Dipole with a reflector	Slot	Dipole	Dipole with a reflector
[illegible]	[illegible]	[illegible]	[illegible]	[illegible]	[illegible]
Input power (W)	[illegible]	[illegible]	[illegible]	[illegible]	[illegible]

TABLE II
THE INPUT POWER TO THE ANTENNA IN THE NEAR FIELD FOR THE WHOLE-BODY AVERAGE SAR EQUAL TO THAT FROM EXPOSURE TO A PLANE WAVE AT 915 MHz of 1 mW/cm² (SHOWN IN BRACKETS)

Polarization	[illegible]	[illegible]
Antenna	Dipole with a reflector	Dipole with a reflector
Input power (W)	[illegible]	[illegible]

TABLE III
THE INPUT TO THE ANTENNA IN THE NEAR FIELD FOR THE AVERAGE SAR IN THE HEAD EQUAL TO THAT FROM EXPOSURE TO A PLANE WAVE OF 1 mW/cm² (SHOWN IN BRACKETS)

Frequency	350 MHz				915 MHz	
[illegible]	[illegible]		[illegible]		[illegible]	[illegible]
	[illegible]	[illegible]	[illegible]	[illegible]	[illegible]	
[illegible]	[illegible]	[illegible]	[illegible]	[illegible]	[illegible]	[illegible]

The SAR measured by us in the head at 350 MHz and the *E*-polarization for the far-field exposure conditions (Table III) is in good agreement with the value calculated for the block model [13]. In the near field, as for the whole-body average, the greater the antenna gain, for a given type of antenna, the smaller input power to the antenna results in the same SAR as 1 mW/cm² of the incident power density in the far field. It can also be noted (Table III) that about three and two times less input power to the antenna than for the whole-body average SAR is needed to obtain the same SAR as in the far field for the *E*-polarization at 350 and 915 MHz, respectively. For the dipole with a reflector at 350 MHz between 0.9 and 2.1 W of input power deposit the same average SAR in the head as 1 mW/cm² for the plane wave.

IV. SPATIAL DISTRIBUTION OF SAR

Both far-field and near-field exposures at the two frequencies investigated produced highly nonuniform spatial patterns of the SAR's. For both exposure conditions, the SAR decreases exponentially in the direction of the wave propagation for the body parts whose radii of curvature are comparable to the wavelength, i.e., in the torso at 350 MHz and in all major body parts at 915 MHz. Furthermore, the attenuation coefficient is equal to that of a wave propagation in a semiinfinite half-space having the same dielectric properties as the model of the human body.

Table IV shows the input power for various antennas in the near field that results in the same maximum SAR at the body surface as for plane waves of 1 mW/cm² at 350 and 915 MHz. It is evident that the SAR at the surface

TABLE IV
THE INPUT TO THE ANTENNA IN THE NEAR FIELD FOR THE SAR ON THE BODY SURFACE EQUAL TO THAT FROM EXPOSURE TO A PLANE WAVE OF 1 mW/cm² (SHOWN IN BRACKETS)

Frequency	350 MHz						915 MHz	
Polarization	E (SAR = 0.22 W/kg)			H (SAR = 0.28 W/kg)		E (SAR = 0.70 W/kg)	E (SAR = 0.53 W/kg)	H (SAR = 0.48 W/kg)
Antenna	Dipole	Dipole with a reflector	Slot	Dipole	Dipole with a reflector	Dipole	Dipole with a reflector	Dipole with a reflector
Input power (W)	0.2	0.08	1.1	0.27	0.11	2.0	2.35	0.20	0.79

can be as high as that for an incident power of 1 mW/cm² (in the far field) for an input power to the antennas of order of 0.1 to 0.2 W, if the antennas are placed close to the body.

The spatial distribution of the SAR in the whole body is illustrated in Figs. 1–6. The experimental results are presented in three different ways: first, as local SAR values measured at locations shown in the midsection of the body (Figs. 1 and 2), second, as the averages of the local values along the direction of wave propagation between the body surfaces in a volume corresponding to the diameter of the measuring probe, i.e., 0.9 cm (Figs. 3 and 4), and third, as the averages of the local values measured in various body cross sections perpendicular to the long body axis (Figs. 5 and 6).

Figs. 1 and 2 show local values of the SAR in the body midsection at 915 MHz for the *E*- and the *H*-polarization, respectively. Exposures in the near field result in very little energy deposition in the lower torso and the legs, which is understandable in view of the location of the antennas in the upper torso region. In the *E*-polarization the maximum SAR's for the far- and the near-field exposures are at the same site (Fig.1), but not so for the *H*-polarization, for which the maximum in the near field is on the antenna axis (Fig. 2).

Figs. 3 and 4 show the far- and near-field data at 350 MHz for the *E*- and *H*-polarizations, respectively. The SAR values are averaged along the direction of the wave propagation between the body surfaces in a volume corresponding to the measuring probe diameter (0.9 cm). Some energy is deposited in the lower torso and the legs in the near field, but relatively little as compared to the far field. One interesting and important feature can be seen in Fig. 3, namely that the maximum SAR occurs in the neck for both the far and the near field for the *E* polarization. This is in marked contrast with other polarizations and at frequency of 915 MHz, where the maximum SAR occurs at the antenna axis for the near-field exposures.

Fig. 5 shows the SAR averaged over the tissue cross sections perpendicular to the long body axis at 350 MHz for two polarizations. The shift of the SAR maximum from the dipole axis to the same position as for the far field is clearly visible for the dipole in the near field and the *E*-polarization even when SAR values are averaged over body cross sections. Similarly as with the local SAR's, the concentration of the energy deposited in the vicinity of the antenna in the near field is evident.

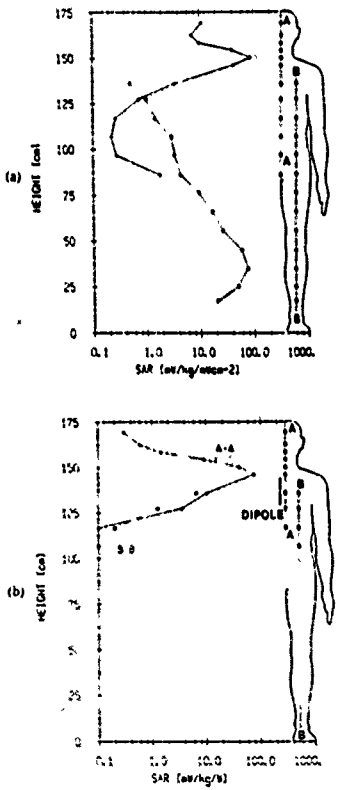

Fig. 1. The specific absorption rate (SAR) (local values) along the *A*-*A* axis (solid lines) and *B*-*B* axis (dashed lines), located in the body midsection, *E*-polarization, $f = 915$ MHz. (a) The far-field exposure and (b) the near field exposure to a resonant dipole with a reflector.

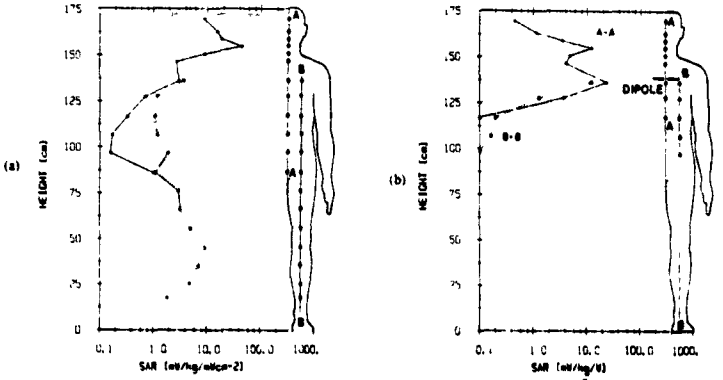

Fig. 2 The specific absorption rate (SAR) (local values) along the *A*–*A* axis (solid lines), and *B*–*B* axis (dashed lines) located in the body midsection, *H* polarization, f = 915 MHz. (a) The far-field exposure. (b) The near-field exposure to a resonant dipole with a reflector

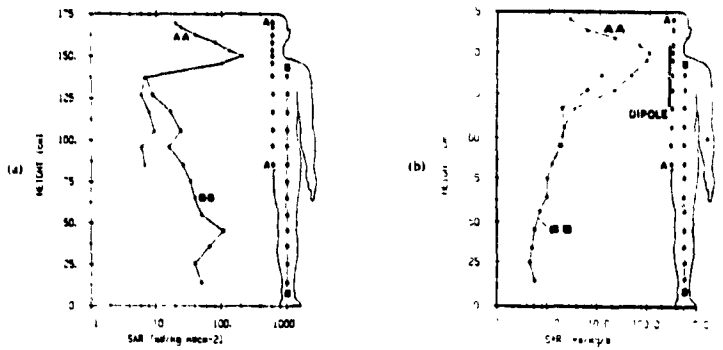

Fig. 3 The specific absorption rate (SAR) averaged over a cylinder 0.9 cm in diameter between the body surfaces in the locations shown. *E*-polarization, f = 350 MHz (a) Far-field exposure (b) Near-field exposure to a resonant dipole

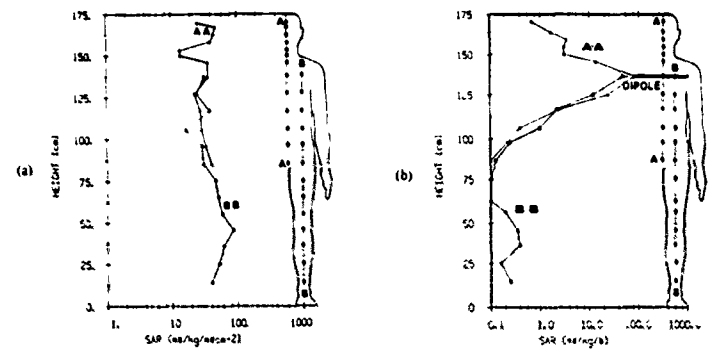

Fig. 4. The specific absorption rate (SAR) averaged over a cylinder 0.9 cm in diameter between the body surfaces in the locations shown, *H* polarization, f = 350 MHz. (a) Far-field exposure, (b) Near field exposure to a resonant dipole.

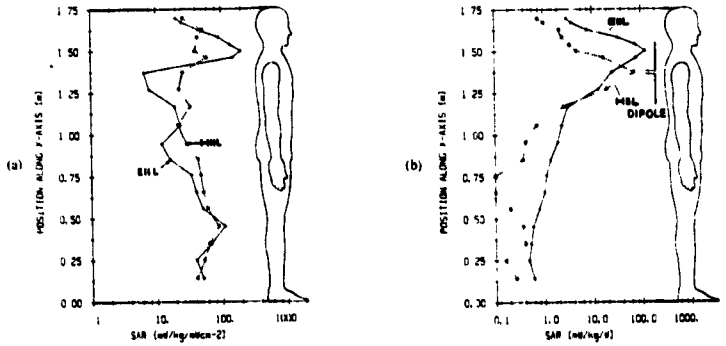

Fig 5 The specific absorption rate (SAR) averaged over tissue layers perpendicular to the body axis for two polarizations, E polarization (EHL)—solid lines, and H-polarization (HHL)—dashed lines, f = 350 MHz. (a) Far-field exposure 1 mW/cm^2 (b) Near-field exposure, a resonant dipole placed 8 cm from the body surface and 137 cm from the feet base

A comparison at 915 MHz for the E-polarization is given in Fig. 6. Here the localized SAR pattern in the near field is even more pronounced. The maximum SAR for the near-field exposure is near the antenna axis.

An interesting comparison between the near- and the far-field exposures is provided in Fig.7 which shows the spatial distribution of the SAR in the neck. The local values in the midsection are shown. In the far field the maximum local SAR occurs close to the center of the neck. However, in the near field the maximum SAR (above 500 mW/kg·W) is at the neck surface upon which the wave is incident, and only a small increase in the SAR (SAR = 55 mW/kg·W) occurs in the neck center. The result obtained in the far field is in agreement with the experimental data at 450 MHz obtained using the thermographic technique [21]

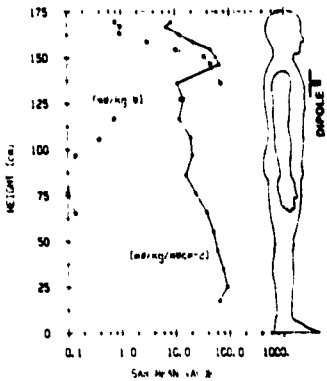

Fig 6 The specific absorption rate (SAR) averaged over tissue layers perpendicular to the body axis, E polarization, f = 915 MHz, solid line far-field exposure, dashed line near-field exposure to a dipole with a reflector, 5 cm from the body surface 137 cm from the feet base

V Conclusions

Experimentally obtained data on the rates of energy deposition in a model of the human body exposed to RF fields at 350 and 915 MHz have been compared for near- and the far-field exposures. Comparisons have been made in terms of the output power of the antenna in the near field required to obtain the same average SAR's for the whole body and body parts as when exposed to a plane wave of 1 mW/cm^2 in the far field. Spatial distributions of the SAR have also been compared.

The antenna output powers for a given whole-body and body-parts average SAR's depend on the antenna type (dipole versus slot), antenna gain, antenna distance from the body surface, and to a lesser degree, on the antenna location with respect to the body and the wave polarization.

At the two frequencies investigated, 350 and 915 MHz, the SAR decreases exponentially in the direction of wave propagation in all body parts whose radii of curvature are comparable to the wavelength. In some typical configurations relatively little input power to the antenna in the near field is needed (only 0.2 W), to obtain the same surface as for a plane wave of 1 mW/cm^2 in the far field

The spatial distributions of the SAR resulting from the near field and the far field are very similar in the vicinity of the antenna (for the near-field exposure). Predictably, in the near-field there is relatively little energy deposition in the regions made from the antenna.

The internally located maxima of the SAR for our model are usually somewhat lower for the near-field exposures than for the far-field exposures resulting in the same whole-body average SAR.

The comparison data presented can also be analyzed from the standard setting point of view and in evaluating

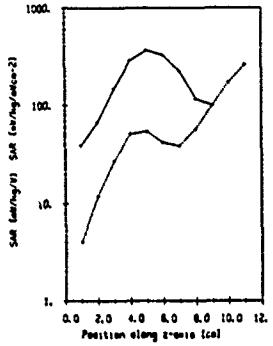

Fig. 7. The specific absorption rate (SAR), local values in the mid-section of the neck along a line perpendicular to the body axis, 350 MHz, *E*-polarization; solid line: far-field exposure (SAR scale in mW/kg•mW in cm^{-2}); dashed line: near field exposure to a dipole 8 cm from the body surface, 137 cm from the feet base (SAR scale in mW/kg•W).

potential hazards of exposure to portable transmitters. For instance, if the far-field exposure limits of 1.2 and 3.0 mW/cm^2 at 350 and 915, respectively, are considered [3], typically, 6 and 24 W of the power to the antenna (a dipole) will produce the same whole-body average SAR's with the antenna about 5–8 cm from the body surface. Greater output powers of the antennas in the near field would be required to exceed the condition of 0.4 W/kg for the whole-body average SAR [3]. However, for the near-field exposures energy is deposited at a greater rate in the head. For a dipole in the near field at 350 MHz the output power of about 2 W deposits the same average SAR in the head as exposure to 1.2 mW/cm^2 in the far field. About 8 W of the output power in the near field would be required to exceed the average of 0.4 W/kg in the head.

For the near-field exposures high rates of energy deposition on the body surface occur. For instance, at 350 MHz approximately 0.25 W of the output power from the dipole deposits the same SAR at the body surface as a plane wave of a power density of 1.2 mW/cm^2. Furthermore, the recommended limit for the spatial peak SAR value of 8 W/kg [3] is exceeded for a dipole at 350 MHz at a distance of 8 cm from the body surface for an output power of less than 8 W.

Resonant dipoles with reflectors can be considered as the worst-case representation of many practical near-field radiators, and their SAR data may be used for estimating potential hazards of exposure when the far-field standard, e.g., [3], is used as a reference.

The results reported here are for a homogeneous model of the human body. Considerable differences in the spatial distribution of the SAR are to be expected when nonhomogeneous properties of the body tissue are included. Even simple body tissue layering (skin-fat-muscle) was shown to increase local SAR's under some conditions [22].

Acknowledgment

The authors gratefully acknowledge the contribution of G. Hartsgrove, D. Adamski, and L. Bonnet from the University of Ottawa, and the editorial help of J. Smith of the Department of Health and Welfare, Canada.

References

[1] "Radiofrequency electromagnetic fields: Properties, quantities and units, biophysical interactions and measurements," NCRP Rep. 67, 1981.

[2] M. A. Stuchly, "Interaction of radiofrequency and microwave radiation with living systems. A review of mechanisms," *Radiat. Environ. Biophys.*, vol. 16, pp. 1–14, 1979.

[3] "Safety levels with respect to human exposure to radio frequency electromagnetic fields, 300 kHz to 100 GHz," IEEE, ANSI C95.1-1982.

[4] "Interim guidelines on limits of exposure to radiofrequency electromagnetic fields in the frequency range from 100 kHz to 300 GHz," *Health Phys.*, vol. 46, pp. 975–984, 1984.

[5] A. Kraszewski, M. A. Stuchly, S. S. Stuchly, G. Hartsgrove, and D. Adamski, "Specific absorption rate distribution in a full-scale model of man at 350 MHz," *IEEE Trans. Microwave Theory Tech.*, vol. MTT-32, pp. 779–782, 1984.

[6] I. Chatterjee, M. J. Hagmann, and O. P. Gandhi, "Electromagnetic absorption in a multilayered slab model of tissue under near-field exposure conditions," *Bioelectromagnet.*, vol. 1, pp. 379–388, 1980.

[7] M. F. Iskander, P. B. Barber, C. H. Durney, and H. Massoudi, "Irradiation of prolate spheroidal models of humans in the near field of a short electric dipole," *IEEE Trans. Microwave Theory Tech.*, vol. MTT-28, pp. 801–807, 1980.

[8] A. Lakhtakia, M. F. Iskander, C. H. Durney, and H. Massoudi, "Near field absorption in prolate spheroidal models of humans exposed to a small loop antenna of arbitrary orientation," *IEEE Trans. Microwave Theory Tech.*, vol. MTT-29, pp. 588–594, 1981.

[9] —— "Absorption characteristics of prolate spheroidal models exposed to the near field of electrically small apertures," *IEEE Trans. Biomed. Eng.*, vol. BME-29, pp. 569–576, 1982.

[10] R. J. Spiegel, "The thermal response of a human in the near-zone of a resonant thin-wire antenna," *IEEE Trans. Microwave Theory Tech.*, vol. MTT-30, pp. 177–183, 1982.

[11] C. H. Durney, C. C. Johnson, P. W. Barber, H. Massoudi, M. F. Iskander, J. L. Lords, D. K. Ryser, S. J. Allen, and J. C. Mitchell, "Radiofrequency radiation dosimetry handbook," USAF School of Aerosp. Medicine, Brooks Air Force Base, TX, 1978, 2nd ed., Rep. SAM-TR-78-22.

[12] C. H. Durney, M. F. Iskander, H. Massoudi, S. J. Allen, and J. C. Mitchell, "Radiofrequency radiation dosimetry handbook," USAF School of Aerosp. Medicine, Brooks Air Force Base, TX, 1980, 3rd ed., Rep. SAM-TR-80-32.

[13] M. J. Hagmann, O. P. Gandhi, J. A. D'Andrea, and I. Chatterjee, "Head resonance: Numerical solutions and experimental results," *IEEE Trans. Microwave Theory Tech.*, vol. MTT-27, pp. 809–813, 1979.

[14] S. S. Stuchly, M. Barski, B. Tam, G. Hartsgrove, and S. Symons, "A computer-based scanning system for electromagnetic dosimetry," *Rev. Sci. Instrum.*, vol. 54, pp. 1547–1550, 1983.

[15] M. A. Stuchly, A. Kraszewski, and S. S. Stuchly, "Implantable electric field probes—some performance characteristics," *IEEE Trans. Biomed. Eng.*, vol. BME-31, pp. 526–530, 1984.

[16] B. Ricci, *Physiological Basis of Human Performance*. Philadelphia, PA: Lea and Febiger, 1967.

[17] M. J. Hagmann, O. P. Gandhi, and C. M. Durney, "Numerical calculation of electromagnetic energy deposition for a realistic model of man," *IEEE Trans. Microwave Theory Tech.*, vol. MTT-27, pp. 804–809, 1979.

[18] C. H. Durney, "Electromagnetic dosimetry for models of humans and animals: A review of theoretical and numerical techniques," *Proc. IEEE*, vol. 68, pp. 33–39, 1980.

[19] H. Massoudi, C. H. Durney, and C. C. Johnson, "A geometrical-optics and an exact solution for internal fields in and energy absorption by a cylindrical model of man irradiated by an electromagnetic plane wave," *Radio Sci.*, vol. 14, pp. 35–42, 1979.

[20] D. A. Hill, "The effect of frequency and grounding on whole-body absorption of humans in E-polarized radiofrequency fields," *Bioelectromagnet.*, vol. 5, pp. 131–146, 1984.

[21] A. W. Guy, "Non-ionizing radiation: Dosimetry and interaction," in *Proc. ACGIH Topical Symp.*, Nov. 26-28, 1979, pp. 75-101.
[22] P. B. Barber, O. P. Gandhi, M. J. Hagmann, and I. Chatterjee, "Electromagnetic absorption in a multilayered model of man," *IEEE Trans. Biomed. Eng.*, vol. BME-26, pp. 400-404, 1979.

Maria A. Stuchly (M'71-SM'76) received the M.S.E.E., degree from the Warsaw Technical University, Warsaw, Poland, in 1962, and the Ph.D. degree from the Polish Academy of Sciences, 1970.

Between 1962 and 1976 she was employed at the Warsaw Technical University, an Institute of the Polish Academy of Science, and at the University of Manitoba, Winnipeg, Canada. Since 1976 she has been with the Radiation Protection Bureau, Department of Health and Welfare, Canada. She is responsible for research and regulations in the area of health protection against electromagnetic fields. She is also an Adjunct Professor in the Department of Electrical Engineering, University of Ottawa, Ottawa, Ont., Canada.

Andrzej Kraszewski was born in Poznań, Poland, on April 22, 1933. He received the M.Sc. degree in electrical engineering from the Technical University of Warsaw, Warsaw, Poland, in 1958, and the D.Sc. degree in technical sciences from the Polish Academy of Sciences (PAN), Warsaw, in 1973.

In 1953 he joined the Telecommunication Institute, Warsaw, Poland, in the research and development of microwave components and systems. In 1963 he joined UNIPAN Scientific Instruments, a subsidiary of the Polish Academy of Sciences, as the Head of the Microwave Laboratory. In 1972 he became the Manager of the Microwave Department of WILMER Instruments and Measurements, a subsidiary of the Polish Academy of Sciences in Warsaw, where he codeveloped microwave instruments for moisture content measurements and control. Since November 1980 he has been a Visiting Professor at the University of Ottawa, Ottawa, Ont., Canada, where he is engaged in the research of interactions between dielectric and electromagnetic fields. He is the author of several books on microwave theory and techniques, has published more than 80 technical papers on the subject, and holds 18 patents.

Dr. Kraszewski is a member of the International Microwave Power Institute, the Polish Electricians Association, and is on the Editorial Board of the *Journal of Microwave Power*. He received several professional awards, among them the State Prize in Science, in 1980.

Stanisław S. Stuchly (M'70-SM'72) was born in Lwow, Poland, on November 20, 1931. He received the B.Sc. degree from the Technical University, Gliwice, Poland, the M.Sc. degree from Warsaw Technical University, both in electrical engineering, in 1953 and 1958, respectively, and the Ph.D. degree from the Polish Academy of Sciences, Warsaw, Poland, in 1968.

From 1953 to 1959 he was a Research Engineer at the Industrial Institute for Telecommunications, Warsaw, Poland, engaged in research in the field of radar and microwave theory and techniques. From 1959 to 1963 he was with the Warsaw Technical University as an Assistant Professor working in the field of microwave measurements. In 1963 he joined UNIPAN-Scientific Instruments, Subsidiary of the Polish Academy of Sciences as a Manager of the Microwave Instruments Division. In 1970 he immigrated to Canada. From 1970 to 1976 he was with the University of Manitoba, Winnipeg, Canada, as an Associate Professor in the Departments of Agricultural Engineering and Electrical Engineering. Since 1977 he has been with the Department of Electrical Engineering, University of Ottawa, Ottawa, Ont., Canada, where he is presently a Professor and teaches courses and carries out research in the field of microwave theory and techniques, as well as digital instrumentation and applications of computers. He is also a nonresident Professor at Carleton University, Ottawa, Canada. He is the author of over 80 scientific papers in the field of microwave theory and techniques, as well as analog and digital instrumentation. He holds 18 patents.

Ref. [17]

Bioelectromagnetics 6:115–129 (1985)

Energy Deposition in a Model of Man in the Near Field

Stanislaw S. Stuchly, Andrzej Kraszewski, Maria A. Stuchly, George Hartsgrove, and Daniel Adamski

Department of Electrical Engineering, University of Ottawa, Ottawa, Ontario (S.S.S., A.K., G.H., D.A.) and Radiation Protection Bureau, Health and Welfare Canada and University of Ottawa (M.S.)

The spatial distribution of the specific absorption rate (SAR) was measured in a full-scale model of man using implantable electric field probes. The model was exposed in the near-field of linear and aperture antennas at 350 MHz. Effects of the wave polarization, antenna position and antenna gain on the SAR distribution and the average SAR in the whole-body and body parts are reported.

Key words: radiofrequency, dosimetry, near-field exposure, SAR distribution

INTRODUCTION

The average specific absorption rate (SAR) has been used in quantifying biological effects of radiofrequency (RF) fields and formulating exposure standards [Cahill, 1983; ANSI, 1982]. Furthermore, it has also been recognized that the spatial distribution of the SAR inside an exposed animal or human being plays an essential role in resulting biological responses. Considerable amount of data has been accumulated on the average SAR obtained through calculations and measurements, particularly in the far-field of antennas [Durney, 1980; Stuchly, 1983; Stuchly and Stuchly, 1985]. However, relatively little information is available on the SAR distribution in the near-field of antennas, even though such exposures are common in practice due to a widespread use of portable and mobile RF transmitters.

Theoretical analysis was previously performed for spheroidal models of man exposed in the near-field of a short dipole (Iskander et al, 1980), a small loop (Lakhtakia et al, 1981), and a small aperture (Lakhtakia et al, 1982). The limitations of these studies in terms of realistic exposures are apparent because of the simplified model and electrically small antennas used. A block model of a man exposed in the near field of a slot antenna [Chatterjee et al, 1980] and monopole and dipole antennas [Spiegel 1982] were also analyzed numerically. In these cases the SARs were calculated with relatively large tissue volumes, typically 300 cm^3.

An alternative approach, which is also most likely to provide accurate data on the spatial distribution of the SAR, employs implantable electric field probes and full-

Received for review July 9, 1984; revision received December 18, 1984.

Address reprint requests to Dr. S.S. Stuchly, Department of Electrical Engineering, University of Ottawa, 770 King Edward Avenue, Ottawa, Ont. K1N 6N5, Canada.

scale realistic models of man [Athey and Cleveland, 1982]. Acquisition of information on the spatial distribution of the SAR in such models is greatly facilitated when an automated scanning system under computer control is used [Stuchly et al, 1983b].

For several reasons, the implantable probe technique was selected rather than the previously developed and successfully used thermographic technique [Guy, 1971; Guy et al, 1976]. One of the main limitations of the thermographic techniques is that high intensities of the exposure field are required, so that a thermographic scan can be taken no later than about 20 s after the commencement of the irradiation. This difficulty is particularly pronounced for near-field exposures and for full-scale models. Furthermore, the probe technique with advanced electronic circuitry provided a wide dynamic range of over 20 dB and an excellent spatial resolution. The thermographic technique, on the other hand, is much faster and provides a complete picture of the SAR distribution in a selected cross-section.

In this paper, we present data on the spatial distribution of the SAR in a full-scale homogeneous model of man exposed in the near-field of linear and aperture antennas at 350 MHz. The frequency of 350 MHz was selected because head resonance at this frequency has been previously reported [Hagmann et al, 1979], and because portable and mobile transmitters are operated at or near this frequency. The antennas selected are typical for practical exposure situations, i.e., a resonant dipole and a resonant dipole with reflector as representatives of linear antennas of radio transmitters, and a resonant slot with a reflector as a representation of leaky housings of RF generators.

MATERIALS AND METHODS

Experimental System

A scanning system consisting of a mechanical structure for supporting and positioning of an electric field probe and a computer system for control of the experiment, data acquisition, storage, display and recording is described in detail elsewhere [Stuchly et al, 1983b]. In brief, the probe can be positioned at any selected location within a volume of 2 m × 0.5 m × 0.5 m with an uncertainty of 0.05 mm. The scanning system with the probe are placed in an anechoic chamber to limit reflections of RF energy. The probe output is fed directly to an amplifier which is connected through an optical fiber link to the remaining electronic circuitry outside the chamber.

To measure the electric field intensity, an implantable triaxial probe EFT 979 was used. The probe had a diameter of 0.9 cm and a sensitivity in the tissue phantom material of 3 $\mu V/V^2/m^2$) [Stuchly et al, 1984]. The probe was calibrated with an estimated uncertainty of $\pm$ 1 dB. With the electronic circuitry utilized it was possible to measure the electric fields equivalent to SARs greater than 0.2 mW/kg with a signal-to-noise ratio of 5.

Model of Man

A full-scale model of an anatomically proportional average man (1.75 m, 70 kg) was constructed from low-density Styrofoam sheets 2.5-cm thick, which were glued together. The mold was positioned horizontally and partly open in the torso area, and holes large enough for inserting the probe were drilled in other locations. The mold was filled with a low-viscosity, water-based mixture having electrical

properties of the average tissue e.g. equal to 2/3 those of muscle. At 350 MHz the dielectric constant was 38, and the conductivity 0.95 S/m.

Antennas and Exposure Conditions

Two linear antennas tested were a resonant (half-wavelength) thin dipole and a resonant dipole with a reflector. The lengths of the dipoles were adjusted to ensure impedance matching to the 50-Ω feeder, while the model of man was placed at the test position close to the antennas.

A resonant slot with a reflector was used as an aperture antenna. All the antennas were well matched (VSWR $\leq$ 1.2). Dimensions and essential electrical parameters of the antennas are summarized in Table I.

The antennas were placed 8 cm from the model surface at various locations close to the head and the torso for the two polarizations investigated, i.e., the E polarization (the electric field parallel to the vertical body axis) and the H polarization. The distance of 8 cm seems to be realistic for typical practical situations of portable backpack radio sets and hand-held portable radios. For k polarization, the dipoles were placed on the axis of the body 14 cm from the head, in which case the wave propagated from head-to-toes. For convenience, the model was positioned horizontally with the antenna placed underneath (for E & H polarizations) (Stuchly, 1983b), see Fig. 1.

To characterize the exposure conditions, the electric field was measured on the dipole axis in the absence of the model. Figure 2 illustrates the square of the total electric field vs distance from the antenna. The model was placed at a distance of 7.6 cm, corresponding to 0.09 of the wavelength in free space. Even though this could be considered as the near-field, it is clear that the contribution of the electric field components, other than those whose amplitudes decay inversely proportionally with the distance from the antenna, was very small.

Calculation of the Average SAR

A curve-fitting method has been developed to facilitate calculations of the average SAR for the whole-body and its parts from the acquired values of the local SARs. The electric-field probe could not be positioned very close to the bottom wall of the model (the probe was introduced to the model from the top and normally was scanned down in the direction of the antenna to a distance of approximately 2 cm from the bottom wall of the model). Since the model was irradiated from the bottom and, in many locations, the SAR decreases with the distance along the direction of propagation, it was essential to include the SAR values in the volume adjacent to the bottom wall in the calculations of the average SAR. To accomplish this task, the

TABLE I. Parameters of the Test Antennas

Antenna type	Resonant dipole	Resonant dipole with a reflector	Slot with a reflector
Length (cm)	37	37	42.5
Length/wavelength	0.43	0.43	0.50
Diameter (cm)	0.63	0.63	—
Width (cm)	—	—	1.6
Reflector distance (cm)	—	18.0	18.0
Gain	1.64	3.28	4.87

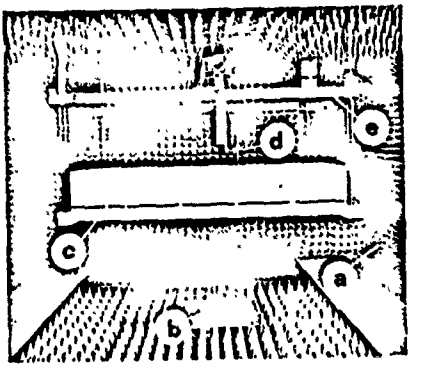

Fig. 1. General view of the experimental system in the anechoic chamber: (a) anechoic chamber, (b) antenna with a reflector, (c) model of the human body, (d) electric field probe, (e) mechanical scanning system.

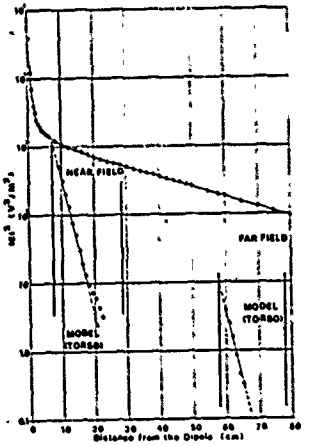

Fig. 2. The square of the electric field intensity (E^2) at 350 MHz, E polarization in air vs distance from the dipole (upper curve) and E^2 in the model placed in the near- and far-field (lower curves). Points are experimental and dashed lines represent extrapolated values.

experimental data were extrapolated into that volume by a least-square curve fitting. In the majority of cases, e.g. in the torso, the SAR follows an exponential function along the direction of wave propagation. Therefore, an exponential function was fitted to the data points, and the SARs in the volume close to the model wall were calculated. Where the SAR changed in a less regular fashion, e.g., in the head or legs, other functions such as polynomials were fitted to the data. The extrapolated values of the SAR were used together with the experimentally obtained values for calculations of the averages.

To calculate the average SARs, the average SARs in twenty body cross-sections were calculated by using the extrapolated data. The cross-sections were perpendicular to the main body axis. Seven cross-sections were located in the head and neck, six in the torso and seven in the legs; the positions of the cross-sections correspond to the points shown in Figure 3. The distances between the cross-sections were from 4 cm in the head to 10 cm in the legs. For each of the cross-sections the SAR data were acquired along three to seven axes spaced about 5 cm apart, and along each of the axes the SAR values (either measured or extrapolated close to the body surface) were spaced 1 cm apart. It is evident that the calculation of the average SARs was more accurate for the head than for the legs. To evaluate the uncertainties involved in the averaging, the average SAR was calculated for a 16-cm diameter dielectric sphere and compared with the calculated value. Three cross-sections and three axes within each cross-section were used. The estimated uncertainty for the calculations of the average SARs is about ± 25%, even though much better agreement was obtained for the sphere.

To calculate the whole-body average SAR the commonly used "rule of nines" (Ricci, 1967) was applied, i.e., the contributions by weight of the various parts of the

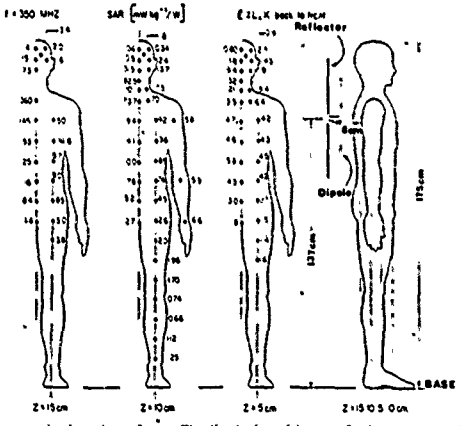

Fig. 3. Resonant dipole with a reflector. The distribution of the specific absorption rate (SAR) in three cross-sections of the body; frequency = 350 MHz, polarization = E ∥ L, power to the antenna = 1W, and dipole at x = 137 cm from the base (feet).

human body were as follows: head and neck, 0.09; upper torso, 0.18; lower torso, 0.18; arms 2 × 0.09; upper legs, 2 × 0.09; lower legs 2 × 0.09. The average SARs were calculated for each body part, then multiplied by the weighing factors and summed to obtain the whole-body average.

RESULTS

The electric field intensity was measured, and the SAR was calculated in over 650 locations within a half of the model for 9 antenna locations and various polarizations. Each complete scan was repeated at least three times by using different input powers to the antenna, or on different days. All the results shown are averages, the repeatability of the data was well within ± 0.5 dB.

A typical distribution of SAR in three cross-sections of the body is shown in Figure 3 for the resonant dipole with a reflector placed 8 cm from the back of the model and 137 cm from the base of the feet.

Variations of the SAR along the direction of the wave propagation on the antenna axis when the antenna was positioned close to the torso, in the E polarization, are illustrated in Figure 4. The same data for other antenna configurations are summarized in Table 2.

Figures 5 to 10 show the spatial distribution of the SAR along the two body axes, where the SAR is averaged over cylinders perpendicular to the points shown on the graphs, contained between the body surfaces and having a diameter of 0.9 cm (the probe diameter). In essence, each point represents the area under the corresponding

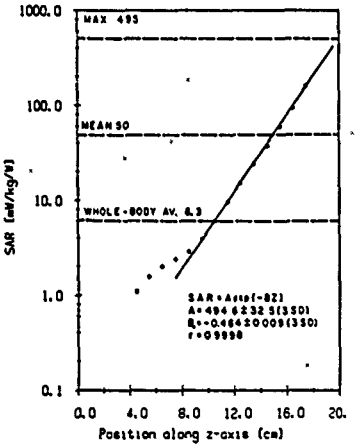

Fig. 4. Resonant dipole. The specific absorption rate (SAR in the torso at the dipole axis vs distance from the body surface at which the wave is incident; frequency = 350 MHz, polarization = E || L, power to the antenna = 1 W, dipole at x = 137 cm from the base (feet).

TABLE 2. Maximum and Mean SAR Along the Direction of Propagation, Whole-Body Average SAR, and Attenuation Coefficient (B) for Antennas in the Near-Field

Antenna	Polarization	x[a] (cm)	SAR(mW/kg) Max[b]	Mean	WB Avg.[c]	B ± 3 SD
Resonant dipole	E	103	1090 ± 86	100	8.1	− 0.567 ± 0.011
	E	137	494 ± 32.5	50	6.3	− 0.464 ± 0.009
	H	137	1053 ± 193	96	6.4	− 0.515 ± 0.027
Resonant dipole with a reflector	E	137	1291 ± 330	139	14.3	− 0.464 ± 0.012
	H	137	2632 ± 516	247	13.2	− 0.503 ± 0.024
Slot with a reflector	E	87	205 ± 54	21.5	6.7	− 0.45 ± 0.03

[a]The distance of the antenna axis from the model (base) feet.
[b]This maximum does not necessarily correspond to the absolute maximum anywhere along the body axis, but represents the maximum at the x position indicated in the table.
[c]WB Avg. = whole-body average.

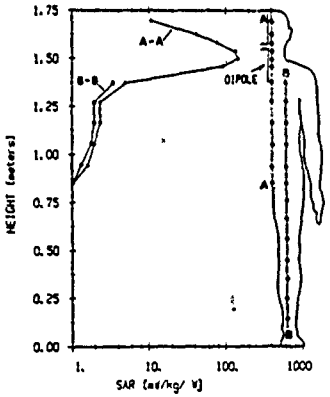

Fig. 5. Resonant dipole. The mean values (averaged over 0.9 cm DIA cylinders perpendicular to the body axis) of the specific absorption rate (SAR) in a number of locations along the selected axis: frequency = 350 MHz, polarization = E || L, power to the antenna = 1 W, dipole at x = 156.5 cm from the base (feet).

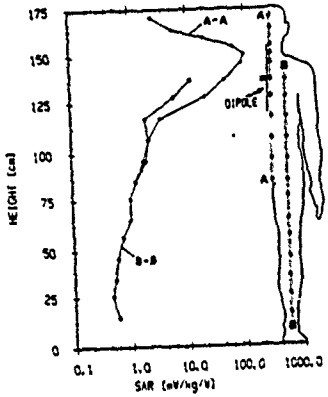

Fig. 6. Resonant dipole. The mean values (averaged over 0.9 cm DIA cylinders perpendicular to the body axis) of the specific absorption rate (SAR) in a number of locations along the selected axis; frequency = 350 MHz, polarization = E ∥ L, power to the antenna = 1 W, dipole at x = 137 cm from the base (feet).

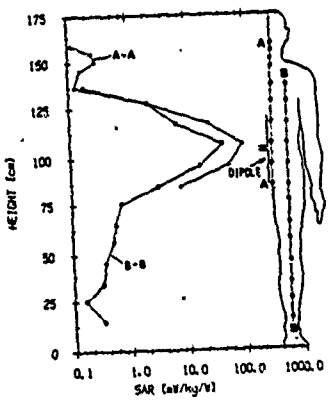

Fig. 7. Resonant dipole. The mean values (averaged over 0.9 cm DIA cylinders perpendicular to the body axis) of the specific absorption rate (SAR) in a number of locations along the selected axis; frequency = 350 MHz, polarization = E ∥ L, power to the antenna = 1 W, dipole at x = 103 cm from the base (feet).

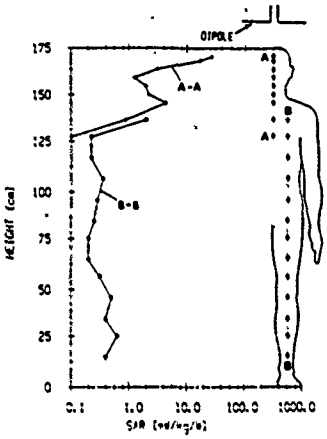

Fig. 8. Resonant dipole. The local values of the specific absorption rate (SAR) along the selected body axis; frequency = 350 MHz, polarization = k ∥ L, power to the antenna = 1 W, the dipole 14 cm from the head.

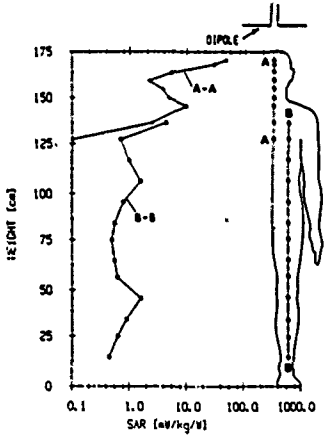

Fig. 9. Resonant dipole with a reflector. The local values of the specific absorption rate (SAR) along the selected body axis, frequency = 350 MHz, polarization = k ∥ L, power to the antenna = 1 W, the dipole 14 cm from the head.

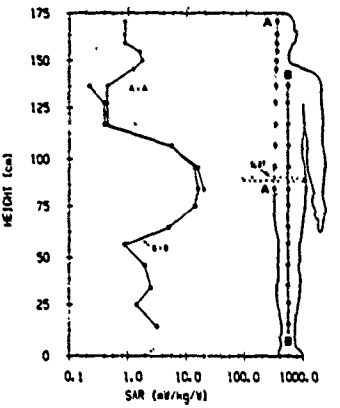

Fig. 10. Resonant slot. The mean values (averaged over 0.9 cm DIA cylinders perpendicular to the body axis) of the specific absorption rate (SAR) in a number of locations along the selected axis; frequency = 350 MHz, polarization = E || L, power to the antenna = 1 W, slot at x = 85 cm from the base (feet).

curve, similar to that shown in Figure 4, divided by the distance between the body surfaces. For instance, the point on curve A-A in Fig. 6 for the height of 137 cm was actually calculated from the data shown in Figure 4.

The distribution of the SAR averaged over horizontal tissue layers along the body vertical axis is shown in Figure 10 for the resonant dipole and the dipole with a reflector, both in the E polarization. The same distribution for the dipole with a reflector for the H polarization is shown in Figure 11.

The average whole-body SAR and those for the parts are summarized in Table 3 for all cases tested, except for the k polarization.

DISCUSSION

The spatial distribution of the SAR in body cross-sections is highly non-uniform for all antennas and their locations, as illustrated in Figure 3 for one of the cases tested. This is characteristic for all tested situations.

For all nine antenna configurations tested, the SAR decreased exponentially along the direction of the wave propagation within the first 10 cm or more, as shown in Figure 4. In some cases small deviations from the exponential behaviour of the SAR were observed at greater depths, particularly in the neck and the limbs, but their magnitude was at least 50 times below the maximum SAR on the irradiated body surface. This behaviour is analogous to the behaviour of the SAR distribution for the far-field exposures at 350 MHz [Kraszewski et al, 1984]. The attenuation coefficients (B), for various antenna configurations are very close to each other, as illustrated in Table 2, and very close to the theoretical value $B = -0.49$, as calculated for a plane

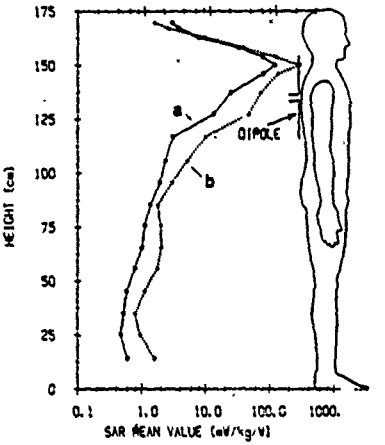

Fig. 11. The mean values of the specific absorption rate (SAR) for horizontal tissue layers along the vertical body axis: frequency = 350 MHz, polarization = E ∥ L, power to the antenna = 1 W, dipole at x = 137 cm from the base (feet), (a) resonant dipole, (b) resonant dipole with a reflector.

TABLE 3. Near-Field Experiments. The Whole-Body Average SAR (mW/kg) and Average SARs (mW/kg) for body parts*

	Antenna configuration						
Body part	Resonant dipole				Resonant dipole with a reflector x = 137 cm		Slot with a reflector
	E∥L, x = 156.5cm	E∥L, x = 137cm	E∥L, x = 103cm	H∥L, x = 137cm	E∥L	H∥L	E∥L, x = 87 cm
Head & neck	58.0[a]	27.8	0.2	2.9	47.5	4.7	1.6
Upper torso	2.8	13.7	6.6	30.8	42.9	65.0	0.4
Lower torso	1.5	1.9	32.4	0.5	3.3	0.7	14.5
Arms	2.4	2.9	5.0	2.5	6.6	5.1	12.3
Legs	0.6	0.7	0.4	0.2	1.5	0.2	4.5
Whole body	6.6	6.3	8.1	6.4	14.3	13.2	6.7

*f = 350 MHz, input power to the antenna = 1 W.
[a]Milliwatts per kilogram

wave of the same frequency incident upon a semi-infinite tissue layer having the electrical properties of the average tissue. The observed exponential decay of the SAR with distance is not surprising in view of the changes of the incident electric field with distance. The incident electric field, as shown in Figure 2, varies nearly inversely proportionally with distance at the location of the model.

Because of the exponential decay of the SAR with distance (Fig. 4), the mean values of the SAR distributions can be easily evaluated. Several features of the energy deposition in the body can be observed. The highest SARs were close to, but not always on, the axis of the antenna. When the antenna was positioned close to the head-neck region and for the E polarization, the maximum SAR shifted off the dipole axis towards the head, as illustrated in Figures 5 and 6. This feature was characteristic for both dipoles, the resonant dipole and the resonant dipole above with a reflector. However, for the H and k-polarizations (Figures 8 and 9), the maximum SAR was on the axis of the dipole. The same holds when a dipole radiating with the E-polarization or a slot were placed close to the lower torso (Figures 7 and 10).

The maximum mean values of the SAR were about 100 mW/kg per 1 W of input power for the resonant dipole with both the E and H polarizations (Figs. 5–7, Table 2), but only about 20 mW/kg for the slot (Fig. 10, Table 2).

The maximum mean SAR value for the k polarization was at the top of the head, i.e., at the irradiated surface for both dipoles tested (Figs. 8 and 9). However, in the neck area there was a small increase in the SAR, approx. 5 mW/kg for the resonant dipole (Fig. 8), and approx. 10 mW/kg for the resonant dipole with a reflector.

The slot created a broader SAR maximum in both directions (only one direction is illustrated in Fig. 10). It can also be observed that for the dipoles, and to a lesser degree for the slot, changes in the mean SAR along the vertical body axis were quite rapid, typically more than an order of magnitude within 10 cm.

The general shape of the SAR distribution along the vertical body axis was preserved for all antennas when the SAR was averaged over horizontal body layers, as shown in Figure 11 and 12. Once again, it should be noted that in a similar manner as for the local SAR distributions and those averaged over the cylinders (Figs. 5–10), the SAR maximum was on the dipole axis (Fig. 12), except when the dipole was located close to the head-neck area.

For linear antennas, the maximum SAR averaged over the tissue layers was very close for the two polarizations (E and H), with slightly greater values (~ 15%–20%) for the E polarization. This point is illustrated in Figures 11 and 12 for the dipole above with a reflector located 137 cm from the feet base.

For linear antennas, an increase in the antenna gain was nearly proportionally reflected in an increase as the local and average SARs. This point is illustrated in Figure 11 showing the SARs averaged over tissue layers for the resonant dipole and the same dipole with a reflector. Further illustration is given in Table 2, for instance, for the H polarization and $x = 137$ cm; the ratios of the maximum, mean, and whole body averaged SAR for the two dipoles are 2.5, 2.6, and 2.1, respectively vs the gain ratio of 2 (Table 1).

The average SAR in various parts of the body, as expected, depends on the position of the antenna with respect to the body and to a certain extent on polarization (Table 3). Whenever an antenna irradiating the body with E-polarization is placed close to the neck, the head-neck SAR is significantly increased, but this increase does not occur with H-polarization.

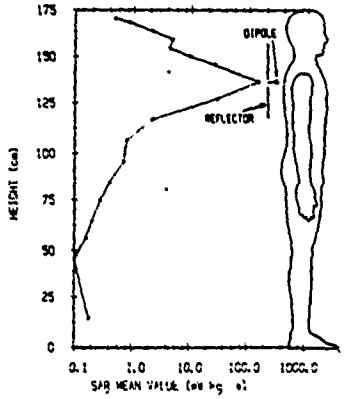

Fig. 12. Resonant dipole with a reflector. The mean values of the specific absorption rate (SAR) for horizontal tissue layers along the vertical body axis; frequency = 350 MHz, polarization = H ⊥ L, power to the antenna = 1 W, dipole at x = 137 cm from the base (feet).

The whole-body average SAR (Table 3) is mainly determined by the antenna gain and, to a much lesser degree, by the antenna location. The dependence on the antenna location basically reflects the dependence on the average distance to the body surface. It should be noted that the antenna axis was always 8 cm from the body surface, but because of the body curvature, the distance between the antenna surface and body surface varied for different antenna positions and polarizations.

One question related to the near-field exposure is worth addressing. According to the ANSI recommendations [ANSI, 1982], the upper limits for near field exposures are an average SAR (whole-body) of 0.4 W/kg and a spatial peak SAR of 8 W/kg as averaged over 1 g of tissue. At a frequency of 350 MHz, the output power of a portable transmitter has to exceed 25 W for the average SAR to be above the limit for practical distances of 7 to 10 cm for the antenna separation from the body surface. However, only about 4 W appear to be sufficient for exceeding the spatial peak SAR, which occurs at the body surface. Whether the limit on the spatial peak SAR should apply when the peak SAR is on the body surface is a separate question.

CONCLUSIONS

The spatial distribution of the SAR in a full-scale homogeneous model of man at 350 MHz with three polarizations of the incident wave has been measured and analyzed for three antennas in the near-field. The whole-body average, the partial body, and selected volume SARs have been calculated. The antennas selected represent typical practical situations, such as portable transmitters and leaky RF transmitter cabinets or similar hardware. For near-field exposure the following conclusions can be drawn:

(i) The spatial distribution of the SAR is highly nonuniform for all polarizations; the nonuniformity occurs along all directions within the body. Typical ratios between the spatial peak and the whole-body average SAR are 150 to 200 for the linear antennas, and 30 for the slot.

(ii) At 350 MHz, and probably at all higher frequencies for all antennas and polarizations, the SAR increases exponentially with distance from the surface upon which the wave is incident, at least within 10 cm. By that distance, the wave is attenuated about 15 dB. This finding is consistent with a previous report for a hand-held transmitter at 806–821 MHz, operating in the E-polarization [Athey and Cleveland, 1982]. The attenuation coefficient is very close to that of a plane wave incident upon a semi-infinite tissue layer. Therefore, a simplified analysis can be used to determine the relative SAR distribution in a multilayered tissue structure. The absolute values of the SAR can only be found through a more complex analysis of measurement since they depend on the antenna type, polarization, and distance from the body.

(iii) For the E-polarization, the maximum absorption is shifted from the axis of the antenna towards the neck region for antenna locations in the nearby region.

(iv) The relative spatial distribution of the SAR depends mainly on the antenna position and polarization, but the whole-body average SAR is basically determined by the antenna gain and distance from the body. The antenna type (e.g. dipole vs slot) affects both the whole-body average and the distribution of the SAR.

(v) The non-uniformity of the SAR distribution in the near-field implies that exposure to some portable radio RF transmitters can result in the peak SAR (averaged over 1 g of tissue) exceeding the recommended limit of 8 W/kg [ANSI, 1982], while the whole-body average SAR remains well within the limit of 0.4 W/kg. For instance, for a resonant dipole with a reflector and H-polarization, an output power from the antenna of 3.1 W is sufficient to deposit the energy at the surface at a rate of 8 W/kg, while for a whole-body average of 0.4 W/kg, an output power of 30 W is required.

ACKNOWLEDGMENTS

Financial support by grants from the U.S. Office of Naval Research, Health and Welfare, Canada, and the Natural Sciences and Engineering Research Council of Canada are gratefully acknowledged.

REFERENCES

American National Standard, ANSI CAS.1 (1982): Safety levels with respect to human exposure to radio frequency electromagnetic fields, 300 KHz to 100 GHz.

Athey TW, Cleveland RF (1982): Power deposition in a head model exposed to hand-held UHF transceivers. Abstracts Bioelectromagnetics Society Fourth Annual Meeting, Los Angeles, CA, p. 27.

Cahill DF (1983): A suggested limit for population exposure to radiofrequency radiation. Health Phys 45:109–126.

Chatterjee I, Hagmann MJ, Gandhi OP (1980): Electromagnetic-energy deposition in an inhomogeneous block model of man for near-field irradiation conditions. IEEE Trans Microwave Theory Tech MTT-28:1452-1459.

Durney CH (1980): Electromagnetic dosimetry for models of humans and animals: A review of theoretical and numerical techniques. Proc IEEE 68:33-40.

Guy AW (1971): Analysis of electromagnetic fields induced in biological tissues by thermographic studies in equivalent phantom models. IEEE Trans Microwave Theory Tech MTT-19: 205-214.

Guy AW, Webb MD, Sorenson CC (1976): Determination of power absorption in man exposed to high frequency electromagnetic fields by thermographic measurements on real models. IEEE Trans Biomed Eng BME-23:361-371.

Hagmann MJ, Gandhi OP, D'Andrea JA, Chatterjee I (1979): Head resonance: numerical solutions and experimental results. IEEE Trans Microwave Theory Tech MTT-27:809-813.

Iskander MF, Barber PW, Durney CH, Massoudi H (1980): Irradiation of prolate spheroidal models of humans in the near field of a short electric dipole. IEEE Trans Microwave Theory Tech MTT-28:801-807.

Kraszewski A, Stuchly MA, Stuchly SS, Hartsgrove G, Adamsky D (1984): Specific absorption rate distribution in a full-scale model of man at 350 MHz. IEEE Trans Microwave Theory Tech MTT-32:779-782.

Lakhtakia A, Iskander MF, Durney CH, Massoudi H (1981): Near-field absorption in prolate spheroidal models of humans exposed to a small loop antenna of arbitrary orientation. IEEE Trans Microwave Theory Tech MTT-29:588-594.

Lakhtakia A, Iskander MF, Durney CH, Massoudi H (1982): Absorption characteristics of prolate spheroidal models exposed to the near fields of electrically small apertures. IEEE Trans Biomed Eng BME-29:569-575.

Ricci B (1967): "Physiological Basis of Human Performance." Philadelphia: Lea and Febiger, Inc.

Spiegel RJ (1982): The thermal response of a human in the near-zone of a resonant thin-wire antenna. IEEE Trans Microwave Theory Tech MTT-30: 177-185.

Stuchly MA (1983): Dosimetry of radio frequency and microwave radiation: Theoretical Analysis. In Grandolfo, M., Michaelson, S.M. (eds): "Biological Effects and Dosimetry of Nonionizing Radiation". Plenum Publ. Co., pp. 163-177.

Stuchly MA, Stuchly SS (1985): Experimental radio and microwave dosimetry. In Polk C, Postow E (eds): "Handbook of Biological Effects of Electromagnetic Radiation." Boca Raton, FL: CRC Press.

Stuchly SS, Barski M, Tam B, Hartsgrove G, Symons S (1983b): A computer-based scanning system for electromagnetic dosimetry. Rev Sci Instrum 54:1547-1550.

Stuchly MA, Kraszewski A, Stuchly SS (1984): Implantable electric field probes—some performance characteristics. IEEE Trans Biomed Eng BME-31:526-531.

ISSN 0243 - 7228

Tirage à Part

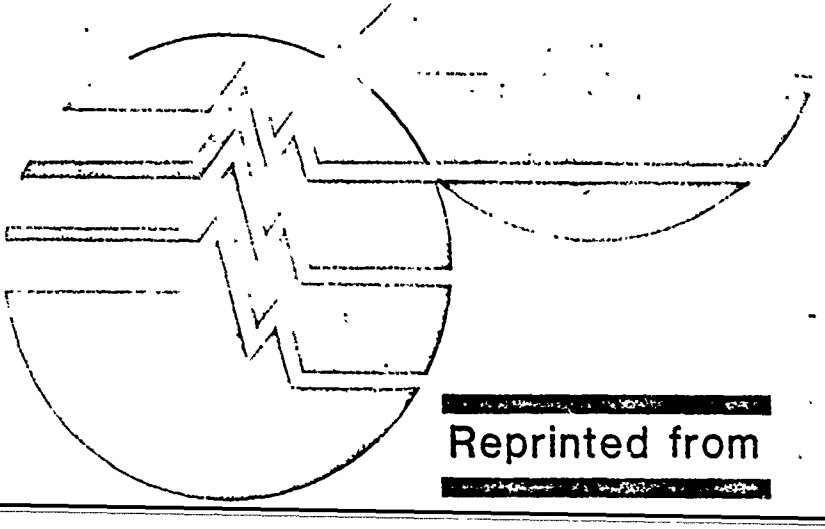

Reprinted from

INNOVATION ET TECHNOLOGIE EN BIOLOGIE ET MEDECINE

SOMMAIRE

VOL. 6, N° 5, 1985

Subscriptions to I.T.B.M. are available from :

ITBM

I.T.B.M. - C.R.D.P.
3, RUE JEAN BART - B.P. 199 - 59018 LILLE CEDEX
FRANCE - TELEX 160315F

PRICES : FRENCH : 280 FF
ELSEWHERE : 330 FF

REPARTITION DE L'ENERGIE DANS LE CORPS HUMAIN SOUMIS AU RAYONNEMENT EN CHAMP PROCHE D'APPLICATEURS RADIOFREQUENCES.

M.A. STUCHLY, S.S. STUCHLY, A. KRASZEWSKI, G. HARTSGROVE

RESUME :

La distribution spatiale du champ électrique ou le taux de répartition de l'énergie (défini par le taux d'absorption spécifique TAS) qui résulte de l'exposition du corps humain au rayonnement émis à partir d'applicateurs radiofréquences est intéressant et important dans le cas de l'hyperthermie induite électromagnétiquement et pour évaluer les risques potentiels pour la santé liés à des expositions involontaires. Un dispositif de balayage contrôlé par ordinateur ainsi qu'une sonde implantable de mesure de champ électrique ont été utilisés pour déterminer la répartition du TAS dans un modèle du corps humain. Les résultats de ces mesures effectuées à 160, 350 et 915 MHz à l'aide de dipôles résonants avec réflecteurs, situés à une distance d'environ $\lambda/10$ de la surface du corps humain, sont présentés.

MOTS CLES : HAUTES FREQUENCES - ABSORPTION - HYPERTHERMIE - CHAMP PROCHE.

ENERGY DEPOSITION IN THE HUMAN BODY FROM RADIOFREQUENCY RADIATORS IN THE NEAR-FIELD.

ABSTRACT :

Spatial distribution of the electric field or the rate of the energy deposition (defined as SAR - specific absorption rate), resulting from exposure of the human body to radiofrequency radiators is of interest and importance in electromagnetically induced hyperthermia and in assessment of potential health hazards due to unwanted (e.g. occupational) exposures. A computer-controlled scanning system and an implantable electric field probe were used to determine distributions of the SAR in a model of man. The results of measurements performed at 160, 350 and 915 MHz for resonant dipoles with reflectors and resonant slots with reflectors placed at a distance of approximately one tenth of the wavelength from the body surface are presented.

KEY WORDS : RADIOFREQUENCIES - ABSORPTION - HYPERTHERMIA - NEAR FIELD.

ENERGY DEPOSITION IN THE HUMAN BODY FROM RADIOFREQUENCY RADIATORS IN THE NEAR-FIELD

M.A. Stuchly(1)(2), S.S. Stuchly(2), A. Kraszewski(2) and G. Hartsgrove(2)
(1) Radiation Protection Bureau, Health and Welfare Canada
(2) Dept. of Electrical Engineering, University of Ottawa, Ottawa, Ontario, Canada, K1N 6N5

INTRODUCTION

Spatial distributions of the electric field or the rates of the energy deposition resulting from exposure of biological bodies to radiofrequency (RF) radiators in the near-field have been of interest and the subject of numerous studies. The interest stems from two important applications. One is in RF induced hyperthermia used in cancer treatment, where it is important to know the spatial distribution of the energy deposited, in order to determine and possibly control the volume of the tissue that is heated. The other application is in evaluating the rates of energy deposition resulting from exposure to various RF sources in the near-field (e.g. portable transmitters, leaky radiofrequency equipment), in order to assess and prevent a potential health hazard.

The quantity frequently used in describing the rates of RF energy deposition is the specific absorption rate (SAR), which is defined as the time derivative of the incremental energy (dW) absorbed by an incremental mass (dm) contained in a volume element (dV) of a given density (ρ) [1]:

$$SAR = \frac{d}{dt}\frac{dW}{dm} = \frac{d}{dt}\left(\frac{dW}{\rho dV}\right) \qquad (1)$$

For sinusoidally time-varying fields the SAR is related to the electric field strength in situ as:

$$SAR = \frac{\sigma}{2\rho}|E|^2 \qquad (2)$$

where: E is the magnitude (peak) of the electric field, and σ is the conductivity of biological material (tissue).

To determine spatial distributions of the SAR, theoretical and experimental methods are employed. Numerical methods used to find the SAR distribution for various hyperthermia applicators have recently been reviewed [2]. In hyperthermia investigations the evaluation of the SAR distribution, either theoretical or experimental, is followed by theoretical and/or experimental evaluation of the resulting temperature distribution. For assessment of a potential health hazard due to exposure to RF energy various methods of analysis have been developed for simplified models. Numerous calculations developed for far-field exposures have been reviewed elsewhere [3,4]. There are numerous theoretically analyzed exposures in the near-field [5,6,7,8,9], however, only a few exposure configurations in the near-field of fairly realistic models, such as a "block model" of man,

REPRINTS : Dr. M.A. STUCHLY, Electrical Engineering Department, University of Ottawa, 770, King Edward Street, OTTAWA, ONTARIO K1N 5N6 CANADA

Innov. Tech. Biol. Med. ; Vol. 6, n° 5, 1985.

have been treated [8,9].

Experimental techniques serve as alternative and frequently complimentary to theoretical methods as reviewed in [10]. These techniques, at least at the present time, provide more detailed information about the spatial distribution of the SAR than the theoretical calculations. There are three viable techniques for measuring SAR distributions. A thermographic technique [11] can be successfully applied for both the evaluation of hyperthermia applicators [12] and for potentially hazardous exposures [13]. The technique is fast and reliable; its main advantage is that a complete thermal picture (or the SAR profile) can be obtained for any selected cross-section of the exposed body. The main limitation of this technique is that high power sources are required, unless only a very limited volume is to be heated. Two other techniques involve use of implantable probes. Either temperature probes or electric field probes can be used. Both types of probes are miniature and implantable, and have been extensively used for measurements in a few points within the volume of interest [10]. Temperature probes are particularly widely used in hyperthermia for treatment monitoring and control. The main limitation of the probes is that unless a special scanning system is used, information about the SAR or temperature is obtained only for a few locations.

We have developed and evaluated a computer-controlled scanning and data acquisition system. This system has been used with implantable electric field probes to determine the spatial distribution of the SAR in models of the whole and parts of the human body. These models have been exposed in the near-field of two types of radiators, namely a resonant slot and a resonant dipole with a reflector. The experimental method and the results obtained at three frequencies (160 MHz, 350 MHz and 915 MHz) are discussed in this paper. The radiators investigated are of interest for both electromagnetically induced hyperthermia and for evaluation of unwanted exposures. For instance, a resonant slot may serve as an approximation of a leaky cabinet. Short dipoles (about 0.1 of the wavelength) have previously been proposed as elements of an efficient hyperthermia applicator [14,15]. Resonant dipoles, because of their greater efficiency in coupling the RF energy into tissue, may offer a better solution.

EXPERIMENTAL SYSTEM

The experimental system consists of the following essential parts: (a) an anechoic chamber, (b) an RF radiation system, (c) an appropriate phantom model of the human body or its part, (d) an electric field probe, (e) a mechanical computer-controlled scanning system, (f) an electronic system interfacing the probe with the computer, (g) a minicomputer. A general description of our earlier system is given elsewhere [16]. Significant modifications have been introduced since then and are described here for the first time.

Figure 1 shows a block diagram of the experimental system. An antenna or a hyperthermia applicator, the E-field probe, the probe holders, the pre-amplifier and the mechanical frame with stepping

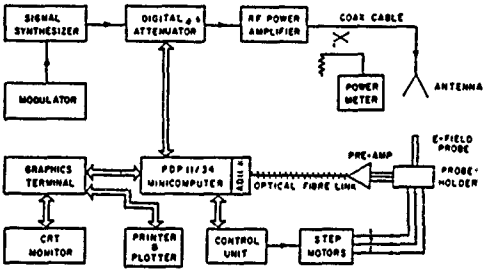

Figure 1 : Block diagram of the experimental system for mapping the electric field in models of a human body or its parts.

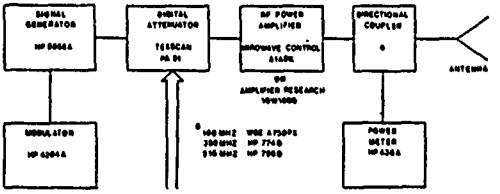

Figure 2 : Radiofrequency radiation system.

motors are placed in the anechoic chamber. For accurate measurements a limited size and quality (reflections below -20 dB) chamber is required to minimize interference by the reflected waves. Although measurements for hyperthermia applicators and other near-field radiators are possible without an anechoic chamber, the accuracy of measurements is usually adversely affected. The RF radiation system, shown in Figure 2, comprises a signal synthesizer modulated at a low frequency (about 500 Hz), a digital attenuator, an RF power amplifier, a power meter and a radiation source (an antenna or a hyperthermia applicator).

The mechanical structure, the drives and the control unit, and their operation are described in detail elsewhere [16]. Briefly, they are capable under the computer control to position the E-field probe within ±0.05 mm in any location within a volume of 190 x 50 x 45 cm. The speed is 0.42 mm/s for a simple motion (a single coordinate changing at a time), and 12 mm/s for a composite motion (two or three coordinates changing simultaneously).

A schematic diagram of the electronic system is shown in Figure 3. This system provides amplification of the 500 Hz signals from the E-field probe, conditioning of the signals, and transmission by an optical fiber link to an A/D converter. The amplitude modulation of the RF signal is employed in order to increase the dynamic range of measurements of the SAR (the electric field strength in tissue). The dynamic range depends on the E-field probes linear range of operation

and on their noise level. The amplitude modulation at about 500 Hz improves the signal-to-noise ratio by about 10 dB with a 1 Hz bandwidth of the amplifier as compared to the operation without modulation [17].

The dynamic range of measurements of the SAR exceeded 30 dB in the frequency range from 150 MHz to 1 GHz.

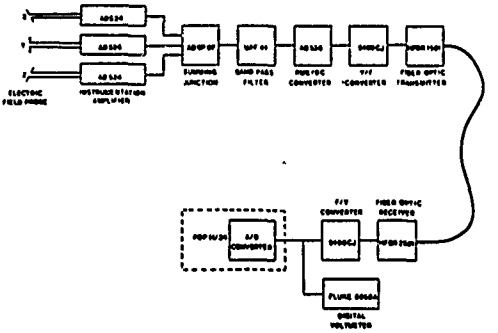

Figure 3 : Schematic diagram of the electronic system.

Two types of radiators operating in the near-field were investigated: a resonant slot and a resonant dipole, both with reflectors. Salient characteristics of these radiators are summarized in Table 1. One of the most important features of these radiators is that they are very well matched to the feeding lines when a phantom model of the human body is placed in front of them at distances of about 0.1 of the wavelength. The voltage standing wave ratio (VSWR) is less than 1.6, which is equivalent to 4 per cent of the reflected power. This is particularly important in hyperthermia applications.

A model of the human body in a form of a shell was made of a thin (1.5 mm) thermoplastic material. The geometrical shape and the dimensions closely approximated an anatomically correct average man of a height of 175 cm and a weight of 70 kg. The shell was filled with a semiliquid material having electical properties equal approximately to those of "average tissue", i.e. 2/3 of the muscle properties. As electrical properties of tissues vary with frequency, different mixtures were prepared for specific frequencies used in the investigations (160, 350 and 915 MHz). The electrical properties of the tissue-equivalent materials used are summarized in Table 2 and the attenuation coefficient, α, is given. Parts of the plastic shell were removed (on some "flat" parts of the torso) or holes were drilled in the shell to allow the E-field probe to penetrate into the interior of the model, which was positioned horizontally. The radiating source was placed under the model, while the probe penetrated vertically from the top of the model.

The electric field strength was measured with an implantable triaxial field probe, consisting of three short dipoles, each loaded

with Schottky diodes (EIT probe, model 979). The overall diameter of the probe was 9 mm. The probe was fully characterized and calibrated as described in [17], and its calibration was spot-checked during the course of experiments. The estimated measurement uncertainty in SARs was ±1 dB, and was mostly due to the uncertainty in the probe calibration [17]. The measurement repeatibility was better than ±0.5 dB.

Table 1. Characteristics of the radiators

TYPE	FREQUENCY (MHz)	LENGTH/ WAVELENGTH	ANTENNA-REFLECTOR DISTANCE (cm)	GAIN (dB)	INPUT VSWR
Dipole	160	0.49	20	3.6	1.5
Dipole	350	0.43	21	3.3	1.6
Slot	350	0.50	16	4.9	1.1
Dipole	915	0.49	8.2	3.2	1.1
Slot	915	0.50	6.5	6.1	1.1

Table 2. Electrical properties of tissue phantom materials

FREQUENCY (MHz)	DIELECTRIC CONSTANT, ϵ'	CONDUCTIVITY, σ, (S/m)	ATTENUATION COEFFICIENT, α
160	40	0.80	0.18
350	38	0.95	0.26
915	37	1.17	0.35

RESULTS AND DISCUSSION

The electric field strength was measured and the SAR calculated on the axis of the radiators in the tissue-equivalent material at three frequencies for resonant dipoles and slots with reflectors. The designation of the radiator placement with respect to the model of man is shown in Figure 4, while Table 3 gives the radiator coordinates at the frequencies investigated. The radiators were placed in the plane corresponding to the body vertical axis, and were oriented in such a way that the electric field vector was parallel to the body vertical axis. Figures 5 and 6 show the results for the dipoles and the slots, respectively. In all cases investigated, for both types of radiators and at all frequencies, the SAR decreases exponentially (notice the logarhythmic scale) with distance from the body surface. Furthermore, the attenuation coefficients are very close to those estimated theoretically for the plane wave as given in Table 3. That means, that the longer the wavelength, the greater the penetration depth in the tissue. The SAR close to the surface is much greater at 350 and 915 MHz than at 160 MHz for the dipoles. For the slots the SAR close to the surface is less than that for the dipoles, and at 915 MHz it is greater than at 350 MHz.

Figures 7 and 8 illustrate the spatial distribution of the SAR in the cross-section of the torso on the radiator axes (see Table 3) for dipoles and slots, respectively. The dashed lines show the equi-SAR profiles in mW/kg per 1W of the radiator output power. A difference in shape of the lines between the dipoles and the slots can be seen. The data presented can be utilized in designing an array to obtain a desired heating contour.

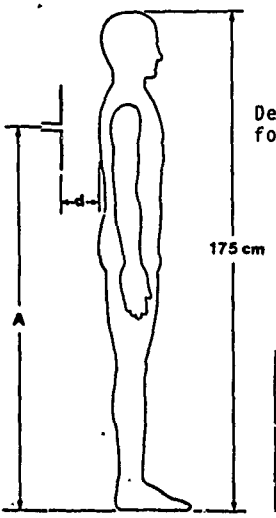

Figure 4

Designation of geometrical coordinates for the radiators investigated.

Table 3. Geometrical coordinates for the radiators investigated (see also Figure 4)

TYPE	FREQUENCY (MHz)	A (cm)	d (cm)	d/λ
DIPOLE	160	134	21	0.112
DIPOLE	350	103	8	0.093
SLOT	350	87	8	0.093
DIPOLE	915	107	5	0.152
SLOT	915	97	5	0.152

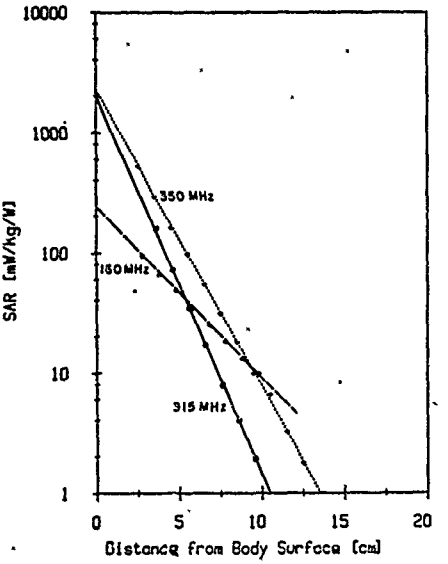

Figure 5 : The specific absorption rate, SAR, in the torso on the antenna axis as a function of distance from the body surface for resonant dipoles with reflectors. Points show the experimental data and the lines are the least-square fit.

Figure 6 : The specific rate, SAR, in the torso on the antenna axis as a function of distance from the body surface for resonant slots with reflectors. Points show the experimental data and the lines are the least-square fit.

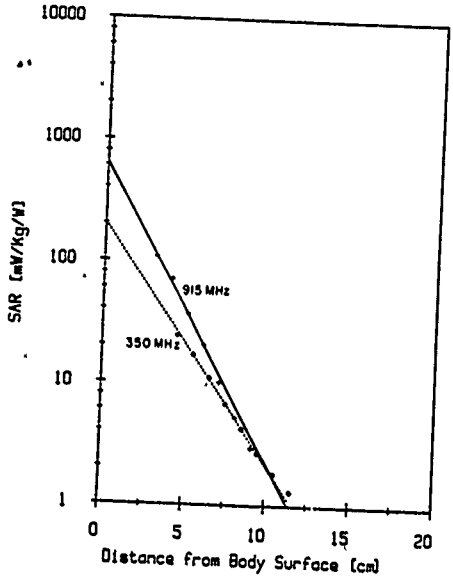

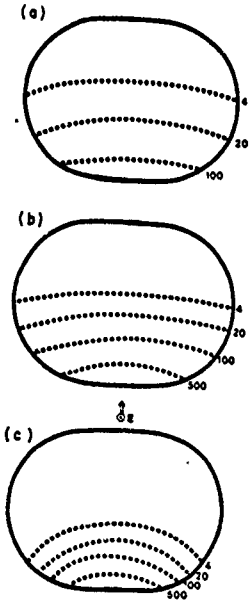

Figure 7 : The specific absorption rate, SAR, in mW/kg, the cross-section of the torso on the axis of the resonant dipoles with reflectors with 1W output power ;
(a) 160 MHz,
(b) 350 MHz,
(c) 915 MHz.

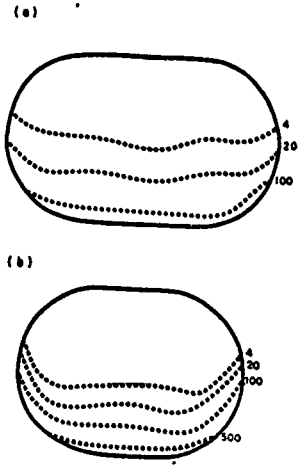

Figure 8 : The specific absorption rate, SAR, in mW/kg, the cross-section of the torso on the axis of the resonant slots with reflectors with 1W output power ;
(a) 350 MHz,
(b) 915 MHz.

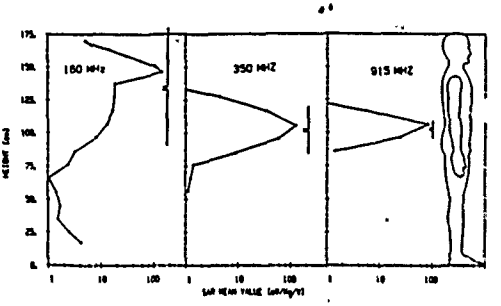

Figure 9

Specific absorption rate, SAR, averaged over tissue layers perpendicular to the body main axis for resonant dipoles with reflectors at three frequencies.

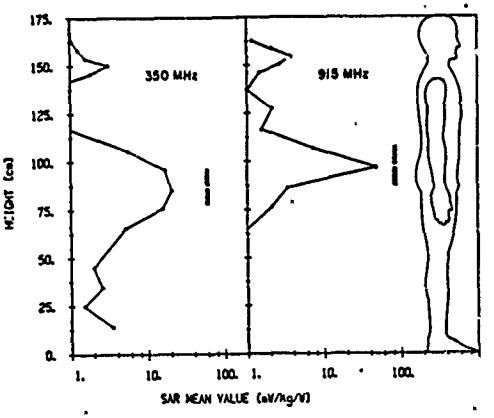

Figure 10

Specific absorption rate, SAR, averaged over tissue layers perpendicular to the body main axis for resonant slots with reflectors at two frequencies.

Spatial distributions of the SAR averaged over tissue layers perpendicular to the body main axis for the dipoles and slots are shown in Figures 9 and 10, respectively. The maximum SARs, except at 160 MHz, occur in the tissue layers on the radiators axes. At 160 MHz, as the radiator axis is close to the neck, the maximum shifts toward the neck, as also observed for far-field exposures [18]. A frequency of 350 MHz appears to be the most advantageous from the three frequencies investigated in terms of the SAR distribution pattern that may be desirable for local hyperthermia. At this frequency a resonant dipole with a reflector is more efficient than a resonant slot with a reflector in terms of coupling the energy to the tissue.

CONCLUSIONS

A computer-controlled scanning system and an implantable electric field probe were used to obtain the specific absorption rate (SAR) profiles in an electrically homogeneous model of man exposed in the near-field of simple radiators. Experiments performed at three frequencies (160, 350 and 915 MHz) with resonant dipoles and slots, both with metal reflectors, indicated localized energy deposition dependent on the frequency and type of radiator. All the frequencies investigated the SAR on the radiator axis decreased exponentially with distance away from the body surface. The most promising for hyperthermia applications were the SAR patterns obtained at 350 MHz for a resonant dipole with a reflector. This exposure situation was characterized by small reflections from the body surface, reasonable penetration depth and the maximum SAR on the antenna axis. Information presented here can be further extended into multiple radiators and nonhomogenous models for design of efficient hyperthermia applicators.

The information on the SAR distributions can also be utilized to assess potential health hazards due to exposure to portable transmitters or leaky sources. A resonant dipole with a reflector may be considered as the worst case (the best energy coupling to the body) of exposure to portable transmitters, and a resonant slot with a reflector as a typical representative of leaky sources (e.g. a transmitter cabinet). For this purpose the values of the SAR obtained can be compared to the values recommended, for instance, in the U.S. ANSI standard [19].

Acknowledgments

The authors gratefully acknowledge grant support from the Health and Welfare Canada, the Natural Sciences and Engineering Council of Canada, and the U.S. Office of Naval Research. We also thank Mrs. D.A. Benwell and Dr. Y. Oeslauriers of the Radiation Protection Bureau for the review of the manuscript and Mrs. J. Smith of the Radiation Protection Bureau for the editorial help.

REFERENCES

[1] Radiofrequency Electromagnetic Fields, Properties, Quantities and Units, Biophysical Interaction, and Measurements. National Council on Radiation Protection and Measurements, Report No 67, 7910 Woodmont Ave., Washington, D.C. 20014, 1981.

[2] J.W. Strohbehn and R.B. Roemer. A survey of computer simulations of hyperthermia treatments. IEEE Trans. Biomed. Eng., Vol. BME-31, pp.136-149, 1984.

[3] C.H. Durney. Electromagnetic dosimetry for humans and animals: a review of theoretical and numerical techniques. Proc. IEEE, Vol.68, pp.33-40, 1980.

[4] M.A. Stuchly. Dosimetry of radio frequency and microwave radiation: Theoretical analyses. In "Biological Effects and Dosimetry of Nonionizing Radiation". Eds. M. Grandolfo and S.M. Michaelson, Plenum Publishing, New York, 1983, pp.163-177.

[5] M.F. Iskander, P.W. Barber, C.H. Durney and H. Massoudi. Irradiation of prolate spheroidal models of humans in the near field of a short electric dipole. IEEE Trans. Microwave Theory Tech., Vol. MTT-28, pp.801-807, 1980.

[6] A. Lakhtakia, M.F. Iskander, C.H. Durney and H. Massoudi. Near-field absorption in prolate spheroidal models of humans exposed to a small loop antenna of arbitrary orientation. IEEE Trans. Microwave Theory Tech., Vol. MTT-29, pp.588-594, 1981.

[7] A. Lakhtakia, M.F. Iskander, C.H. Durney and H. Massoudi. Absorption characteristics of prolate spheroidal models exposed to the near fields of electrically small apertures. IEEE Trans. Biomed. Eng., Vol. BME-29, pp.569-575, 1982.

[8] I. Chatterjee, M.J. Hagmann and O.P. Gandhi. Electromagnetic Energy deposition in an inhomogeneous block model of man for near-field irradiation conditions. IEEE Trans. Microwave Theory Tech., Vol. MTT-28, pp.1452-1459, 1980.

[9] R.J. Spiegel. The thermal response of a human in the near-zone of a resonant thin-wire antenna. IEEE Trans. Microwave Tech., Vol. MTT-30, pp.177-185, 1982.

[10] M.A. Stuchly and S.S. Stuchly. Experimental radio and microwave dosimetry. In "Handbook of Biological Effects of Electromagnetic Fields". Eds. C. Polk and E. Postow, C.R.C. Press, Inc. 1985.

[11] A.W. Guy. Analysis of electromagnetic fields induced in biological tissues by thermographic studies in equivalent phantom models. IEEE Trans. Microwave Theory Tech., Vol. MTT-19, pp.205-214, 1971.

[12] J.F. Lehmann, A.W. Guy, J.B. Stonebridge and B.J. DeLateur. Evaluation of a therapeutic direct-contact 915 MHz microwave applicator for effective deep-tissue heating in humans. IEEE Trans. Microwave Theory Tech., Vol. MTT-26, pp.556-563, 1978.

[13] A.W. Guy, M.D. Webb and C.C. Sorensen. Determination of power absorption in man exposed to high frequency electromagnetic fields by thermographic measurements on real models. IEEE Trans. Biomed. Eng., Vol. BME-23, pp.361-371, 1976.

[14] P.F. Wahid, M.J. Hagmann and O.P. Gandhi. Multidipole applicators for regional and whole-body hyperthermia. Proc. IEEE, Vol.70, pp.311-313, 1982.

[15] Y.G. Gu and O.P. Gandhi. Phased-dipole applicators for torso heating in electromagnetic hyperthermia. IEEE Trans. Microwave Theory Tech., Vol.MTT-32, pp.645-647, 1984.

[16] S.S. Stuchly, M. Barski, B. Tam, G. Hartsgrove and S. Symons. Computer-based scanning system for electromagnetic dosimetry. Rev. Sci. Instrum., Vol.54, pp.1547-1550, 1983.

[17] M.A. Stuchly, A. Kraszewski and M.A. Stuchly. Implantable electric field probes - Some performance characteristics. IEEE Trans. Biomed. Eng., Vol.BME-31, pp.526-531, 1984.

[18] A. Kraszewski, M.A. Stuchly, S.S. Stuchly, G. Hartsgrove and D. Adamski. Specific absorption rate distribution in a full-scale model of man at 350 MHz. IEEE Trans. Microwave Theory Tech., Vol. MTT-32, pp.779-783, 1984.

[19] Safety levels with respect to human exposure at radio frequency electromagnetic fields, 300 kHz to 100 GHz. ANSI C95.1-1982. The Institute of Electrical and Electronic Engineers, Inc., 345 East 47th Street, New York, N.Y. 10017.

Article reçu le : 8 avril 1985 ; Accepté le : 3 juin 1985.

SEVENTH ANNUAL MEETING OF THE BIOELECTROMAGNETICS SOCIETY
SAN FRANCISCO, CALIFORNIA, JUNE 16-20, 1985

ABSTRACT SUBMISSION FORM

FIRST AUTHOR'S MAILING ADDRESS:

Name Maria A. Stuchly, Health and Welfare Canada

Address Rm.233, EHC, Tunney's Pasture

City Ottawa State Ontario Zip K1A 0L2
Canada

First author's signature

Please check preference for method of presentation:

Platform ☒

Poster ☐

No preference ☐

Sponsored by _____ (a full member of BEMS).
Type abstract in space outlined below. Follow instructions (see opposite side).

Please check if this is a student paper ☐

ENERGY DEPOSITION IN A MODEL OF MAN; FREQUENCY EFFECTS IN THE FAR FIELD. Maria A. Stuchly[1], Andrzej Kraszewski, Stanislaw S. Stuchly and George Hartsgrove, Dept. of Electrical Engineering, University of Ottawa, Ottawa, Ont. K1N 5N6; 1) Radiation Protection Bureau, Health and Welfare Canada, Ottawa, Ont. K1A 0L2.

A previously described computer-controlled system and implantable electric field probes were used to measure spatial distributions of the SAR in a full-scale homogeneous model of man having properties of the average tissue. The model was exposed in the far-field at three frequencies, 160, 350 and 915 MHz in E and H polarizations. For all frequencies and polarizations investigated, large spatial gradients of the SAR inside the body were observed. In the torso the SAR decreased exponentially in the direction of the wave propagation, with the attenuation coefficient very close to that of a plane wave incident upon a semi-infinite slab having the same electrical properties as the model. At 160 MHz and 350 MHz, for the E polarization a maximum was found inside the neck where the SAR was about 10 times greater than the whole-body average, which at 160 MHz was more than 1 W/kg (v.s. whole-body average SAR of 0.105 W/kg). The SAR values at the model surface ranged from approximately 16 times the whole-body average at 160 MHz to about 65 times at 350 MHz, and to about 10 times at 915 MHz. The mean SARs in the head-neck region were about 2 to 2.5 times the whole-body average SAR at 160 and 350 MHz for the E polarization. The whole-body average SARs were slightly (less than 15%), but consistently, greater than the calculated values for the block model of man and/or the spheroidal model for the E polarization, and considerably greater (20-50%) for the H polarization.

To assist in program scheduling, please underline the category below which best characterizes the subject matter of your paper:

Electric and Magnetic Properties	Instrumentation and Exposure Systems
Mechanism of Interaction	ELF Studies
Modulated Fields	*In Vivo* Studies
Dosimetry and Exposure Assessment	*In Vitro* Studies
Medical Application and Technique	Other: _____

Provide three (3) key words that characterize this work: 1. SAR distribution
2 Radiofrequency 3. model of man

Authors are requested to send abstracts and three (3) copies by February 1, 1985, to.

Elliot Postow
Naval Medical R&D Command
Naval Medical Command National Capital Region
Bethesda, Maryland 20814-5044

ACCEPTED FOR PUBLICATION IEEE TRANS. MICROWAVE THEORY TECH., JAN. '86.

EXPOSURE OF MAN IN THE NEAR-FIELD OF A RESONANT DIPOLE: COMPARISON BETWEEN THEORY AND MEASUREMENTS

Ref. [20]

Maria A. Stuchly, Senior Member IEEE, Ronald J. Spiegel, Member IEEE, Stanislaw S. Stuchly, Senior Member IEEE, and Andrzej Kraszewski

Abstract

The rate of the radiofrequency energy deposition in a block model of the human body exposed in the near-field of a resonant dipole at 350 MHz was calculated using the moment method. Detailed maps of the electric field strength in a homogeneous model of a realistic shape under the same exposure conditions were obtained using a computer-controlled scanning system and an implantable electric field probe. A comparison of the measurement data with the calculations shows a relatively good agreement when average values over relatively large volumes are concerned; however the calculations do not show large spatial gradients and tend to underestimate the magnitude of "hot spots" observed experimentally.

The authors are (M.A.S.) with the Radiation Protection Bureau, Health and Welfare Canada, Ottawa, Ont. K1A 0L2, (RJS) with the U.S. Environmental Protection Agency, Health Effects Research Laboratory, Research Triangle Park, NC 27711, (SSS) and (AK) with the Department of Electrical Engineering, University of Ottawa, Ont. K1N 6N5.

This work was supported by grants from the U.S. Office of Naval Research, Health and Welfare Canada and the Natural Sciences and Engineering Research Council of Canada.

I. INTRODUCTION

Recent progress in telecommunications technology and applications has resulted in wide spread and continuously growing use of portable and mobile radio transmitters. One aspect of these developments is the resulting exposure to radiofrequency fields, and consequently, a need to assess the safety of the device user.

The dose rate, or the rate at which radiofrequency (RF) electromagnetic energy is imparted into the body, defined as the specific absorption rate (SAR), is used in quantifying biological effects and formulating standards on exposure to RF fields [1,2]. It is also recognized that the spatial distribution of the SAR within the exposed body, and in some interactions also other parameters play an essential role [3].

Numerical methods have been developed to calculate the SAR distribution in very simplified block models of man [4-6], and in a more realistic model [7], both in the far-field. The more realistic model has also been employed for evaluation of the SAR distribution in the near-field, when there is no coupling between the radiation source and the irradiated object [8]. Several recent reviews have summarized the computational methods [9-11].

The SAR distribution can also be determined experimentally, usually in scaled down models of man by thermography [12], or by implantable electric field probes.

Because of the geometrical and electrical complexity of the human body, the spatial distribution of the SAR resulting from exposures in the near-field of antennas, as in the case for portable

transmitters, is difficult to determine by analytical or experimental methods. The tensor integral method has been used to calculate the SAR distribution in a block model of man consisting of 180 cells exposed to a resonant dipole in the near field with mutual coupling between the antenna and body due to their close proximity [13,14]. A computer-controlled measurement-system and implantable electric field probes were utilized in obtaining detailed maps of the SAR in a full-scale model of the human body [15,16].

In this paper we present the calculations and measurements of the spatial distribution and average SARs for various body parts for a full-scale model of man exposed in the near field of a resonant dipole at 350 MHz. The frequency of 350 MHz was selected because of the previously reported resonance of the head [17], and because it is relatively close to the frequencies used in FM portable/mobile radio (403-430 MHz). The results obtained by the two methods are compared, and limitations and advantages of both methods are outlined.

II. CALCULATIONS

The electric fields and therefore the SAR distribution inside a model of the human body near a dipole antenna are calculated by the tensor integral method described in detail in [13] and briefly in [14]. The human block model consists of 180 cubical cells of varying sizes arranged to best fit the contour of a 70 kg man [7]. Because of body symmetry, only the values within one half of the body are presented. A thin resonant dipole is located close to the head in a location whose coordinates are given in Table 1. Other essential exposure and model parameters are also summarized in Table 1.

III. MEASUREMENTS

The electric field intensity was measured, and the SAR subsequently calculated in more than 650 locations within half of the model of the human body. An implantable isotropic electric field probe, EIT, model 979 (manufactured by Electronic Instrumentation and Technology, Inc., 1439 Sheppard Ave., Sterling, VA 22170) was used. The probe was fully evaluated and calibrated prior to the experiment [18] and the calibration was spot checked during the measurements. The computer-controlled scanning system [15,16] performed a set of measurements at 650 locations in less than 1.5 hours. The repeatability of the SAR measurements was better than $\pm$0.5 dB, as tested on up to 15 repetitions under various power levels and on various days. The uncertainty of the SAR determination was estimated to be approximately $\pm$1 dB. The main contribution to the SAR measurement uncertainty was due to the limitations of performance of the electric field probe and its calibration [18]. Each data point presented in this paper is an average of four to five measurements.

A full-scale model of an anatomically proportional average man (175 cm, 70 kg based on a plastic model Remcal, manufactured by Alderson Research Lab. Inc., Stamford, Conneticut) was made of low density Styrofoam sheets 2.5 cm thick, which were glued together. The model was positioned horizontally (face up) in an anechoic chamber (dimensions 4.6 x 3 x 2.1 m). The antenna was placed under the model, and the electric field probe was immersed in the model from its top. The distance between the chamber floor, which was covered with RF absorber, and the antenna was 60 cm (from the absorber); the distance

between the mold and the chamber walls and ceiling was 1.5 m or more. The reflections from the chamber walls, floor and ceiling were measured, and were found to be below -20 dB at a frequency of 350 MHz.

The mold was partly open in the torso area, and holes large enough for inserting the probe were drilled in other locations, more details about the mold are given elsewhere [16]. The mold was filled with a low viscosity (to facilitate probe immersion) mixture having average tissue properties (2/3 muscle tissue) at a frequency of 350 MHz (Table 1). Essential model and exposure parameters are given in Table 1. The resonant dipole was shortened to 0.43λ, to achieve matching to a 50Ω transmission line. The dipole input VSWR was less than 1.2 with the model of man placed at a distance of 8 cm.

IV. RESULTS AND DISCUSSION

The measured local values of the SAR in the center cross-section of the model (dashed lines) are compared with the calculated SAR values in the corresponding cells (solid-line bars), as illustrated in Figure 1. The contours of the two models were matched along the main axis of the body. A small difference (less than 3%) in the height of the two models (see Table 1) resulted mainly from the curvature of the head. When the measured location was on the border of two cells or very close to it, the average SAR for the two cells was utilized for the comparison. Both the calculated and the measured SAR values were normalized to 1 W input power to the dipole. It can be seen that the theoretical and measured SARs in the neck region in the center of the body are in reasonably good agreement. However, overall, the spatial distribution of the SAR predicted by the calculation is

significantly different from the measured values, with differences of an order of magnitude at some locations (notice the logarithmic scale). This may be an unfair comparison, as the local values of the SAR within spheres of a diameter of 0.9 cm (the probe diameter) are compared with the average values in cubes of approximately 7 cm (the average cell size). In the comparisons that follow the calculated values are compared with the measured values averaged over certain volumes.

Figure 2 shows a comparison of the spatially averaged calculated and measured SARs along two selected body axes. The SAR values are, in both cases, averaged over the tissue volume contained between the body surfaces in the direction of the wave propagation. This means that the values are the averages over two or three cells, except in the legs, for the calculated SARs, and the averages over the cylindrical volume of 0.9-cm diameter for the measured SARs. Since the probe did not penetrate to the very bottom of the back surface of the mold appropriate curves (exponential) were fitted to the measurement points using the least-square method to calculate SARs at the model surface. These data points together with the measured SAR values were used to calculate the average SARs.

The general shape of both spatial distributions looks similar. It is clear that the theory does not predict to the same extent an increase in the SAR in the neck region. However the largest differences between the predicted and measured values are about 5 to 6 times rather than 10, as it was for the previous comparison (see Figure 1).

A much better agreement between the theory and the experiment can be seen in the SAR values averaged over the horizontal tissue

layers presented in Figure 3. The arms are not included in these averages. The calculations in this case underestimate the maximum SAR in the neck by a factor of three.

The whole-body average SARs calculated and measured are 7.9 and 6.3±1.2 mW/kg, respectively. The difference is within the uncertainty of measurements (because of the extrapolation involved the accuracy of the whole-body average estimated at ±25% is much worse than that of the local SARs) and can be attributed to the difference in the distance between the dipole and the body in the calculations and experiment (7.3 vs. 8 cm). As an example of regional SAR differences, the head/neck area calculated average SAR is 17 mW/kg, while the measured value is 28 mW/kg. The difference in this case is relatively large, but consistent with previously noted differences in the spatial distribution of the SAR. The SAR in the neck is extremely sensitive to the shape of the neck.

A very important feature of the RF energy deposition in the human body in the near-field of radiators at 350 MHz, which is not evident from the analysis of the block model of man, is illustrated in Figure 4. This figure shows the SAR in the torso on the center point of the dipole along the direction of the wave propagation. The dipole center point is located at 38 cm from the head top. The wave is incident at the torso wall at z = 20 cm and the torso extends to approximately z = 0. The vertical columns show the calculated SAR in the three body cells, the points show the experimental data. The dashed line represents a least-square fit of an exponential relationship

$$SAR = A \exp(-\alpha z) \qquad (1)$$

Two important observations can be made. Firstly, at a frequency of 350 MHz the SAR decreases exponentially in the torso within about one-half of the torso width. Beyond that point the SAR values are very low, more than 100 times below those on the surface. Furthermore, the attenuation coefficient, $\alpha = 0.46 \pm 0.01$ is, within the fitting error, equal to that calculated for the planar model with electrical properties of the tissue simulating material, $\alpha = 0.49 \pm 0.02$. Secondly, the theory does not show the decrease of the SAR with distance away from the plane of the incident wavefront. It is apparent from Figure 4, that the average SARs for the layers of about 7 cm corresponding to the cells width are significantly different, particularly for the two outer cells. The exponential decay in the SAR is typical for other locations along the torso and the head. Only in the center of the neck, 150 cm from the feet base, can an increase in the SAR close to the neck center be observed (Figure 5). The SAR close to the neck center is approximately 50 mW/kg, as compared with 440 mW/kg at the neck surface and the average SAR of 115 mW/kg for the cylinder of 0.9 cm in diameter on the neck axis between the neck surface of the wave incidence and the opposite surface.

Our results are to certain extent different from the previously reported agreement between the calculated and measured SAR distributions [4-6]. However, the comparisons were done for much simpler shapes and different exposure conditions. The reported agreement is even more impressive in view of a relatively simple

electric field probe that was used for the measurements reported in [4,6]. On the other hand for more realistic models, for some regions such as the neck, differences of the order of 10 to 20 between the calculated and measured values of the SAR were previously reported [7].

We feel that the differences between the calculated and the measured values of the SAR are due to the limitations of the calculations, because the accuracy of the measurements was verified using simple geometrical bodies [19]. Although it was stipulated that the analysis of the block model of man can be used up to 500 MHz [4-7], the limits on the cell size were suggested [20]. The cell size used in our calculations is greater than the suggested limit [20]. Furthermore, other deficiencies of the numerical analysis using the cubical block model of man in calculating the SAR distribution have recently been suggested [21]. These, however, have also been questioned [22].

V. CONCLUSIONS

The specific absorption rate (SAR) averaged over various body volumes and the spatial distributions of the SAR calculated and measured were compared for the near-field exposure by a resonant dipole at 350 MHz. The calculations were performed using the method of moments to solve the tensor integral equations for a block model of man consisting of total of 180 cubical cells. A computer-controlled scanning system and an implantable electric field probe were used to measure local values of the SAR in 650 locations within half of the model of a human body with an uncertainly of approximately ± 1 dB.

The whole-body average SARs obtained by both methods are in a

good agreement. The values of the SAR averaged over smaller volumes and the spatial distribution of the SAR are different by factors ranging from 3 to 10. The theoretical analysis does not predict an exponential decrease in the SAR values in the direction of the wave propagation away from the surface upon which the wave is incident. Relatively large spatial gradients of the SAR are similarly not apparent from the calculations.

The main limitations of the calculations result from a relatively small number of blocks and the resulting relatively large size of the blocks as compared to the wavelength in the tissue [20]. Furthermore, limited accuracy is inherent in the method employed [21]. Differences in the shapes of the models may play some role, but probably less significant than the other factors. The neck may be considered as the region where shape differences have been sufficiently large, to affect the SAR.

In view of the computational difficulties in extending the available theoretical methods to more refined realistic models of the human body, at present experimental methods appears to be a viable alternative for determination of the spatial distribution of the SAR in models of humans exposed in the near-field of radiofrequency antennas.

FIGURE CAPTIONS

1. Comparison of the specific absorption rate (SAR) calculated and measured along selected axis shown by vertical dashed lines. Blocks represent the calculated values, while the measured values are depicted by horizontal dashed lines, for f = 350 MHz, 1 W input power to the antenna, E polarization, and for the location of the dipole given in Table 1.

2. Comparison of the calculated and measured specific absorption rate (SAR) averaged along the direction of the wave propagation (perpendicular to the axis of the body). The blocks show the calculated values, averaged over the cells in the direction of wave propagation, and the points represent the measured data averaged over cylinders 0.9 cm in diameter, for f = 350 MHz, 1 W input power to the antenna, E polarization, and for the location of the dipole given in Table 1.

3. Comparison of the specific absorption rate (SAR) averaged over horizontal tissue layers. The blocks show the calculated values, and the points the measured data, for f = 350 MHz, 1 W input power to the antenna, E polarization, and for the location of the dipole given in Table 1.

4. The specific absorption rate (SAR) on the dipole axis in the torso. The blocks show the calculated values, the points the measured data, the straight line shows the least square fit into

data points for $z \geq 8$ cm of the curve SAR = A exp ($-\alpha z$). The body surface at which the wave is incident is at z = 20 cm, and the wave propagates toward z = 0, with f = 350 MHz, 1 W input power to the antenna, E polarization, and for the location of the dipole given in Table 1.

5. The specific absorption rate (SAR) in the neck. The points show the measured data at the height 150 cm from the feet base, the neck surface at which the wave is incident is at z = 12 cm, and the wave propagates toward z = 0, with f = 350 MHz, 1 W input power to the antenna, E polarization, and for the location of the dipole given in Table 1.

REFERENCES

1. Radiofrequency electromagnetic fields; properties, quantities and units, biophysical interactions and measurements. NCRP Report No.67, 1981.

2. Safety levels with respect to human exposure to radio frequency electromagnetic fields, 300 kHz to 100 GHz. ANSI C95.1-1982.

3. W.R. Adey, "Tissue interactions with non-ionizing electromagnetic fields", Physiol. Rev., Vol.61, pp.435-513, 1981.

4. B.S. Guru and K.M. Chen, "Experimental and theoretical studies on electromagnetic fields induced inside finite biological bodies", IEEE Trans. Microwave Theory Tech., Vol. MTT-24, pp.433-440, 1976.

5. K.M. Chen and B.S. Guru, "Induced electromagnetic field and absorbed power density inside human torso. IEEE Trans. Microwave Theory Tech., Vol. MTT-24, pp.1450-1453, 1976.

6. K.M. Chen and B.S. Guru, "Internal EM field and absorbed power density in human torso induced by 1-500 MHz EM waves", IEEE Trans. Microwave Theory Tech., Vol. MTT-25, pp.746-756, 1977.

7. M.J. Hagmann, O.P. Gandhi and C.H. Durney, "Numerical calculation of electromagnetic energy deposition for a realistic model of man." IEEE Trans. Microwave Theory Tech., Vol. MTT-27, pp.804-809, 1979.

8. I. Chatterjee, M.J. Hagmann and O.P. Gandhi, "Electromagnetic energy deposition in an inhomogeneous block model of man for near-field irradiation conditions." IEEE Trans. Microwave Theory Tech., Vol. MTT-288, pp.1452-1459, 1980.

9. R.J. Spiegel, "A review of numerical models for predicting the energy deposition and resultant thermal response of humans exposed to electromagnetic fields", IEEE Trans. Microwave Theory Tech., Vol. MTT-32, pp.730-746, 1984.

10. C.H. Durney, "Electromagnetic dosimetry for models of humans and animals: A review of theoretical numerical techniques". Proc. IEEE, Vol.68, pp.33-40, 1980.

11. O.P. Gandhi, "Electromagnetic absorption in an inhomogeneous model of man in realistic exposure conditions". Bioelectromagn., Vol.3, pp.81-90, 1982.

12. A.W. Guy, "Analysis of electromagnetic fields induced in biological tissues by thermographic studies in equivalent phantom models", IEEE Trans. Microwave Theory Tech., Vol. MTT-19, 205-214, 1971.

13. K. Karimullah, K.M. Chen, and D.P. Nyquist, "Electromagnetic coupling between a thin-wire antenna and a neighboring biological body: theory and experiment". IEEE Trans. Microwave Theory Tech., Vol.MTT-28, pp.1218-1225, 1980.

14. R.J. Spiegel, "The thermal response of a human in the near-zone of a resonant thin-wire antenna", IEEE Trans. Microwave Theory Tech., Vol.MTT-30, pp.177-185, 1982.

15. S.S. Stuchly, M. Barski, B. Tam, G. Hartsgrove and S. Symons, "A computer-based scanning system for electromagnetic dosimetry", Rev. Sci. Instrum., Vol.54, pp.1547-1550, 1983.

16. A. Kraszewski, M.A. Stuchly, S.S. Stuchly, G.Hartsgrove and D. Adamski, "Specific absorption rate distribution in a full-scale model of man at 350 MHz", IEEE Trans. Microwave Theory Tech., Vol.MTT-32, pp.779-783, 1984.

17. M.J. Hagmann, O.P. Gandhi, J.A. D'Andrea and I. Chatterjee, "Head resonance: numerical solutions and experimental results", IEEE Trans. Microwave Theory Tech., Vol.MTT-27, pp.809-813, 1979.

18. M.A. Stuchly, A. Kraszewski and S.S. Stuchly, "Implantable electric field probes - some performance characteristics", IEEE Trans. Biomed. Eng., Vol.BME-31, pp.526-530, 1984.

19. C.H. Wong, S.S. Stuchly, A. Kraszewski and M.A. Stuchly,

"Probing electromagnetic fields in lossy spheres and cylinders", IEEE Trans. Microwave Theory Tech., Vol. MTT-32, pp.824-828, 1984.

20. M.J. Hagmann, O.P. Gandhi and C.H. Durney, "Upper bound on cell size for moment-method solutions", IEEE Trans. Microwave Theory Tech., Vol. MTT-25, pp.831-832, 1977.

21. H. Massoudi, C.H. Durney and M.F. Iskander, "Limitations of the cubical block model of man in calculating SAR distributions", IEEE Trans. Microwave Theory Tech., Vol. MTT-32, pp.746-751, 1984.

22. M.J. Hagmann, Comments on "Limitations on the cubical block model of man in calculating SAR distributions", IEEE Trans. Microwave Theory Tech., Vol.MTT-33, pp.347-350, 1985.

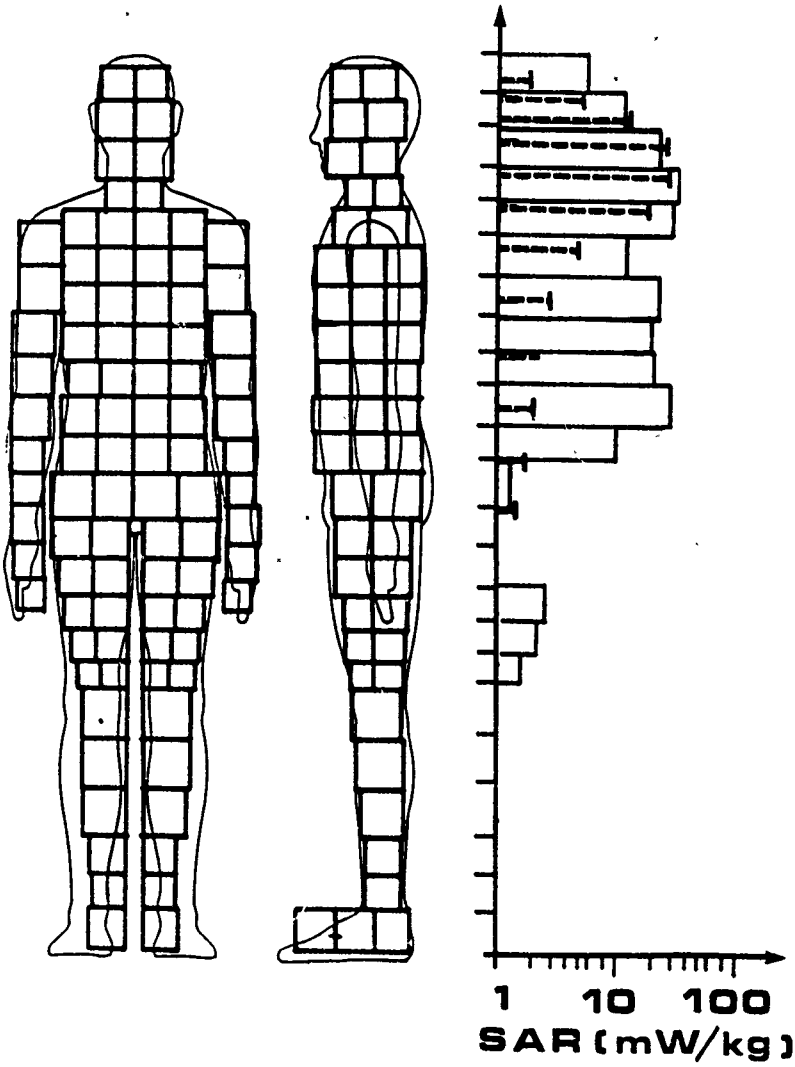
1
10
100
SAR (mW/kg)

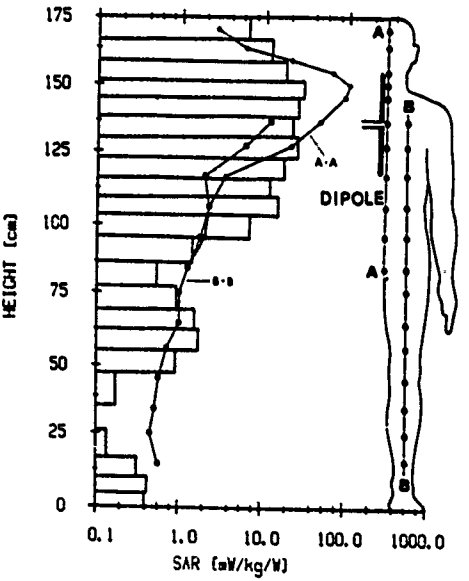

Fig 2

Hendy et al

Near-field comparison

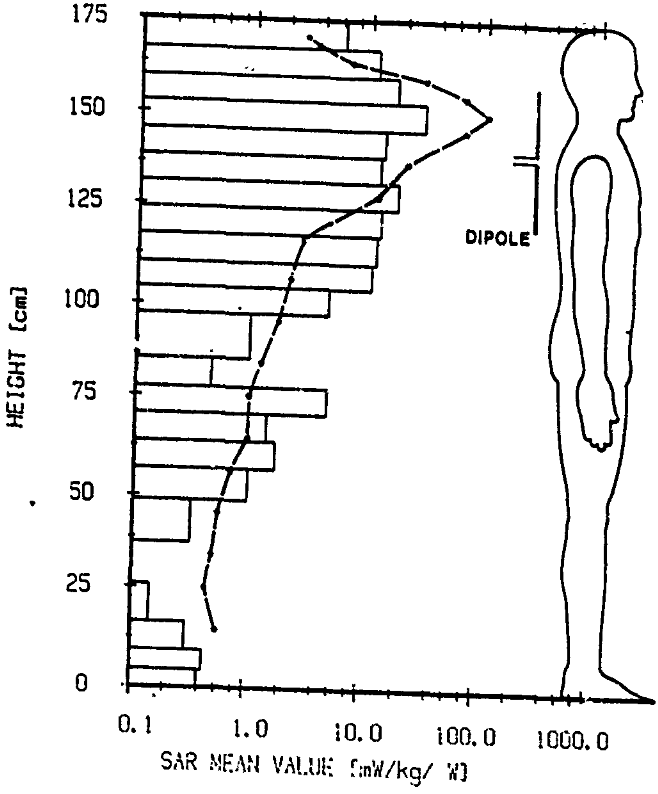

[illegible] et al

[illegible] field comparison

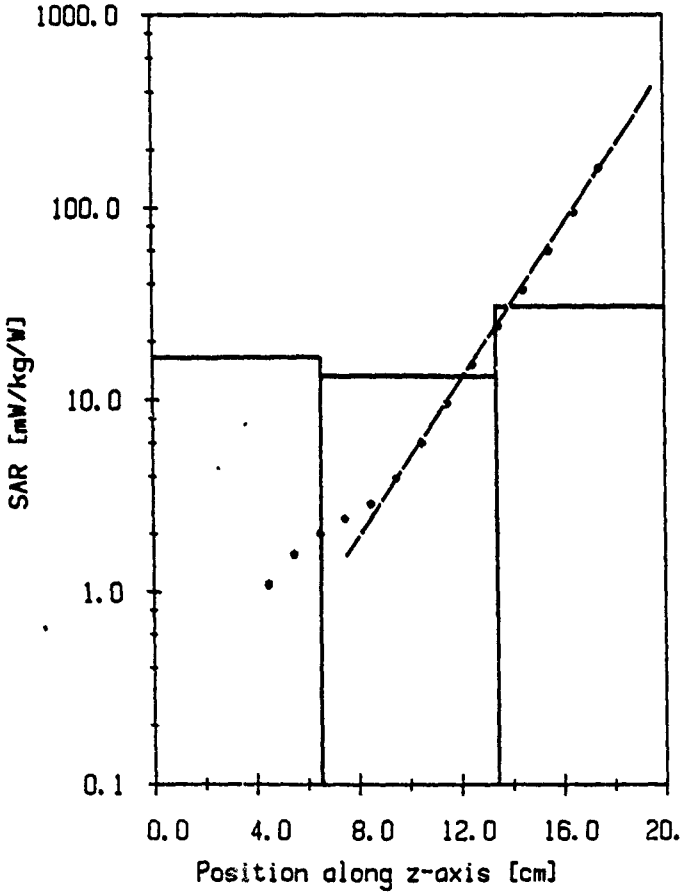

Fig 4

Smythe, et al

Near field comparison

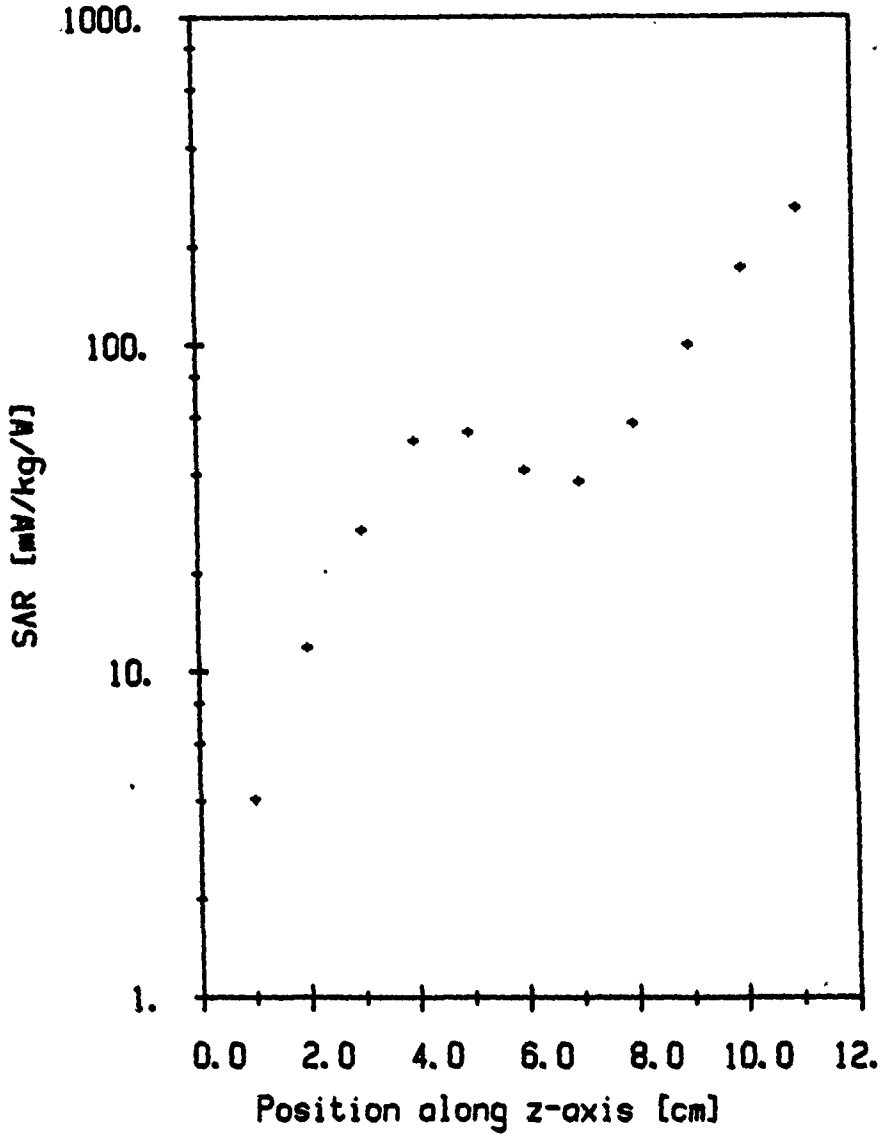

Fig 5

Pinney et al

Near field comparison

Table 1.

Essential Model and Exposure Parameters

Parameter	Calculations	Experiment
Frequency	350 MHz	350 MHz
Actual dipole length	0.5 λ	0.43 λ
Dipole length/radius	200	117
Input impedance	48.3 Ω	50 Ω
Distance from the body	7.3 cm	8 cm
Distance dipole axis/head top (vertically)	34.8 cm	38 cm
Model height	170 cm	175 cm
Dielectric constant	37	37
Conductivity	0.95 S/m	0.95 S/m

ENERGY DEPOSITION IN A MODEL OF MAN;

FREQUENCY EFFECTS

S.S. Stuchly, M.A. Stuchly*, A Kraszewski and G. Hartsgrove

Dept. of Electrical Eng., University of Ottawa, Ottawa, Ont. Canada

*Radiation Protection Bureau, Health and Welfare Canada, Ottawa, Ont. Canada

ABSTRACT

A computer-controlled scanning system and implantable, nonperturbing electric field probes were used to measure spatial distributions of the electric field in a full scale homogeneous model of a human body. The measurements were performed at three frequencies (160, 350 and 915 MHz) in the far-field and in the near-field of resonant dipoles. The specific absorption rate (SAR) distributions and the averages for body parts and the whole body are analyzed as functions of frequency. In the far-field, the SAR decreases exponentially in the direction of wave propagation in the torso at all frequencies, and large gradients of the SAR are observed along the body main axis, particularly for the E polarization. At 160 and 350 MHz high local SARs are produced in the neck. It appears that for plane wave exposures the ratio of the peak SAR to the whole-body average SAR does not exceed 20, In the near field, large SAR gradients are also produced, and the ratios of the peak spatial SAR to the whole-body average SAR vary from about 30 to 250 depending on the frequency and polarization. It is suggested that for near-field exposures the whole-body average SAR is not a proper dosimetric measure, and the SAR averaged over any 0.1 of the tissue volume is recommended instead.

This work was supported by grants from the U.S. Office of Naval Research, Health and Welfare Canada and Natural Sciences and Engineering Research Council of Canada.

I. INTRODUCTION

To quantify interactions of radio waves with biological systems, it is important to know both spatial distributions and average values of the specific absorption rate, SAR, [1]. Various theoretical and experimental methods have been developed and used for this purpose, as reviewed elsewhere [2-4]. Recently, an experimental technique, which utilizes implantable nonperturbing electric field probes and a computer-controlled scanning system, was used to obtain SAR distributions in a full scale model of man at 350 MHz in the far-field [5], and at 350 MHz and 915 MHz in the near-field [6,7]. A homogeneous model certainly has some limitations, particularly at 915 MHz, where for instance layered structure has been shown to increase absorption efficiency [8].

In this paper we report new results of measurements at 160 MHz in the far- and the near-fields, the far-field measurements at 915 MHz and discuss effects of frequency on the SAR distribution and various SAR averages at the three frequencies investigated, namely 160, 350 and 915 MHz. The average values and spatial distributions of the SAR in the far-field are also compared with the previously published theoretical and experimental data.

II. MEASUREMENT METHOD

The measurement system was described in our earlier publications [7,9]. Models of man were made of thin plastic (1.5 mm) (160 MHz and 915 MHz) or low density styrofoam (350 MHz). The dimensions of the model corresponded to a 50 percentile man (175 cm, 70 kg). The models were filled with a semi-liquid tissue-equivalent material having electrical properties

given in Table 1, corresponding to those of the average tissue at a given test frequency. More details about the models are given in [7].

All measurements were performed in an anechoic chamber. The reflections were less than -16 dB at frequencies above 100 MHz.

Far-field exposure conditions were produced by antennas located at sufficiently large distances from the model surface. The power density at the model location was measured with an uncertainty of about 10% without the model in place. Since the antennas produced non-planar wavefronts, corrections were introduced to normalize the SAR data to 1 mW/cm^2 of the incident power on the model surface closest to the antennas as described elsewhere [7]. For resonant dipoles the spatial distribution of the fields was calculated from using well known analytical expressions and incorporated into the data processing routine as a correction factor. Theoretical calculations were also verified experimentally.

For measurements in the near-field, resonant dipoles were positioned as illustrated in Fig. 1. Two polarizations were used. For the E polarization the antenna was placed parallel to the long body axis while for the H polarization the antenna was positioned perpendicular to the axis, shoulder-to-shoulder. Table 2 gives the geometrical coordinates and characteristics of the antennas.

The SAR was calculated using the three components of the electric field which were measured with an electric field probe as described in [7]. The estimated uncertainty of measurements of local SARs was about 12%, and of average SARs about 25%. The latter uncertainty includes both the uncertainty in measurements and in calculation of averages using a finite number

of measurement points. The values of the SARs for each exposure were determined in approximately 650 points within one-half of the model.[1])

In order to calculate the averages for the body parts and the whole body averages the model was divided into 23 slices perpendicular to the main body axis as shown in Fig. 1. In each slice, the field measurements were done in several locations as described in Table 3. In each of the test locations electric fields were measured in several points, separated by 1 cm, along the direction of propagation. Due to the mechanical and electrical limitations of the model and the electric field probes it was not possible to probe the fields very close to the irradiated surface of the model (closer than 1 to 2 cm) and therefore, the electric fields on and in the immediate vicinity of the irradiated surface were obtained by extrapolation of the fields measured deeper in the model. Since in the majority of the test locations the electric fields decay exponentially (see Table 4) a simple expression $E^2 = E_0^2 \exp(-\alpha z)$ was used, where E_0 is the electric field on the irradiated surface, α is the attenuation coefficient (see Table 4) and z is the distance along the direction of propagation. In a few test locations a linear or a polynomial extrapolation was found to be more appropriate. Although the curvature of the body can potentially affect the SAR close to the surface, we were not able to notice such behaviour for the homogeneous model.

By selecting an appropriate number of points in the direction of wave propagation in each of the test locations (Fig. 1), the model was divided into 4×4×1 cm and 10×10×1 cm blocks. The average SARs were calculated in each block and then partial body SARs were calculated. The average whole body SARs were obtained using the "rule of nines" which gives an estimate of

[1]) The model was assumed to be symmetrical with respect to the main plane.

the contributions of various parts to the total weight of the human body (see Table 3)[10].

III. FAR-FIELD EXPOSURES

At all test frequencies an exponential decay of the SAR in the torso in the direction of the wave propagation was observed. The attenuation coefficient was found equal to that of a plane wave propagating in a semi-infinite slab having the same electrical properties as the torso. The pertinent data are summarized in Table 4. However, the SAR distribution along the main body axis is much more complex, and even a relatively sophisticated analysis utilizing a block model of man consisting of a few hundred cells does not provide reliable data as found at 350 MHz [5].

Figure 2 illustrates maximum values of the SAR anywhere on the body surface, for two polarizations[1]). At 915 MHz the maximum SAR on the surface is not much different for the two polarizations. At 160 MHz and 350 MHz for the E polarization high SARs occur on the surface of the neck. However, for the torso the SARs on the surface are not much different at all three frequencies.

In general, for the E polarization at all test frequencies (and it may be inferred at all frequencies between 160 and 915 MHz), higher than whole-body average SARs are deposited in the neck. The location and magnitude of the maximum is, frequency dependent. Figure 3 shows the SAR distri-

[1]) The data on the surface were obtained by extrapolation of the data measured inside the model at several depths.

bution along the main body axis for the E polarization. The mean values averaged over the tissue slices perpendicular to the main body axis are shown. The mean SAR in the neck decreases with frequency from about 1000 mW/kg at 160 MHz to about 70 mW/kg at 915 MHz for an incident power density of 1 mW/cm^2. The high mean SAR values do not necessarily reflect high SARs ("hot spots") in the center of the neck, as illustrated in Figures 4 and 5. For instance, at 350 MHz the maximum SAR of over 400 mW/kg is located in the neck center, as compared with the mean of about 200 mW/kg, while at 160 MHz the SAR in the neck center is 900 mW/kg while the mean is 1000 mW/kg.

Figures 3 and 4 also illustrate that relatively high SARs are produced in the legs. This is even more clearly visible from Figure 6 showing contributions of rates of energy deposition in various parts of the body as a fraction of the whole body average power absorbed. A conclusion can be drawn, that at all frequencies higher SARs are produced in the legs than in the torso (the weight of the legs is equal to that of the whole torso, see Table 3).

Figure 7 shows the whole-body average and the head-neck average SARs. It can be seen that 2 to 2.5 times greater rates of energy deposition occur in the head at 160 and 350 MHz, but not at 915 MHz, and only for the E polarization. The latter data are compared in Table 5 and Figure 8 with theoretical results published earlier [11-13].

IV. NEAR-FIELD EXPOSURES

Similarly as in the far-field, the SAR on the dipole axis decays exponentially in the direction of propagation with an attenuation coeffi-

cient very close to that of a plane wave, see Figure 9 and Table 4. This behaviour is characteristic for resonant dipoles placed at distances of one tenth or more from the body surface, as analyzed in detail at 350 MHz in [6]. For other types of antennas the situation can be different because of the amount of energy contained in evanescent waves [14]. The maximum SAR on the body surface is on or very close to the antenna axis. The frequency dependence of the maximum SAR on the body surface (shown in Figure 9 for the E-polarization; similar values of the SAR on the body surface were also obtained for the H polarization) is quite different from that in the far-field (Figure 2). The differences in the normalized distances between the antenna and the body surface at all three frequencies are small (0.09 to 0.15 λ, Table 2), so these differences cannot account for the differences in the SARs.

Figures 10 and 11 show the local values of the SAR in the body mid-plane at three frequencies, for the E and H polarizations, respectively. At all frequencies coupling of energy is stronger in the E polarization (Figure 10) than in the H polarization (Figure 11) by a factor from about 4 to 10. Generally, the energy is deposited in the tissue relatively close to the antenna at much greater rates than in remote parts of the body, e.g. legs. As may be expected, the lower the frequency the more energy deposited further away from the antenna.

Figure 12 shows the SARs averaged over tissue slices perpendicular to the main body axis for resonant dipoles in the E-polarization. The maximum SAR in the tissue slice is produced in the slice facing the antenna axis for the H polarization and the E polarization in all cases except when the

antenna is located close to the neck at 160 and 350 MHz. There is no apparent correlation in the shape of the SAR distributions along the main body axis and the frequency. Similarly, the maximum SAR in the tissue slice (Figure 13) does not appear to be correlated with frequency or polarization. However, there is an apparent correlation between the SAR profiles in the torso cross-sections perpendicular to the main body axis and the frequency, as illustrated in Figure 14. This figure shows the iso-SAR curves for 500, 100, 20 and 4 mW/kg for 1 W input power to the antenna. The data presented in this figure may be useful in designing applicators for inducing hyperthermia in various volumes of tissue by use of radiofrequency energy.

In the near-field most energy is deposited in the tissue volume close to the antenna location. This is clearly shown in Figures 12 and 15. At all three frequencies, the dipoles were placed in the upper shoulder area (Table 2), and consequently most of the energy was deposited in the head-and-neck and upper torso. It is interesting to note, that as in the far-field at 160 and 350 MHz and the E polarization (Figure 7), the head-and-neck SARs are considerably greater than the whole-body-average SARs (Figure 15).

IV. DISCUSSION

A. Measurement Method

The experimental method used in this study was developed with the main objective of providing data on distributions of the SAR in the near-field of various devices, such as portable transmitters, leaky transmitter cabinets, hyperthermia applicators, etc. For such applications the thermo-

graphic dosimetry method [15, 16] has considerable limitations. The most serious limitation is due to the required high radiated power, so that a short exposure (about 20s [15]) is sufficient to obtain the required temperature increase in the tissue-equivalent material. Other limitations are related to the difficulties in scaling near-field exposure conditions for more complex antennas. For far-field exposures the superiority of one method over the other is debatable, as both have their advantages and limitations. The thermographic technique, particularly with the improved iterative computer data processing [15], provides a complete profile of the SAR in any selected plane. However, in practical situations investigations are limited to one and sometimes two or three planes.

In the implantable electric field probe technique, measurements are performed in various planes, but because of practical constraints electric fields are measured at a limited number of points and therefore the resolution in any cross-section is limited. As a consequence of the method limitations, we have selected a large number of measurement points in anatomically important locations such as the head, neck and torso, at the expense of a relatively small number of points in the legs and arms. The selection was made arbitrarily, as we considered "hot spots" in the limbs of less importance. The limited number of points has also affected the uncertainty in calculated average SARs. For the worst case, i.e. whole body, the legs, and the arms, an estimate is 25%, but for the head and neck and torso it is 15%. The latter is determined to a large extent by the accuracy of the electric field probe calibration of 12%.

The implantable probe technique can also be used for inhomogeneous models, as the probe calibration factor should not depend on the permittivity of the material in which the probe is immersed; at least for insulated probes [17]. However, a careful evaluation of the probe behaviour at interfaces between different tissues will have to be performed.

The accuracies of the two methods are similar, as compared in measurements of the SAR distribution in spheres [18,19]. In the thermographic method the measured peak SAR values are in some cases (for small spheres) lower by about 20% than the actual values [18]. In the implantable-probe method the peak SAR values are very accurately reproduced, but some errors may be introduced when the probe size is large compared with the object size [19].

Far-field Exposures

The exponential decrease of the SAR in the torso for far-field exposures is a significant finding, indicating that at frequencies above 160 MHz a simple model can be used to predict theoretically the SAR distribution in the direction of wave propagation. Although not explicitly analysed, the exponential decay of the SAR was observed experimentally by others at 1.29 and 2 GHz [20, 21]. At these frequencies, and at 915 MHz, as indicated by our measurements, the SAR in the head and the legs also decays exponentially for a homogeneous model. This would indicate that simple calculations can be used to account for tissue layering, i.e., the skin, bone, fat, etc.

At all frequencies, there are gradients of the SAR along the main body axis. In the far-field these gradients are much greater for the E-polarization than the H polarization at all test frequencies. This observation is in agreement with the experimental data obtained thermographically at 450 MHz [15]. For all test frequencies which are above the whole-body resonant frequency of about 80 MHz [2,11,13] for the E polarization in the far-field, there appears to be certain consistency in the SAR distribution. When rates of energy deposition in the body parts (Fig. 6), the tissue layer average SARs (Fig. 3) and the local values of the SAR in the body mid-section (Fig. 4) are scrutinized, it is apparent that large SARs are produced in the head-and-neck, and the legs. Also large SARs occur at 160 and 350, but not at 915 MHz, in the arms. These observations are again consistent with the data at 450 MHz [15].

The mean SAR in the slice about 4 cm thick in the neck is about 10 times greater then the whole-body average SAR at 160 MHz, about 5 times at 350 MHz, and about 3 times at 915 MHz for the E polarization. Only in the legs and possibly arms (not investigated in detail) at 350 and 915 MHz are the SARs in the slices comparably large. It is also interesting to note, that the distribution of the SAR across the neck is strongly frequency dependent (Fig. 5). While the mean SAR in the neck at 350 MHz is less than at 160 MHz, the maximum SAR is produced close to the center. The value of the SAR in the neck center at 350 MHz is about 400 mW/kg at 1 mW/cm^2 of the incident power. At 160 MHz the maximum SAR is of 1.67 W/kg occurs on the surface while it is about 0.9 W/kg in the center (Fig. 5).

It appears that at frequencies above 160 MHz in the far-field, in spite of large SAR gradients, local values of the SAR are only up to about 20 times the whole-body average SAR. The condition on which the ANSI exposure standard [22] is based, i.e. the peak local SAR less than 8 W/kg, is not exceeded at least for a homogeneous model. This is to a large extent due to low whole-body average SARs, below 0.11 W/kg, at those frequencies. The results obtained at frequencies between 160 and 915 MHz, suggest that investigations of the SAR distribution should be carried out also below 160 MHz, close to the resonant frequency of the body. At those frequencies the SARs in the neck may reach even higher values. Presently available theory offers little guidance in this respect. As it may be seen from Table 5, the head and neck SAR at 160 MHz estimated from calculations [11] is 3 to 5 times lower than the measured value. A good agreement between the calculations and measurements for head and neck at one frequency (350 MHz, Table 5) does not provide a solid argument for the accuracy of the calculations.

The measured whole-' 'erage SARs (Fig. 8) are relatively close to the calculated values for spheroidal models [2, 13]. Figure 8 depicts the theoretical predictions for an average and ectomorphic man, our experimental data (at 160, 350, 915 MHz) and those reported by others (40 MHz [23], 450 MHz [15], 1.29 GHz [14] and 2 GHz [21]). The data point at 2 GHz appears to be highly questionable, large errors were likely as a result of calculation of the average based on a relatively small number of points [21]. For both polarizations (E and H) the measured SAR is higher than the predicted (our data points at 350 and 915 MHz are somewhat lower; it may be

due to the uncertainties in our calculations of the average SAR in the legs, whose contribution to the total SAR increases with frequency, as shown in Fig. 6). As pointed out previously [15], when a large part of energy is absorbed in the legs (Fig. 6), the shape of the model plays significant role in determining the average SAR. A spheroid is obviously very different in shape. Less apparent but equally important are the differences in the shape between the block model of man and the actual man geometry, particularly when a small number of cells are used to represent the legs.

C. Near-field Exposures

At all frequencies investigated for near-field exposures with the antenna-body surface separation of about one tenth of the free-space wavelength, energy deposition is mostly concentrated within a limited volume, close to the antenna, i.e. for the positions of the antennas reported here in the neck-head and upper torso (Fig. 15). The width of the SAR distribution (Figures 10, 11, 12) is not strongly dependent on frequency. At two frequencies (160 and 350 MHz) for the E polarization the maximum SAR is shifted off the antenna axis toward the neck, when the antenna axis is positioned on the shoulder level (similarly to the far-field exposure).

For resonant dipoles in the H-polarization the SARs in the neck-head region are comparable with the whole-body averages (Fig. 15). However, in the E polarization, at 160 and 350 MHz, the SAR in the head-and-neck is about five times greater than the whole-body average. Because of highly localized energy deposition for near-field exposures, in our view the whole-body average SAR is not the most suitable parameter for quantification of exposures. The SAR averaged over any 0.1 of the body mass is suggested as a better dosimetric measure.

The maximum mean SARs in tissue slices (see Table 3) is between 10 to 30 times greater than the whole-body average SAR (Figures 13 an 15). There is no consistent frequency dependence.

The ratio of the local peak SAR to the whole body average SAR can be very high at all frequencies and both polarizations. The ratio increases with frequency from about 30 to 140 at 160 MHz, to 150 to 190 at 350 MHz, to 200 to 250 at 915 MHz. The local peak SARs are invariably at the body surface.

As indicated in our earlier publications [6, 7], the high SARs at the body surface at 350 and 915 MHz, as compared with the whole-body averages results in the ANSI peak local limit of 8 W/kg [22] being exceeded for very moderate levels of input power to the antennas, while large antenna power is required to exceed the average SAR limit of 0.4 W/kg [22]. The situation is less critical at 160 MHz for a resonant dipole, however this conclusion must not be extended to other types of antennas. It was earlier indicated that antenna type, not only its gain, play a crucial role in how efficiently the energy is coupled to the body [6].

D. General Remarks

The ANSI exposure standard [22] was based on the theoretical prediction that for plane waves the local peak SAR is about 20 or less times the whole-body average SAR. Our experimental studies, at least at frequencies above 160 MHz for a homogeneous model of man confirm this estimate. This conclusion may not be valid for an inhomogeneous model and also at frequencies close to or below the resonance. There is actually already some evidence for a man standing on a ground plane, the local SAR in the ankles is more than 20 times the average at and below the resonance for the E polarization [23].

In the near-field, the whole-body average SAR may not be a proper dosimetric measure, as most of the power is absorbed in a volume not greater than one tenth of the total. Furthermore, because of very high ratios of the peak- to-average SARs and the location of the peak SAR on the body surface, the limits of exposure may have to be reevaluated. We suggest that instead of the whole-body-average SAR, the SAR averaged over any 0.1 of the tissue volume should not exceed a specified limit, whether the limit of 0.4 W/kg selected for the whole body exposures is applicable is a separate question. The local peak SAR poses a more difficult problem. Some consideration should be given regarding its location, as the same SAR on the surface of the eye for instance may have a dramatically different effect than on the surface of the torso. Selection as a reference level of the SAR averaged over 0.1 of the tissue volume instead of the whole-body average would reduce the peak-to-average ratio, for instance at 350 MHz, and E polarization from about 150 to about 40. Additional difficulty in establishing exposure limits for the near-field is due to the fact that practically all experiments with animals have been performed in the far-field.

REFERENCES

[1] Radiofrequency electromagnetic fields; properties, quantities and units, biophysical interactions and measurements. NCRP Report, No. 67, National Council on Radiation Protection and Measurements, 7910 Woodmont Ave., Washington, DC. 20014, March 1981.

[2] C.H. Durney, "Electromagnetic dosimetry for models of humans and animals: A review of theoretical numerical techniques", Proc. IEEE, Vol. 68, pp. 33-40, 1980.

[3] R.J Spiegel, "A review of numerical models for predicting the energy deposition and resultant thermal response of humans exposed to electromagnetic fields", IEEE Trans. Microwave Theory Tech., Vol. MTT-32, pp. 730-746, 1984.

[4] M.A. Stuchly and S.S. Stuchly, "Experimental radio and microwave dosimetry", In: Handbook of Biological Effects of Electromagnetic Radiation. C. Polk and E. Postow (Eds) CRC Press, Inc. 1985.

[5] A. Kraszewski, M.A. Stuchly, S.S. Stuchly, G. Hartsgrove and D. Adamski, "Specific absorption rate distribution in a full-scale model of man at 350 MHz", IEEE Trans. Microwave Theory Tech., Vol. MTT-32, pp. 779-783, 1984.

[6] S.S. Stuchly, A. Kraszewski, M.A. Stuchly, G. Hartsgrove and D. Adamski, "Energy deposition in a model of man in the near-field", Bioelectromagnetics, Vol. 6, pp.115-130,1985.

[7] M.A. Stuchly, A. Kraszewski and S.S. Stuchly, "Exposure of human models in the near-and far-field - a comparison", IEEE Trans. Biomed. Eng., Vol. BME-32, pp. 609-615, 1985.

[8] P.W. Barber, O.P. Gandhi, M.J. Hagman and I. Chaterjee, "Electromagnetic Absorption in a Multilayered Model of Man", IEEE Trans. Biomed. Eng., Vol. BME-26, pp. 400-404, 1979.

[9] S.S. Stuchly, M. Barski, B. Tam, G. Hartsgrove and S. Symons, "A computer-based scanning system for electromagnetic dosimetry", Rev. Sci. Instru., Vol. 54, pp. 1547-1550, 1983.

[10] B. Ricci, Physiological Basis of Human Performance, Philadelphia, PA: Lea and Febiges, 1967.

[11] M.J. Hagmann, O.P. Gandhi and C.H. Durney, "Numerical calculation of electromagnetic energy deposition for a realistic model of man", IEEE Trans. Microwave Theory Tech., Vol. MTT-27, pp. 804-809, 1979.

FIGURE CAPTIONS

1. Coordinates of the antenna shown here for the E polarization.

2. Maximum SAR on the body surface for the far-field exposures to 1 mW/cm^2.

3. Mean SARs averaged over tissue slices perpendicular to the main body axis, the far-field exposure in the E polarization.

4. Local values of the SAR in the mid-section of a homogeneous model of man exposed in the far-field in the E polarization.

5. Spatial profiles of the SAR in the neck for the far-field exposure in the E polarization. The wave is incident at z = 12 cm in the direction of negative z (neck diameter is 12 cm).

6. Energy deposition rates in various parts of the human body exposed in the far-field of a power density of 1 mW/cm^2 in the E-polarization. The diameter of the circles corresponds to the whole-body-average SAR.

7. Whole-body-average (low density hatch) and the head-and-neck average (high density hatch) SARs for far-field exposures to 1 mW/cm^2.

[12] O.P. Gandhi, M.H. Hagmann and J.A. D'Andrea, "Part-body and multibody effects on absorption of radio frequency electromagnetic energy by animals and by models of man", Radio Sci., Vol. 14 (65), pp. 15-29, 1979.

[13] C.H. Durney, C.C. Johnson, P.W. Barber, H. Massoudi, M.F. Islander, J.L. Lords, D.K. Riper, S.J. Allen and J.C. Mitchell, "Radiofrequency Radiation Dosimetry Handbook", Second Edition, Report SAM-TR-78-22, USAF School of Aerospace Medicine, Brooks Air Force Base, TX 78235, 1978.

[14] I. Chatterjee, O.P. Gandhi, M.J. Hagman and A. Riazi, "Plane wave spectrum approach to calculation of electromagnetic absorption under near-field exposure conditions", Bioelectromagnetics, Vol. 1, pp. 363-377, 1980.

[15] A.W. Guy, C.K. Chou and B. Neuhaus, "Average SAR and SAR distribution in man exposed to 450 MHz radiofrequency radiation", IEEE Trans. Microwave Theory Tech., Vol. MTT-32, pp. 752-762, 1984.

[16] A.W. Guy, M.D. Webb and C.C. Sorensen, "Determination of power absorption in man exposed to high frequency electromagnetic fields by thermographic measurements on scale models", IEEE Trans. Biomed. Eng., Vol. BME-23, pp. 361-371, 1976.

[17] G.S. Smith, "A comparison of electrically short bare and insulated probes for measuring the local radio frequency electric field in biological systems", IEEE Trans. Biomed. Eng., Vol. BME-22, p. 477-483, 1975.

[18] C.K. Chou and A.W. Guy, "Absorption of microwave energy by muscle models and by birds of differing mass and geometry", J. Microwave Power, Vol. 20, pp. 75-84, 1985.

[19] G.H. Wong, S.S. Stuchly, A. Kraszewski and M.A. Stuchly, "Probing electromagnetic fields in lossy spheres and cylinders", IEEE Trans. Microwave Theory Tech., Vol. MTT-32, pp. 824-828, 1984.

[20] R.G. Olsen, "Preliminary studies: far-field microwave dosimetric measurements of a full scale model of man", J. Microwave Power, Vol. 14, pp. 383-388, 1979.

[21] R.G. Olsen, "Far-field dosimetric measurements in a full-sized man model of 2 GHz", Bioelectromagnetics, Vol. 3, pp. 433-441, 1982.

[22] ANSI C95.1-1982: "American national standard safety levels with respect to human exposure to radio frequency electromagnetic fields, 300 kHz to 100 GHz", IEEE Inc., New York, N.Y.

[23] O.P. Gandhi, I. Chatterjee, D. Wu and Y.G. Gu, "Likelihood of high rates of energy deposition in the human legs at the ANSI recommended 3-30 MHz RF safety levels", Proc. IEEE, Vol. 73, no. 4, 1985.

8. Comparison of the calculated (lines) and measured (points) whole-body average SARs. The lines show the limits of the SAR for spheroidal models of ectomorphic (dotted lines) and average (solid lines) man; dots and crosses show the measured SARs for the E polarization and the H polarizations, respectively. Data points at 160, 350 and 915 MHz are from our measurements, at 40 MHz from [21], at 450 MHz from [15], at 1.2 GHz from [18] and at 2 GHz from [19].

9. The SAR in the direction of the wave propagation on the antenna axis for exposures in the near field of resonant dipoles with reflectors in the E polarization. Input power to the antenna 1 W. Antennas located at A = 134 cm at 160 MHz, A = 103 cm at 350 MHz, and A = 107 cm at 915 MHz.

10. Local values of the SAR in the mid-section of a homogeneous model of man exposed in the near field in the E polarization. Input power to the antenna 1 W.

11. Local values of the SAR in the mid-section of a homogeneous model of man exposed in the near field in the H polarization. Input power to the antenna 1 W.

12. Mean SARs averaged over tissue slices perpendicular to the main body axis for the near field exposure in the E polarization. Input power to the antenna 1 W.

13. Maximum SARs in the tissue slice perpendicular to the main body axis for near field exposures. Input power to the antenna 1 W.

14. Equi-SAR lines of 500, 100, 20 and 4 mW/kg in the torso in the plane of the antenna axis; exposures in the near field of resonant dipoles with reflectors in the E polarization and 1W of input power. Antennas located at A = 134 cm at 160 MHz, A = 103 cm at 350 MHz, and A = 107 cm at 915 MHz.

15. Whole-body average and head-and-neck average SARs for near-field exposures with 1 W of input power to resonant dipoles with reflectors located as shown in Figure 1 and described in detail in Table 2.

LIST OF TABLES

Table 1

Electrical properties of tissue equivalent materials

Frequency MHz	Relative dielectric constant, ε'	Conductivity, σ (S/m)	Plane wave attenuation coefficient*, α (cm^{-1})
160	40	0.80	0.36
350	38	0.95	0.51
915	37	1.17	0.70

* Defined as a power ratio for a plane wave in a uniform and homogeneous dielectric.

Table 2

Characteristics and coordinates of the antennas
for near-field exposures(see Fig. 1)

Frequency (MHz)	160	350	915
Dipole length/λ	0.49	0.43	0.49
Gain without reflector (dB)*	1.8	1.65	1.6
Input VSWR*	1.5	1.6	1.1
A (cm)	134	137	137
d (cm)	21	8	5
d/λ	0.11	0.09	0.15

* Experimental values.

Table 3

Test grid of the full scale model (also see Fig. 1)

Part of the body	Slices		Number of test locations	Contribution to the total body weight (rule of nines) %
	Thickness (cm)	Number		
Head & neck	4	8	3	9
Upper torso	10	3	5	18
Lower torso	10	3	7	18
Arms (both)	10	5	1	18
Legs (both)	10	9	1	36

*In one-half of the slice (body), perpendicular to the frontal surface of the body, within each location the electric field was measured in points separated by 1 cm.

Table 4

Attenuation coefficients in the torso[1)]

Frequency (MHz)	Polarization	Plane wave (±3 SD)	Experimental values	
			Far-field (±3 SD)	Near-field[3)] (±3 SD)
160	E	0.36 ± 0.02	0.34 ± 0.01	0.32 ± 0.01
160	H		0.25 ± 0.07	0.31 ± 0.03
350	E	0.51 ± 0.02	0.50 ± 0.03	0.46 ± 0.02
350	H		0.49 ± 0.02	0.515± 0.02
915	E	0.70 ± 0.02	0.73 ± 0.05	0.72 ± 0.04
915	H		0.72 ± 0.02	0.63 ± 0.04

1) Defined as a power ratio.
2) In a uniform and homogeneous dielectric.
3) Measured on the axis of the dipoles positioned as shown in Fig. 1 and Table 2.

Table 5

Comparison of the whole-body-average and head-and-neck average SARs for the far-field exposure to 1 mW/cm^2

Frequency (MHz)	Polarization	Whole-body average SAR (mW/kg)			Head/neck average SAR (mW/kg)	
		This work	Theory	Other techniques	This work	Theory
160	E	104.7	90 [1]		234.2	45-80 [2]
160	H	29.2	19 [3]		13.4	
350	E	40.7	44.5 [1]		102.2	108 [2]
	H	47.0	27 [3]		41.2	
450	E		34 [3]	46-50 [4]		
	H		30 [3]	40-42 [4]		
915	E	30.4	31 [3]		32.0	
915	H	49.3	38 [3]		54.8	

[1]) Block-model of man [11]
[2]) Block-model of man [12]
[3]) Spheroidal model of man [13]
[4]) Thermographic measurements [15]

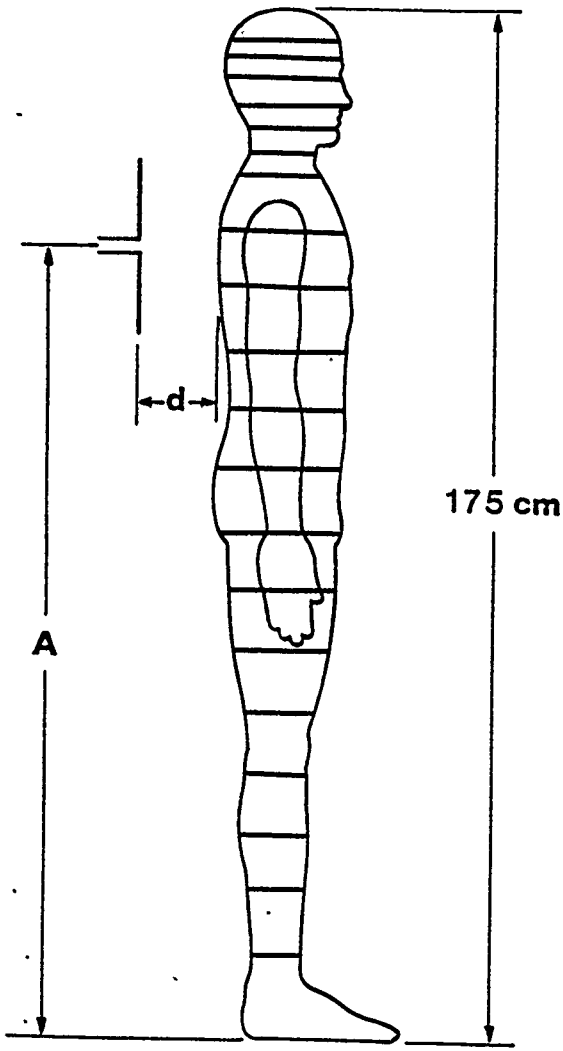

FIG.1

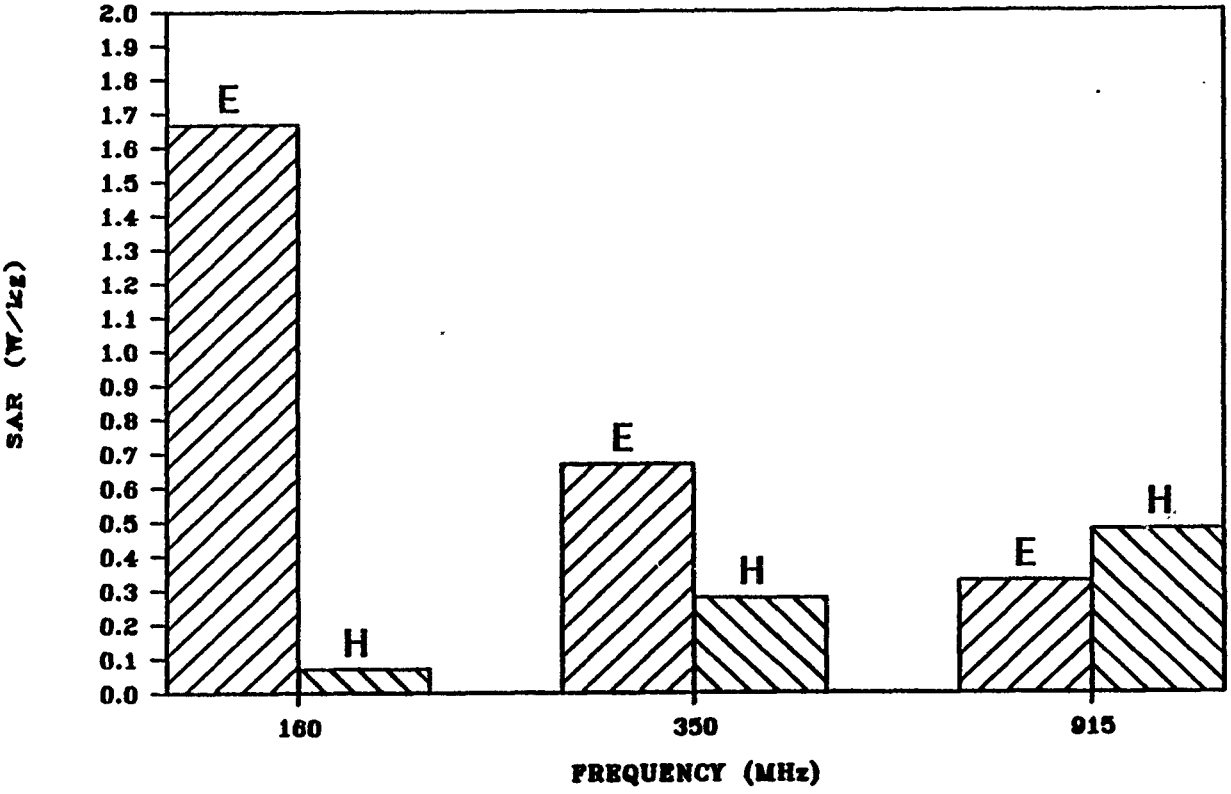
2.0
1.9
1.8
1.7
1.6
1.5
1.4
1.3
1.2
1.1
1.0
0.9
0.8
0.7
0.6
0.5
0.4
0.3
0.2
0.1
0.0
SAR (W/kg)
E
H
E
H
E
H
160
350
915
FREQUENCY (MHz)

Fig. 2

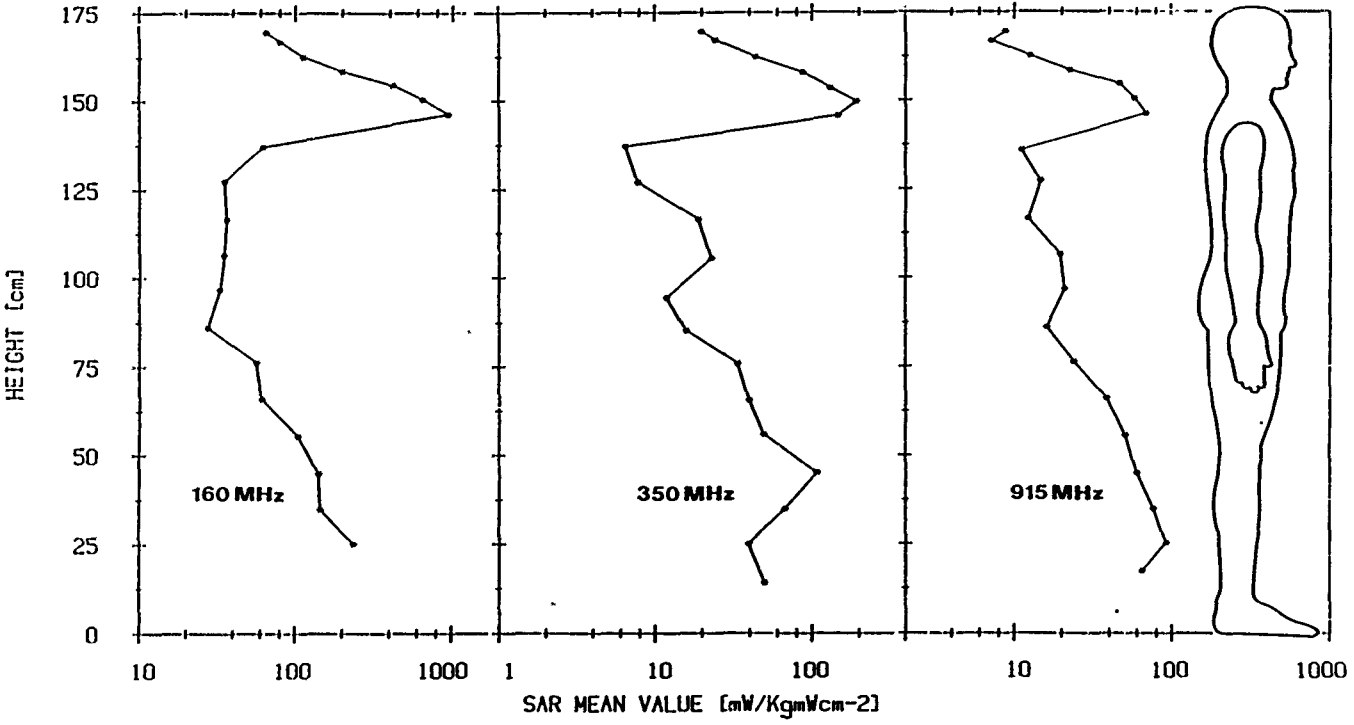
175
150
125
100
75
50
25
0
HEIGHT [cm]
160 MHz
350 MHz
915 MHz
10
100
1000
1
10
100
10
100
1000
SAR MEAN VALUE [mW/KgmWcm-2]

Fig. 3

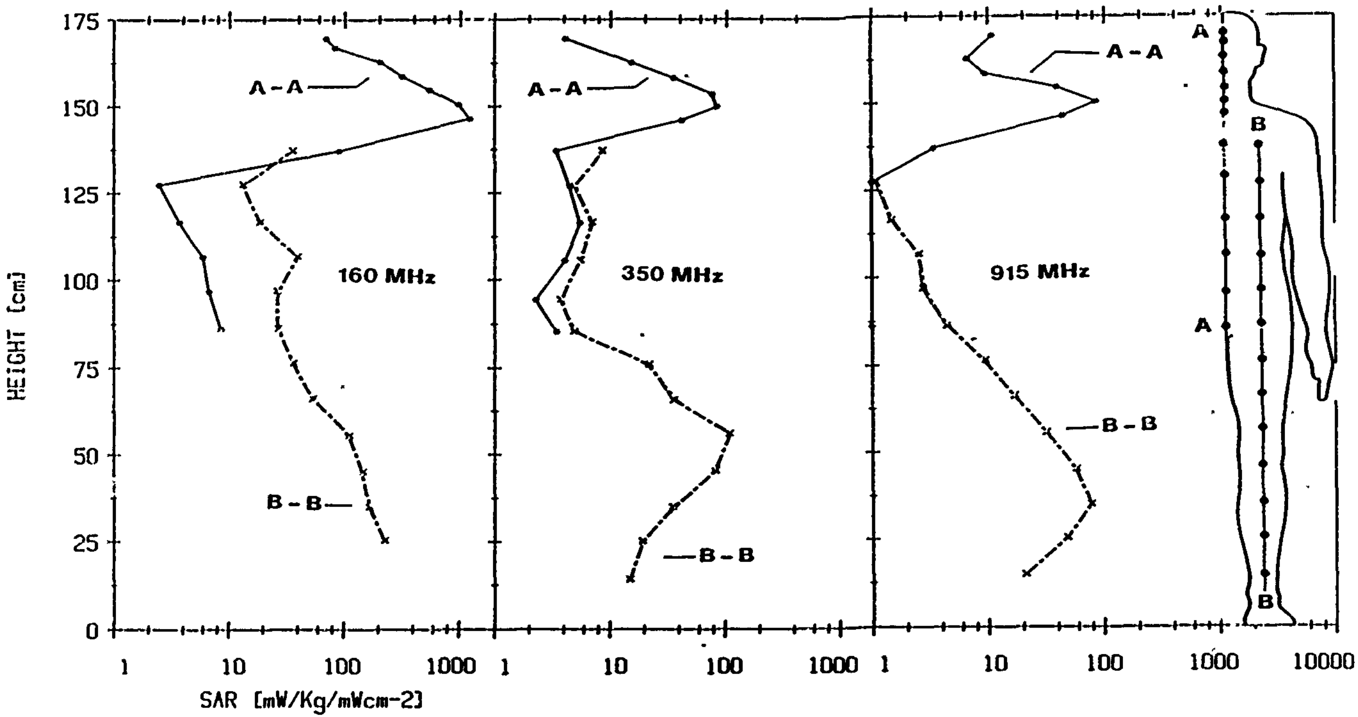
HEIGHT [cm]
175
150
125
100
75
50
25
0
1
10
100
1000
10000
SAR [mW/Kg/mWcm-2]
160 MHz
350 MHz
915 MHz
A - A
B - B
A
B

FIG. 4

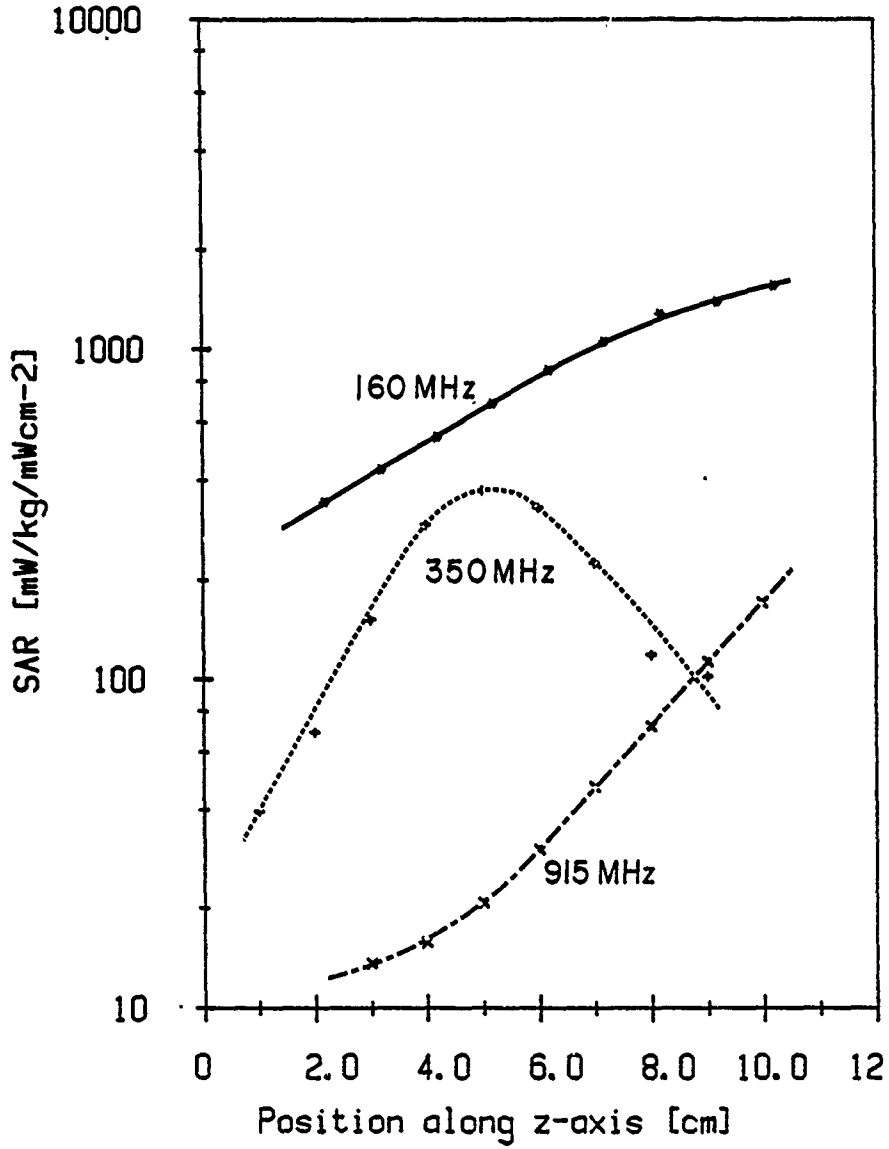
10000
1000
100
10
SAR [mW/kg/mWcm-2]
160 MHz
350 MHz
915 MHz
0
2.0
4.0
6.0
8.0
10.0
12
Position along z-axis [cm]

FIG 5

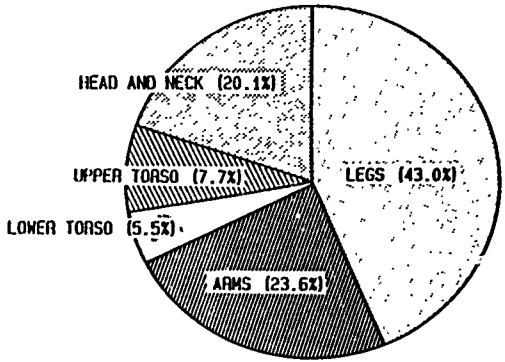

160 MHz
SAR = 104.7 mW/kg

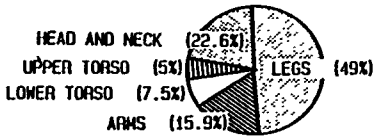

350 MHz
SAR = 40.7 mW/kg

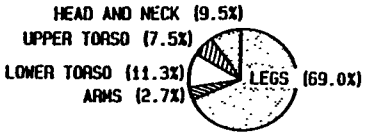

915 MHz
SAR = 30.4 mW/kg

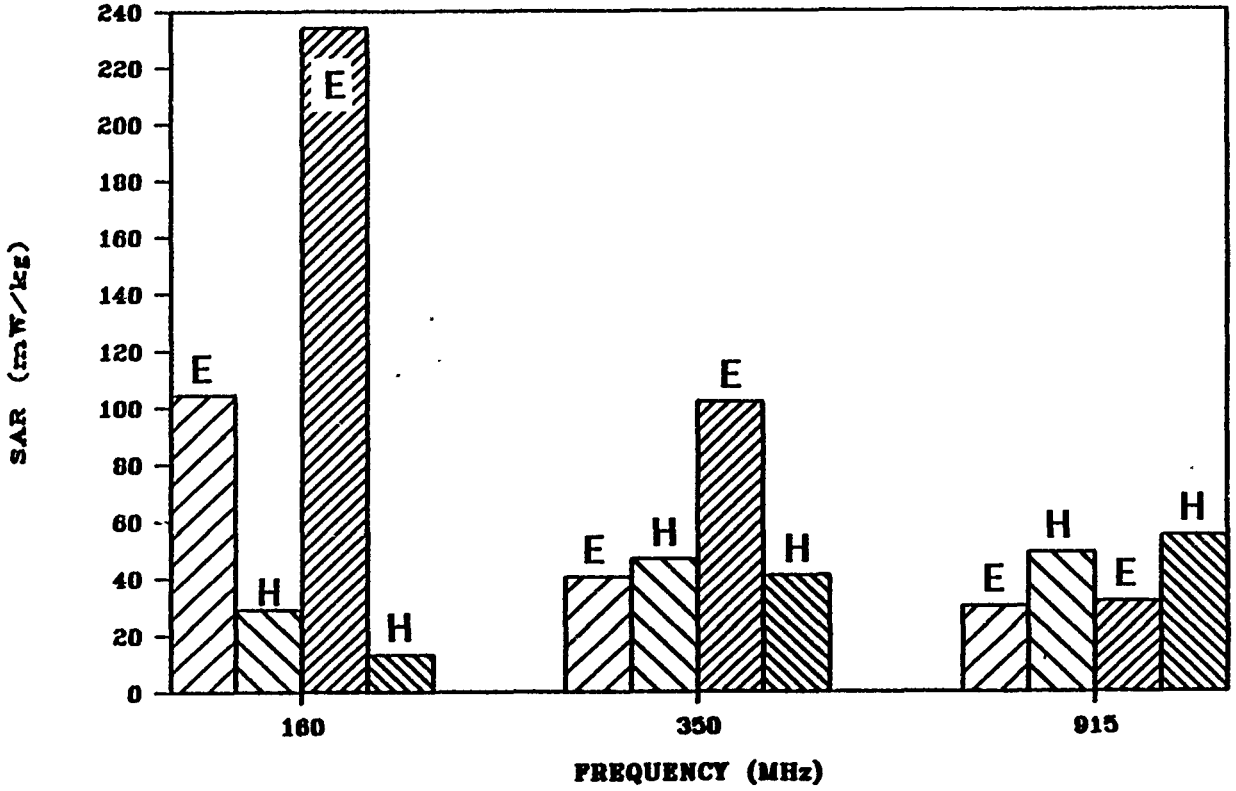
240
220
200
180
160
140
120
100
80
60
40
20
0
SAR (mW/kg)
E
H
E
H
E
H
E
H
E
H
E
H
160
350
915
FREQUENCY (MHz)

Fig 2

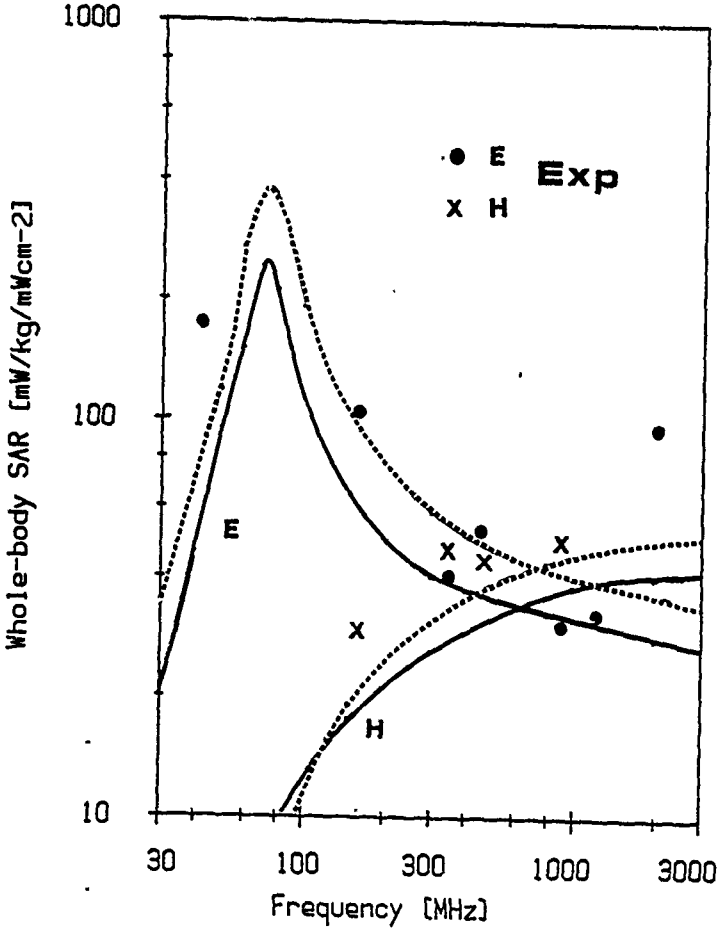
1000
100
10
Whole-body SAR [mW/kg/mWcm-2]
E
X H
Exp
E
X
X
X
X
H
30
100
300
1000
3000
Frequency [MHz]

Fig.8

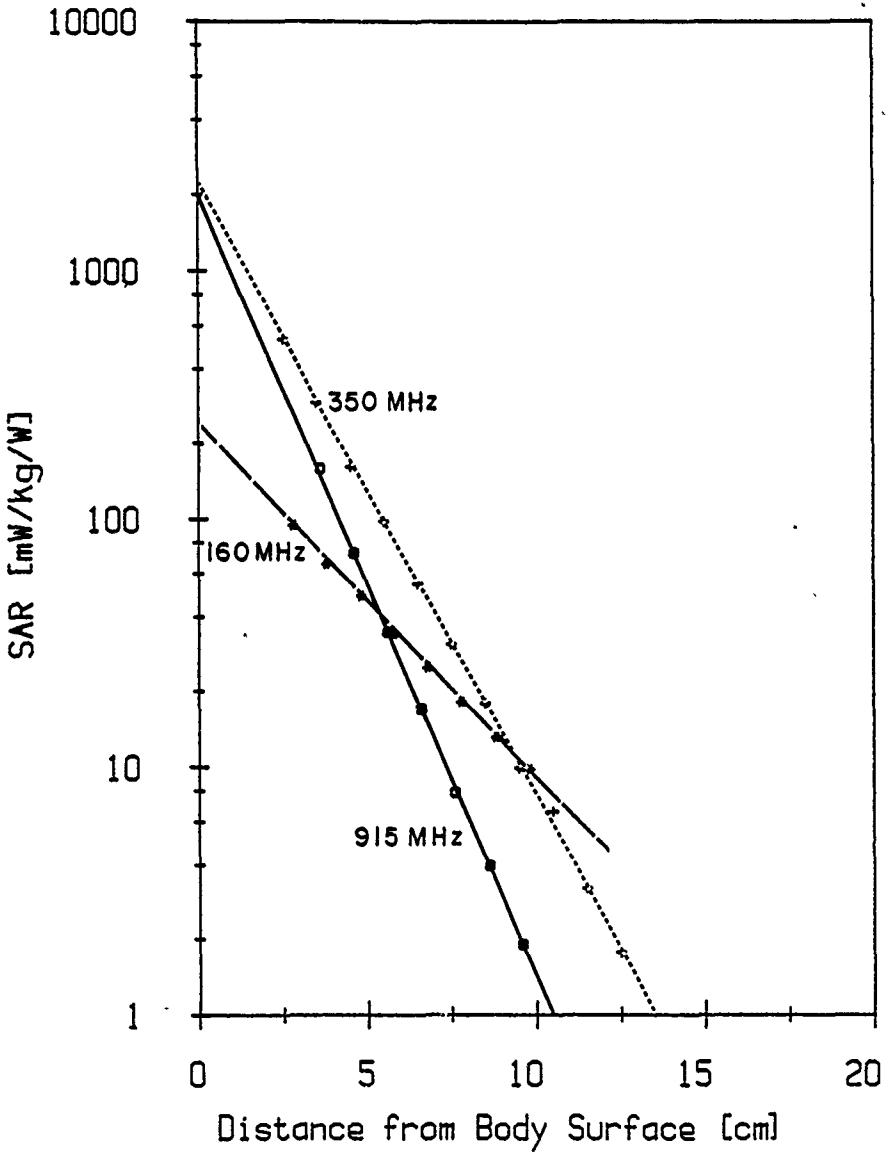
10000
1000
100
10
1
SAR [mW/kg/W]
350 MHz
160 MHz
915 MHz
0
5
10
15
20
Distance from Body Surface [cm]

Fig. 6

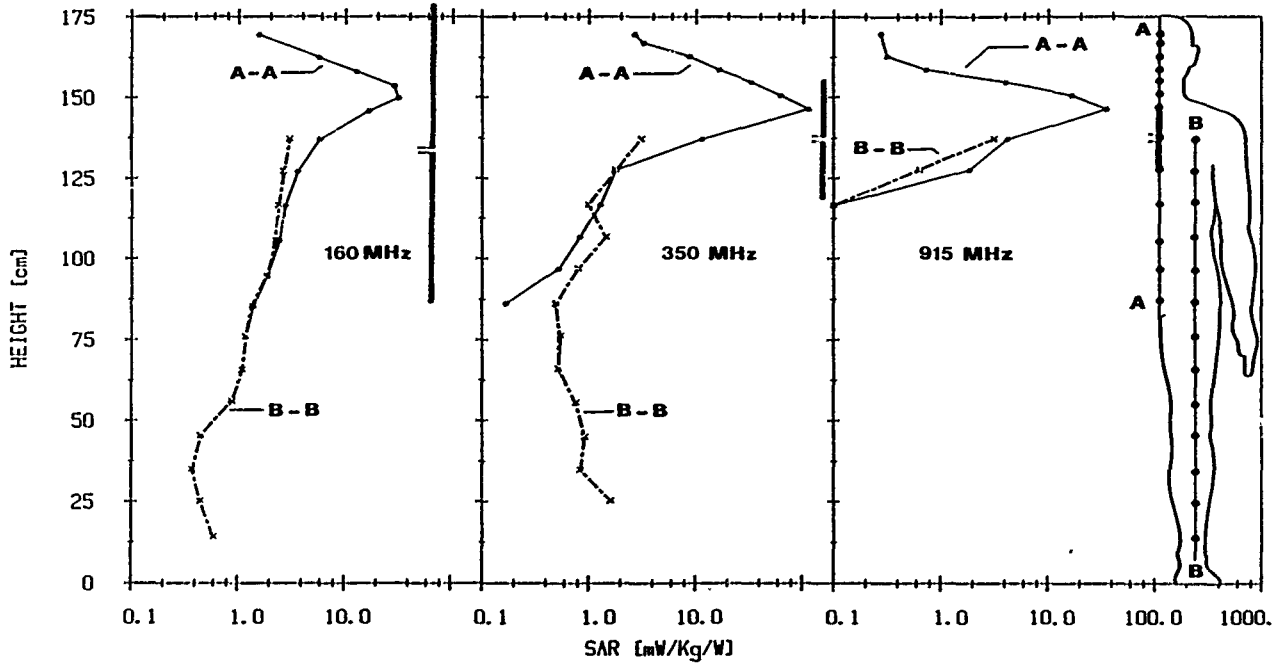
HEIGHT [cm]
175
150
125
100
75
50
25
0
A-A
B-B
160 MHz
350 MHz
915 MHz
A
B
0.1
1.0
10.0
100.0
1000.
SAR [mW/Kg/W]

FIG.10

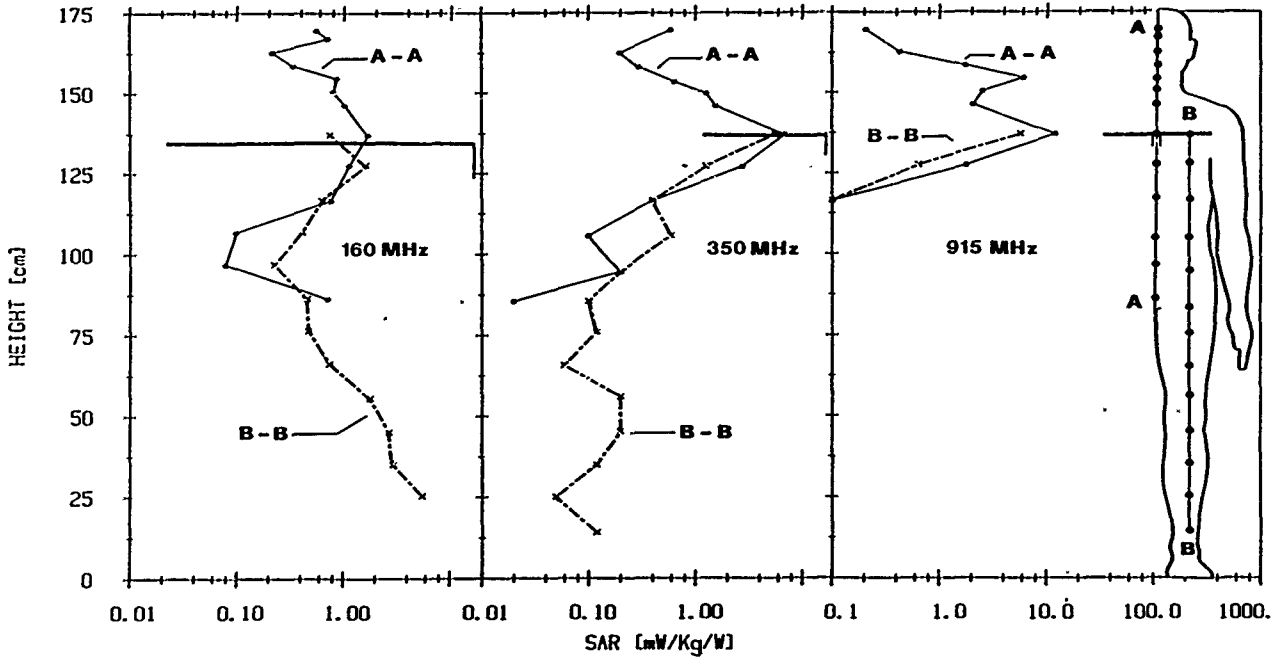
HEIGHT [cm]
175
150
125
100
75
50
25
0
A - A
B - B
160 MHz
350 MHz
915 MHz
A
B
0.01
0.10
1.00
0.01
0.10
1.00
0.1
1.0
10.0
100.0
1000.
SAR [mW/Kg/W]

Fig. 11

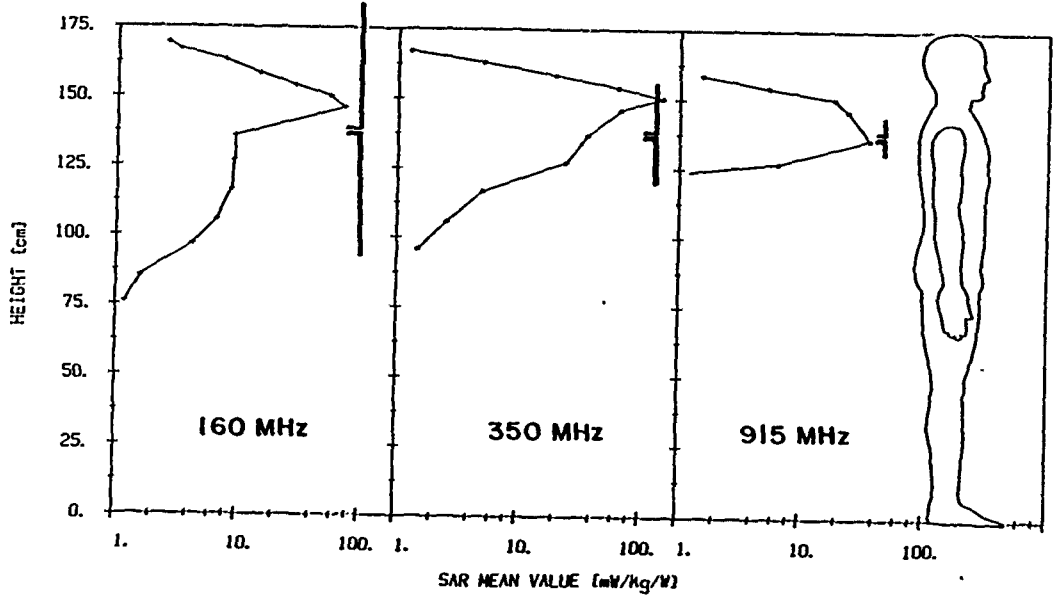
175.
150.
125.
100.
75.
50.
25.
0.
HEIGHT [cm]
160 MHz
350 MHz
915 MHz
1.
10.
100.
SAR MEAN VALUE [mW/Kg/W]

Fig. 2

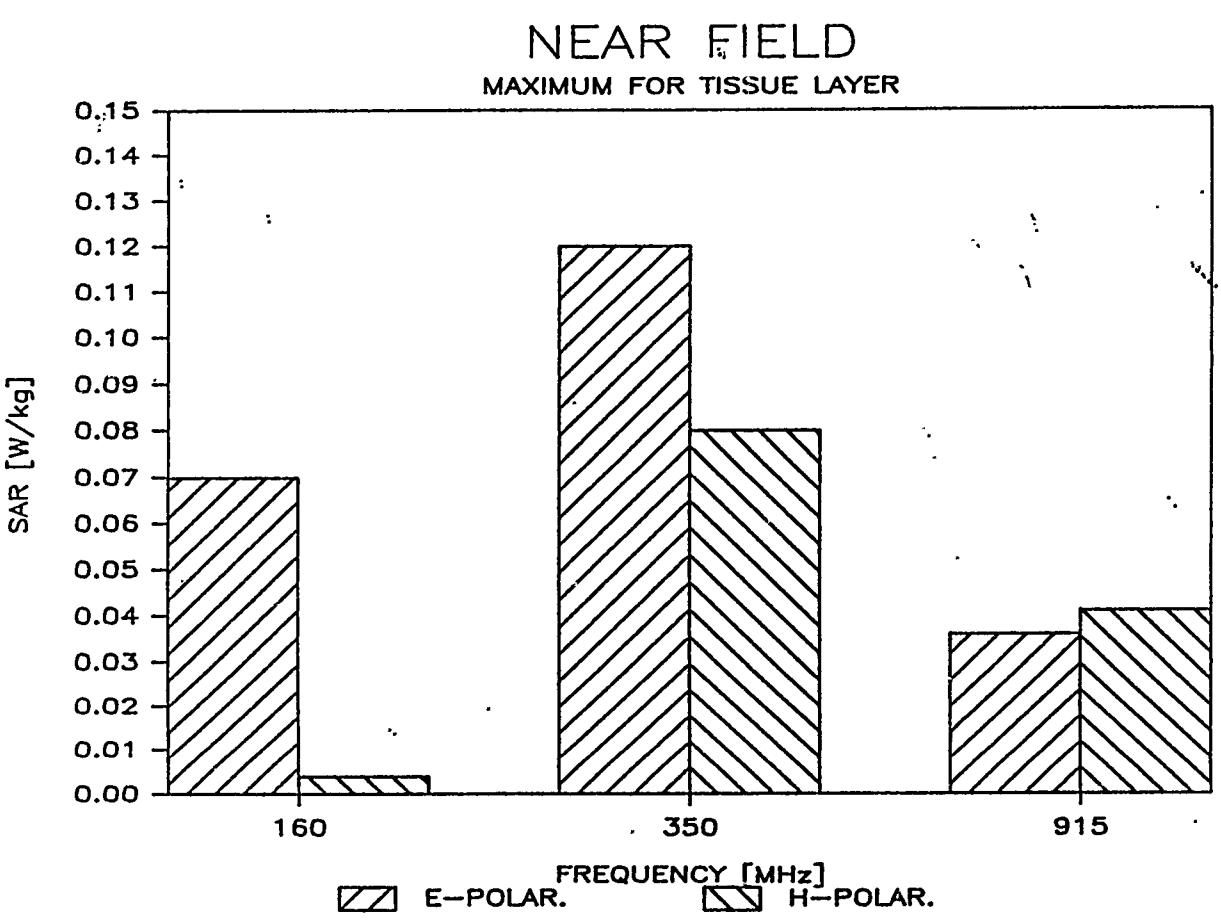
NEAR FIELD
MAXIMUM FOR TISSUE LAYER
SAR [W/kg]
0.15
0.14
0.13
0.12
0.11
0.10
0.09
0.08
0.07
0.06
0.05
0.04
0.03
0.02
0.01
0.00
160
350
915
FREQUENCY [MHz]
E—POLAR.
H—POLAR.

Fig 13

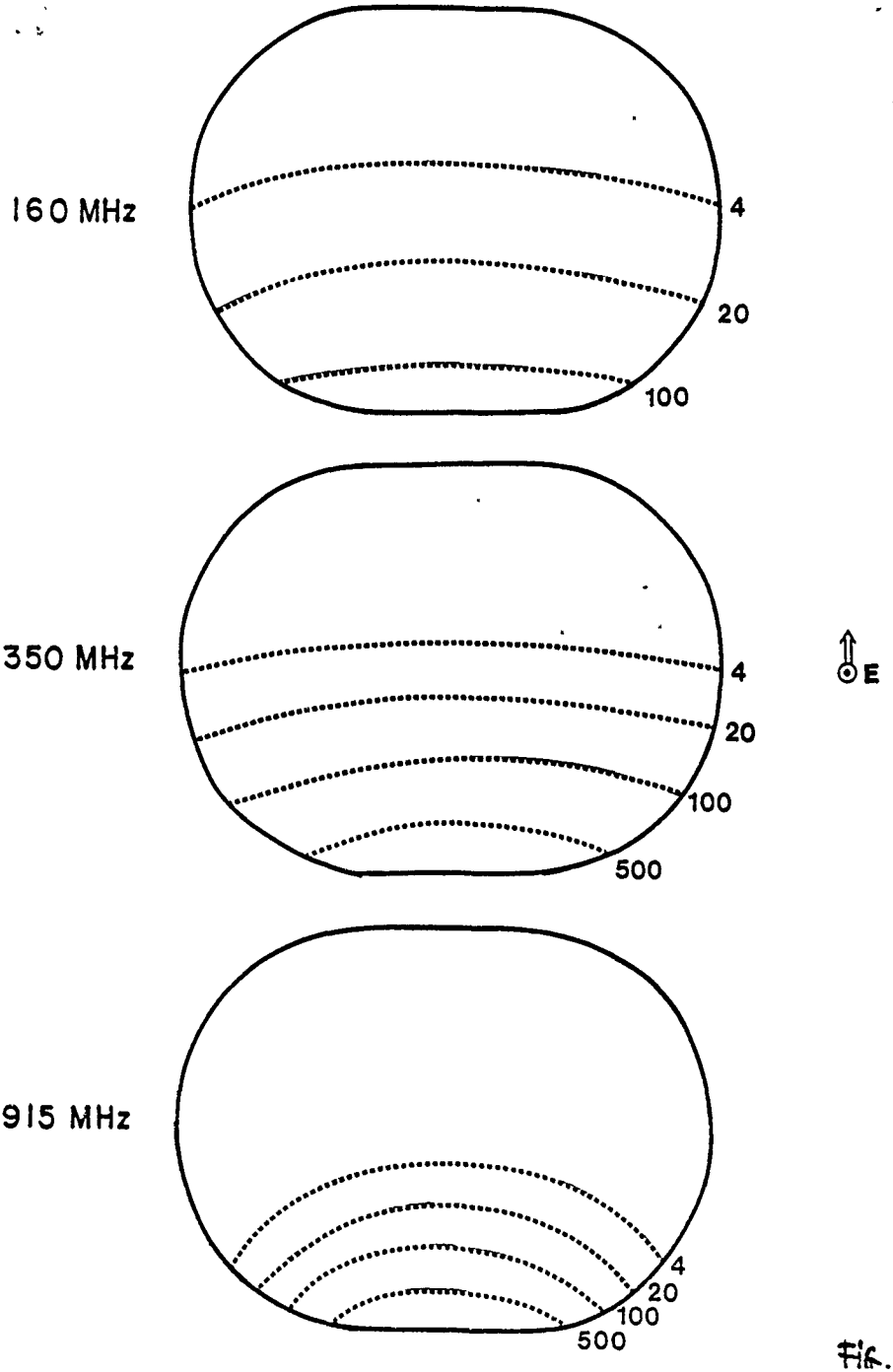

Fig. 14

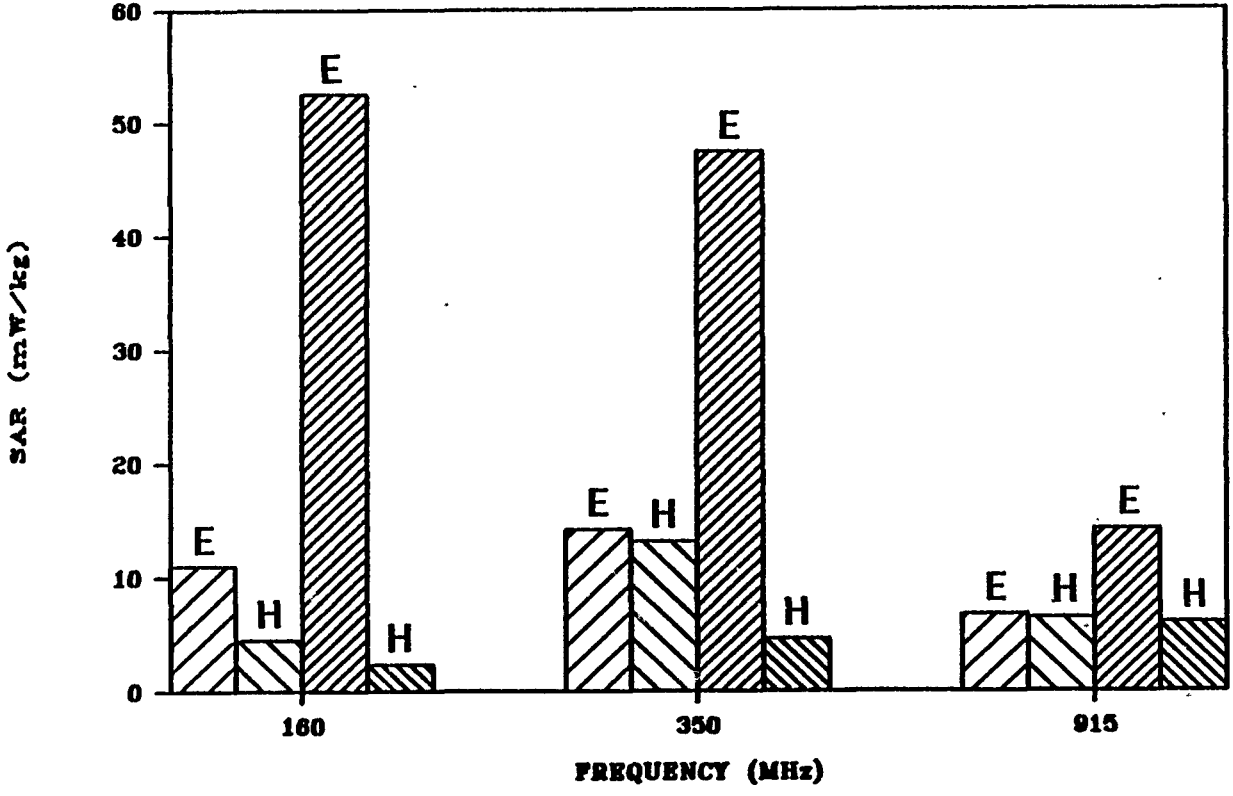
60
50
40
30
20
10
0
SAR (mW/kg)
E
H
E
H
E
H
E
H
E
H
E
H
160
350
915
FREQUENCY (MHz)

Fig. 15

IEEE IMTC 186 Instrumentation/Measurement Technology Conference Ref [22]
Boulder Co, March 25-27, 1986

INSTRUMENTATION FOR MEASUREMENTS OF ELECTRIC FIELDS AT RADIO FREQUENCIES

M.A. Stuchly*, S.S. Stuchly, G.W. Hartsgrove,
J. Markowski and A. Kraszewski

Department of Electrical Engineering,
University of Ottawa,
Ottawa, Ontario, Canada K1N 6N5
(613)564-3472
*Radiation Protection Bureau, Health & Welfare Canada

Introduction

Knowledge of the spatial distribution of the electric field around various objects and inside dielectric objects is important in numerous applications. Such applications include surveying complex exposure fields for evaluation and protection against health hazards, measurements of fields in situ in models of humans and in animals for electromagnetic dosimetric purposes, and measurements of exposure fields for EMI and field generated for EMC purposes. Dosimetric measurements are essential in exposure hazard assessment, control of electromagnetically induced hyperthermia and NMR imaging.

Numerous probes have been developed for measurements of the electric and magnetic field strength in air [1-6] and dielectric media [2,6-9]. Recent developments include also probes capable for simultaneous measurements of the electric and magnetic field strength in air [5]. Probes designed for measurements in air are of a relatively large size (a few centimeters in diameter) and are, in commercial versions, usually equipped with a meter of the total field strength. Probes intended for measurements of the fields in dielectrics (sometimes also called implantable probes) are considerably smaller (usually less than 1 cm. in diameter), are not normally equipped with a metering device, and when used with proper instrumentation allow measurement of all three spatial components of the field. Implantable probes can also be used in air.

Mapping of electromagnetic fields in air or dielectric media, unless automated, is time consuming and frequently inaccurate. In this paper we describe a computer-controlled scanning system for automated measurements of electric fields in air and dielectric media.

The System

A block diagram of the experimental system developed in our laboratory is shown in Figure 1, while the external views are shown in Figures 2 and 3. Figure 2 shows the scanning system with an electric field probe, a radiating antenna and a model of a human body in which electric fields strengths are measured. This part of the system is placed in an anechoic chamber to avoid reflections of the radiated RF energy. Figure 3 shows the operating console.

The system consists of a computer-controlled mechanical scanning system, electric field probes, electronic circuitry interfacing the probes with the computer, a minicomputer, and a source of the RF energy with associated antennas. For mapping of electric fields in models of objects or around them, appropriate models are required. To avoid interference with reflections of RF energy reflected by the surrounding objects, part of the system is placed in an

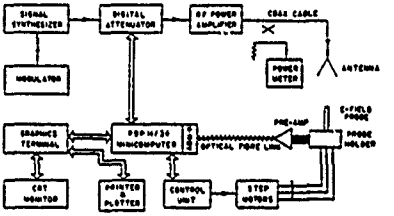

Figure 1. Block diagram of a computer-controlled system for mapping the electric field strength.

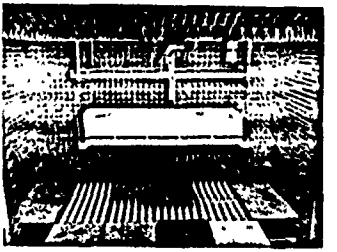

Figure 2. Radiofrequency part of the system and a model of the human body. This part is placed in an anechoic chamber.

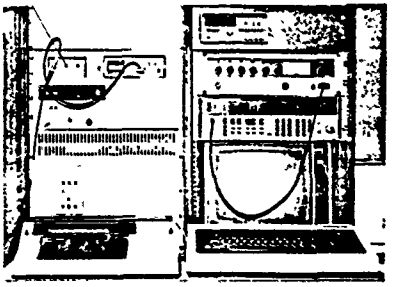

Figure 3. Operating console of system.

anechoic chamber as illustrated in Figure 2. The source of the RF energy is amplitude modulated at low frequency (~500 Hz) and its output level is digitally controlled by the computer.

The mechanical structure which supports and positions the electric field probe consists of three independent guiding slides in three mutually perpendicular directions. The probe can be placed in any location within a volume 1.9 × 0.5 × 0.45 m, using three stepping motors, each controlled by a separate driver. The system can operate in a manual or computer- supervised mode. In the manual mode the probe motion is controlled by switches on a portable, hand-operated unit. Selected coordinates of the probe position are stored in a file in the computer memory, forming a map of operator-selected test points. In the computer-supervised mode the probe scans automatically through the selected set of points. The motion-control unit is based on a 8085 microprocessor linked to a PDP 11/34 minicomputer. The accuracy of the probe position is within ±0.01 mm. The travel speed is 0.42 mm/s for a simple motion (a single coordinate changed) and 12 mm/s for a composite motion (two or three coordinates changed)[10].

Electronic Circuitry

An analysis of the performance of the electric field probes indicates that a significant improvement in sensitivity can be obtained by using amplitude modulated RF signals [11]. For probes used in our investigations the modulation frequency of 500 Hz was selected [11].

Three versions of the electronic system were developed and tested. An early version shown in Figure 4 consisted of three instrumentation amplifiers, a summing junction, an active filter, a voltage to frequency converter, a line driver, an LED and an optical-fiber link to the computer. This optical fiber link brings the signal from the amplifier out of the anechoic chamber to a circuit containing a fiber optic receiver and a frequency to voltage converter. This voltage which represents the electric field is then sent to the PDP/1134 where an A/D converter inputs the signal to the computer. In the next version a substitution of FET amplifiers for the instrumentation amplifiers resulted in an improvement of the signal to noise ratio (S/N) of 7 dB. In the last version shown in Figure 5 flexibility of the system and lower S/N were achieved by use of an integrated optical-fiber transmitter, which allows for use of a lock-in amplifier at the receiving end resulting in narrow-band detection without imposing extreme requirements on the stability of the modulating signal. The system gain is adjustable up to 10^5.

Electric Field Probes

Many electric field probes either designed for operation in air [2,4,5] or in the dielectric media [2,7] can be used in our system, as long as they contain three independent antennas loaded with detecting diodes and connected to the external terminals by high resistance leads. Alternatively, magnetic field probes [6] can be used, or with some system modifications, even probes that measure simultaneously the electric and magnetic field [5] can also be employed. We have used three triaxial electric field probes, namely, a Holaday IME-01, an EIT 979, and a NARDA 2608. The diameters of these probes are 17, 9 and 3 mm, respectively. The probes were fully characterized in terms of their sensitivity, noise, dynamic range, directional response and modulation characteristics.

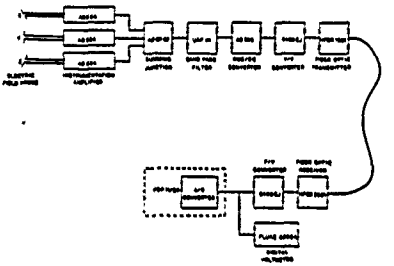

Figure 4. Electronic circuitry for interfacing the probes with the computer.

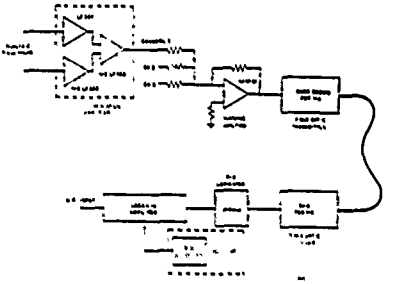

Figure 5. Electronic circuitry with an integrated optical fiber transmitter.

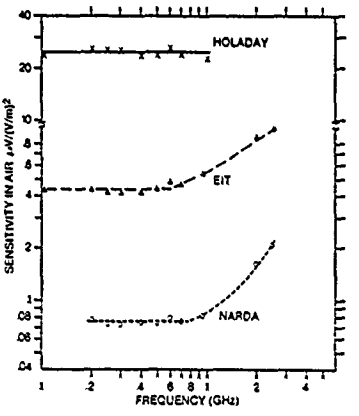

Figure 6. Sensitivity of the probes in air as a function of frequency.

The sensitivity in air of the three probes as a function of frequency is shown in Figure 6 [11]. The sensitivities at a few frequencies in a dielectric medium having a dielectric constant of about 50 and a conductivity of about 1.5 S/m (except at 2.45 GHz where the conductivity is 2.3 S/m) are summarized in Table 1. The sensitivity of probes in dielectric media is determined by measuring the output voltage of the electric field probe, placed at various locations in a sphere made of that dielectric medium (the medium is usually liquid or jello contained in a styrofoam mold). The output signal is compared (using the least-square fit method) with theoretically values of the electric field in the same locations [12]. The sphere is irradiated by a plane wave of a known power density. A typical calibration curve is shown in Figure 7. The calculated values of the square of the electric field strength are shown by the solid line while the dots depict the measured values.

Figure 8 presents the relative sensitivity of the NARDA probe as a function of the modulation frequency with the input amplifier (Figure 5) having an input resistance of 2.2 MΩ. The roll-off frequency in this system is considerably higher than in a previously used system [11], so that a frequency of modulation up to about 2 kHz can be used. However, except for the IME-01 probe, modulation frequency higher than 500 Hz does not results in any improvements of the signal-to-noise ratio (S/N) [11].

Software

The software used in the data collection and analysis consists of three programs developed by ourselves and a software package purchased for display of contour and mesh. views of the data. The first program called MAP is used in conjunction with the hand-held control unit driving the scanning system to generate a map of coordinates. This map is stored on disk file in the PDP/11/34. The second program called SCAN uses this map to automatically take electric field measurements at all of the stored locations. For each location the electric field is measured five times and averaged. The same program also controls a digital attenuator which is used to adjust the power to the antenna, in order to keep the signal from the amplifier in a limited, highly linear range. Each X,Y,Z location and the associated electric field strength are then stored in another disk file. The third program called CHART allows us to display or plot a graph of, for instance, the electric field strength vs. distance (X,Y,Z). The software purchased from Data Plotting Services called DPICT provides the capability of displaying the electric field strength or SAR, in the form of a contour diagram of equi-potential lines or as a 3-dimensional representation (Fig. 9).

Experimental Results

Some of the recent results illustrating the capabilities of the system are presented in Figures 9 and 10. Figure 9 shows the square of the electric field strength in a dielectric sphere ($\varepsilon' = 50, \sigma = 1.5$ S/m) irradiated by a plane wave at 450 MHz and 1 mW/cm^2.

Figure 10 depicts dosimetric data obtained for a full-size model of man exposed in the near-field of resonant dipoles. A dosimetric measure, the specific absorption rate (SAR), shown on the abscissa, is defined as the rate of energy absorption in a unit mass, and is related to the electric field strength, in situ E(rms), and the conductivity of the medium, σ.

$$SAR = \sigma E^2$$

Table 1. Sensitivity of electric field probes in a lossy dielectric medium (ε=50, σ=1.5 S/m), in $\mu W_{rms}/(V/m)^2$

Frequency	Probe Holaday IME-01	EIT 979	Narda 2608
160 MHz	208	3.9	NA
350 MHz	146	3.1	0.8
915 MHz	54	1.1	0.5
2.45 GHz	NA	1.3	0.8

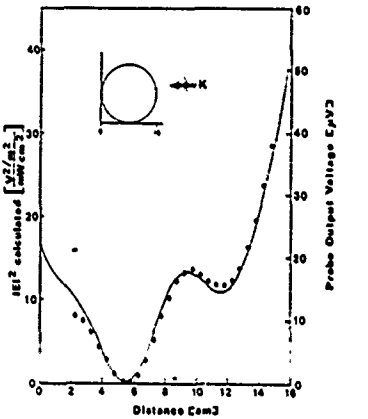

Figure 7. Probe calibration in a dielectric material. The solid line shows theoretical values of the square of the electric field strength and the points show the measured values. A sphere of 16 cm contained a liquid having ε'=50 and σ=1.5 S/m and was exposed to a plane wave of 1 mW/cm^2 at 475 MHz.

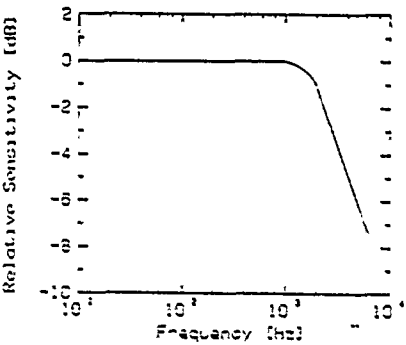

Figure 8. Relative probe (NARDA 2608) sensitivity (as a function of the modulation frequency. Amplifier input resistance 2.2 MΩ.

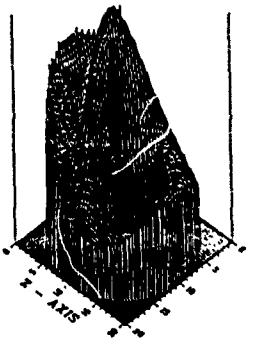

Figure 9. The square of the electric field in a cross-section of a 14-cm diameter sphere filled with a dielectric having $\varepsilon'=50$ and $\sigma=1.5$ S/m irradiated by a plane wave at 450 MHz.

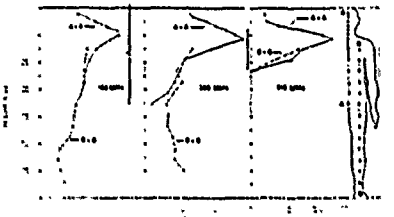

Figure 10. Specific absorption rate (SAR) in the mid-plane of a full-scale model of man exposed to RF fields from resonant dipoles at three frequencies. At each frequency d the dipole was one-half wavelength long and was placed about one-tenth of the wavelength from the body surface.

The values of the SAR were measured in the mid-section of a full-scale model of a standard man (175 cm, 70 kg.). The model of man consisted of a thin plastic shell (wall thickness ~2 mm), filled with semiliquid material having electrical properties equal to the properties of the average tissue. The antennas were located about one tenth of the wavelength from the body surface in locations shown in the figure. This type of date is needed in evaluation of potential hazards due to use of portable RF transmitters [13,14].

Conclusions

A computer-controlled mechanical scanning system together with triaxial electric field probes provide a viable method for mapping electric fields in air and dielectric materials at radio frequencies. The electronic circuitry associated with the probes facilitates measurements of weak fields and a relatively wide dynamic range of over three decades.

The system has been successfully used to obtain spatial distribution of the electric field in full-scale models of man and simple geometrical objects exposed in the near- and far-field of various antennas.

Acknowledgements

This work was supported by grants from the U.S. Office of Naval Research, the Canadian Department of Health and Welfare and the Natural Sciences and Engineering Council of Canada.

REFERENCES

[1] R.A. Tell, "Instrumentation for measurement of electromagnetic fields: equipment, calibrations and selected application," In Biological Effects and Dosimetry of Nonionizing Radiation, M. Grandolfo, S.M. Michaelson and A. Rindi, Eds. Plenum Press Co., 1983, pp. 95-162.

[2] H.I. Bassen and G.S. Smith, "Electric field probes - A Review," IEEE Trans. Antennas Prop., vol. AP-31, pp. 710-718, 1983.

[3] E. Aslan, "An ANSI radiation protection guide conformal probe," Microwave J., vol. 26, pp. April, 1983.

[4] M. Kanda, "A broad-band isotropic real-time electric-field sensor (BIRES) using resistively loaded dipoles," IEEE Trans. Electrom. Compat., vol. EMC-23, pp. 122-132, 1981.

[5] M. Kanda, "An electromagnetic near-field sensor for simultaneous electric and magnetic-field measurements," Trans. Electrom. Compat, vol. EMC -26, pp. 102-110, 1984.

[6] L.D. Driver and J.E. Cruz, "Development of the NBS isotropic magnetic field meter (MFM-10) 300 kHz-100 MHz," EMC Symp., Tokyo, Japan, 1984.

[7] G.S. Smith and R.W.P. King, "Electric field probes in material media and their application to EMC," IEEE Trans. Electrom. Compat., vol. EMC-17, pp. 206-211, 1975.

[8] G.S. Smith, "Analysis of miniature electric field probes with resistive transmission lines," IEEE Trans. Microwave Theory Tech., vol. MTT-29, pp. 1213-1224, 1981.

[9] G.S. Smith, "Limitations on the size of miniature electric-field probes," IEEE Trans. Microwave Theory , vol. MTT-32, pp. 594-600, 1984.

[10] S.S. Stuchly, M. Barski, B. Tan., G. Hartsgrove and S. Symons, "Computer-based scanning system for electromagnetic dosimetry," Rev. Sci. Instrum., vol. 54, pp. 1547-1550, 1983.

[11] M.A. Stuchly, A. Kraszewski and S.S. Stuchly, "Implantable electric field probes-some performance characteristics", IEEE Trans. Biomed. Engg., vol. BME-31, pp. 526-531, 1984.

[12] G.H. Wong, S.S. Stuchly, A. Kraszewski and M.A. Stuchly, "Probing electromagnetic fields in lossy spheres and cylinders", IEEE Trans. Microwave Theory Tech., vol. MTT-32, pp. 824-828, 1984.

[13] M.A. Stuchly, A. Kraszewski and S.S. Stuchly, "Exposure of human models in the near- and far-field - A Comparison", IEEE Trans. Biomed. Engg., vol. BME-32, pp. 609-615, 1985.

[14] S.S. Stuchly, A. Kraszewski, M.A. Stuchly, G. Hartsgrove and D. Adamski, "Energy deposition in a model of man in the near-field", Bioelectromagnetics, vol. 6, pp. 115-130, 1985.

R4 [24]

Probing Electromagnetic Fields in Lossy Spheres and Cylinders

GARY H. WONG, STANISLAW S. STUCHLY, SENIOR MEMBER, IEEE, ANDRZEJ KRASZEWSKI, AND MARIA A. STUCHLY, SENIOR MEMBER, IEEE

Abstract—Distributions of electric fields in lossy spheres and infinite lossy cylinders simulating biological objects were measured at 350, 920, and 2450 MHz. The measurements were performed in a computer-controlled scanning system using three different implantable nonperturbing probes. The results are compared with theory, and use of lossy spheres and cylinders for calibration of implantable probes is quantitatively evaluated.

I. Introduction

DOSIMETRY OF electromagnetic fields is essential in quantifying biological effects of these fields and developing exposure standards for humans. Dosimetry is concerned with the determination of the electric-field intensity and the rate of energy deposition in biological bodies and their electrical models. The rate of energy deposition is defined as the specific absorption rate (SAR) usually expressed in W/kg [1]. The SAR is directly related to the intensity of the electric field *in situ* and the electric properties of the tissue.

Considerable progress in theoretical and experimental dosimetric methods has taken place in recent years, as reviewed elsewhere [1]–[3].

Lossy dielectric spheres serve as convenient models of biological bodies and their parts [1]–[3]. These models are relatively easy to analyze theoretically and to construct for experimentation. They also provide adequate simulation of some biological systems under certain exposure conditions [1].

The distribution of electric fields in a lossy sphere was previously obtained theoretically [4], and a computer program was developed [5]. Qualitative experimental verification was obtained [6]; however, a quantitative analysis of the accuracy with which the electric-field distribution can be measured by implantable electric-field probes is wanting. The SAR distribution was also measured by the thermographic technique [7].

The electric fields in lossy cylinders were determined analytically for an infinite cylinder [8] and analytically and experimentally for cylinders of finite length [9]. In the latter case, the experimental technique used had serious limitations when used for cylinders of small diameters

Manuscript received October 12, 1983; revised March 8, 1984. This work was supported in part by grants from the Natural Sciences and Engineering Research Council of Canada and the U.S. Office of Naval Research.

G. H. Wong, S. S. Stuchly, and A. Kraszewski are with the Department of Electrical Engineering, University of Ottawa, Ottawa, Ontario, Canada K1N 6N5.

M. A. Stuchly is with the Radiation Protection Bureau, Health and Welfare Canada, Ottawa, Ontario, Canada.

0018-9480/84/0800-0824$01.00 ©1984 IEEE

compared with the wavelength. This technique is also not acceptable for probing of the fields in biological bodies.

The purpose of this study was twofold, firstly, to evaluate the application of lossy spheres and cylinders for calibration of implantable probes used in bioeffects dosimetry, and secondly, to obtain quantitative experimental data and comparison with theoretical results at 350, 920, and 2450 MHz for the electric-field distribution in spheres and cylinders simulating the human body and its parts. This information can be further used for comparison with the electric-field distributions in models more closely resembling the human body.

II. Theoretical Analysis

A. Spherical Models

The electric-field and SAR distributions in lossy spheres irradiated by a plane wave were calculated using the Mie method [4]. The numerical calculations were obtained using a computer program provided courtesy of the Bureau of Devices and Radiological Health [5].

B. Cylindrical Model

The electric-field and SAR distributions in an infinite lossy cylindrical model were obtained under plane-wave irradiation. A recursive method, derived by Bussey and Richmond [8], was employed to solve the scattering amplitude of a lossy multilayered infinite cylinder for TE and TM modes as shown in Fig. 1. The infinite cylinder solution can be used to approximate a finite-length cylinder within a limited range of the cylinder length.

C. Limitations of the Numerical Techniques

Dimensions of the spherical and cylindrical models are restricted by the computational instability of the angular functions due to the arguments which are either too small or too large.

Restrictions of the program for the spherical model are as follows:

- the maximum number of layers is 10,
- each layer is homogeneous,
- $|k|r < 90.83$, where r is the radius of a homogeneous sphere and k is the propagation constant in the medium.

Limitations on the calculation for a homogeneous infinite cylinder are as follows:

- $|k|R < 22.8$,
- $|k|r > 1.87$, where R is the radius of the cylinder, r is the radius of the observation point, and k is the propagation constant in the medium.

III. Materials and Methods

A. Materials

Molds for the 6.6-cm, 12-cm, and 16-cm diameter spheres were made of 5-cm-thick RF transparent polystyrene foam. The mold for the 24.8-cm diameter cylinder of a length of 1.83 m was made of 3.2-mm-thick solid acrylic having a dielectric constant of 2.6.

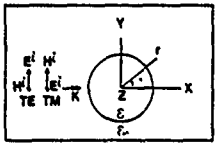

Fig. 1. TE and TM modes for a lossy circular infinite cylinder.

TABLE I
Sensitivities of the Implantable Probes Determined Using Various Models

A semisolid phantom material which simulates the electrical properties of the average tissue was used at 350 MHz [10]. At frequencies of 920 MHz and 2.45 GHz, saline solutions were used as phantom materials because of their low viscosity, simplicity of preparation, and elimination of the mechanical perturbation of the phantom by the probe. The permittivities of different phantom materials, as measured by an automatic measurement system with an uncertainty of less than 3 percent [11], are given in Table I.

The electric-field intensities in different models were measured using a computer-based scanning system and an electric-field-probe technique [12].

The molds filled with phantom materials are placed in the far field of a selected antenna and accurately positioned to ensure a desired orientation of the incident electric field with respect to the scanning direction.

B. Probes

Three-dipole electric-field probes, a Narda Model 2608 (3 mm in diameter), an EIT model 979 (9 mm in diameter), and a Holaday Model IME-01 (19 mm in diameter), were used to measure the electric-field intensity. The characteristics of these probes are described elsewhere [13].

The sum of three voltages (V_T) detected by the diode-loaded dipoles is related to the square of the total electric-field intensity $|E_T|^2$ by the following expression:

$$V_T = B|E_T|^2$$

where B is the sensitivity of the probe in the tissue phantom material.

The sensitivity of each probe was determined for each model from the following expression:

$$B = \frac{\sum_{i=1}^{N} (V_T)_i (|E_T|^2)_i}{\sum_{i=1}^{N} (|E_T|^2)_i^2}$$

where $(V_T)_i$ is the total voltage at the probe detector diodes (a sum of the three voltages of the three dipoles), measured at an experimental point i, $(|E_T|^2)_i$ is the theoretical value of the internal electric-field intensity in the same point, and N is the number of points. The final value of the sensitivity was arrived at by an iterative process, in which only an unperturbed part of the distribution was included, i.e., that part for which the relative difference between the theoretical and experimental values was less than 10 percent.

C. System Uncertainties

There are several sources of errors in the system that may affect the accuracy of experimental results. Some of the errors can be limited to be negligibly small through proper arrangements and care. These include reflections from the walls and the scanning system. In this work, they have been eliminated by placing the whole system in an anechoic chamber and covering the frame of the scanning system with absorbing tiles. The incident electric field has to be well defined in terms of its amplitude and direction. The field intensity in our tests was determined from the antenna gain calibration and measurements of the input power to the antenna. The uncertainty in the intensity was estimated at ±0.5 dB. The direction (alignment) of the antenna with respect to the probe was arranged within ±1°. The intensity of the field was always adjusted so that the probes operated in the linear region.

The main accuracy limitations in this experiment are due to the probes themselves, namely to the cross-coupling of the dipoles, lack of a perfectly isotropic response (due to small differences between the three dipole-diode assemblies), remnant pick-up of their high-resistance leads and the field perturbation by the leads.

IV. Results and Discussion

A. Spherical Models

A comparison of the theoretical and experimental data for a 16-cm diameter sphere at 350 MHz is shown in Fig. 2. On all illustrations, the probe is introduced from the positive z direction, while the wave is incident from the negative z direction. An excellent agreement can be seen for a smaller diameter probe (9 mm, EIT model), except at one end where the probe is introduced to the phantom. For a large-diameter probe (19 mm, Holaday model), significant deviations are also seen at the other end of the distance scanned. This is due to the smearing because of a poor spatial resolution of the probe.

The experimental error close to the point of probe entrance is due to a formation of a neck through which the phantom material is flowing outside the sphere.

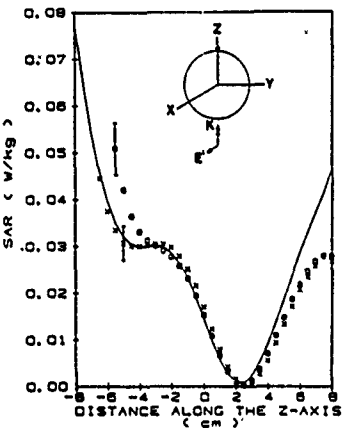

Fig. 2. Comparison of the calculated and measured SAR distribution along the z-axis of an average-tissue-phantom sphere. Solid line indicates the calculated values. ×× measured values with the Holaday probe. □□ measured values with the Holaday probe, $\epsilon' = 38.9$, $\sigma = 1.04$ S/m, $f = 350$ MHz. Incident Power Density = 1 mW/cm². Diameter = 16 cm, Diameter/$\lambda_0 = 0.19$. Sensitivity $B = 3.1 \pm 0.3$ μV/(V²/m²) for the EIT probe and 12 ± 2 μV/(V²/m²) for the Holaday probe. The vertical bars show the uncertainty of measurements, the double arrow indicates the direction of incidence of the wave, and the single arrow shows the point where the probe is introduced into the phantom.

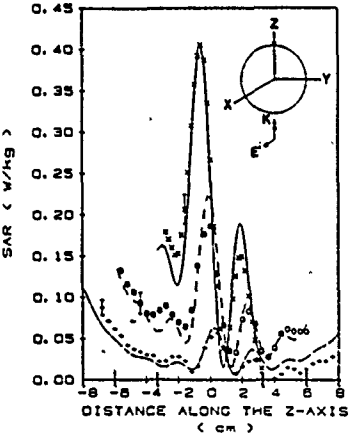

Fig. 3. Comparison of the calculated and measured SAR distributions along the z-axis for three spheres filled with the muscle-equivalent saline. $\epsilon' = 76.0$, $\sigma = 1.58$ S/m, $f = 920$ MHz. Incident Power Density = 1 mW/cm². Probe Narda. Solid line indicates the calculated values. ×× measured values for a sphere of a diameter = 6.6 cm, Diameter/$\lambda_0 = 0.2$. Sensitivity $B = 0.71 \pm 0.04$ μV/(V²/m²) Dashed line indicates the calculated values, □□ measured values for a sphere of a diameter = 12 cm, Diameter/$\lambda_0 = 0.37$. Sensitivity $B = 0.63 \pm 0.8$ μV/(V²/m²) The dash-dot line indicates the calculated values. ++ measured values for a sphere of a diameter = 16 cm, Diameter/$\lambda_0 = 0.49$, Sensitivity $B = 0.71 \pm 0.06$ μV/(V²/m²) The vertical bars indicate the uncertainty of measurements, the double arrow indicates the direction of incidence of the wave, and the single arrow shows the point of probe insertion.

Fig. 3 provides a comparison of theoretical and experimental results for three spheres at 920 MHz for the Narda probe. This is the smallest diameter (3 mm) probe, and smearing effect is very small. The "neck effect" is eliminated as a result of using a liquid phantom material.

Fig. 4 gives the results for 6.6-cm and 12-cm diameter spheres at 2.45 GHz as measured with the Narda and EIT probes. The spatial resolution limitations of both probes are apparent. For instance, for the 6.6-cm diameter sphere, where rapid changes of the SAR occur within about 1 cm, some smearing is evident in the second peak even for the Narda probe.

B. Cylindrical Model

Fig. 5 illustrates the data for the cylindrical model. The computational instability of the theoretical results close to the cylinder center was caused by the divergence of the Bessel functions in the region near the center.

The measurements were performed at the center of the cylinder and at a distance of 0.44 λ_0 from the end of the cylinder (points 1 and 3). Very good agreement was obtained for both probes for all locations except close to the point of the probe introduction. This was due to a small truncation of the cylinder.

C. General Discussion

As previously indicated, the agreement between theoretical and experimental SAR distributions is affected by several factors, e.g., limitations of the theoretical solution for the cylindrical model investigated, probe spatial resolution, model perturbation by the probe ("the neck" for semisolid phantom). Also, the agreement between the permittivity assumed in calculations and that of the material used plays a certain role.

The probe sensitivities as determined by a comparison of the experimental and theoretical SAR distributions in different models for the three probes at 350, 920, and 2450 MHz are summarized in Table I and compared with the data for slab phantoms [13]. A rather good agreement between the sensitivity values obtained using different models was obtained.

V. Conclusions

A quantitative comparison between the distributions of the specific absorption rate (SAR) obtained by analytical methods and by probing the electric fields in lossy spheres and cylinders using implantable probes was performed.

An excellent agreement between the theory and experiment was found within the limitations of the probes. The main limitations of the field probing are due to the spatial resolution of the probes, which in turn depends on the probe size. Other probe limitations include the probe symmetry, cross-coupling between the dipoles, and the field perturbation. The experiments confirmed that the computer-controlled experimental dosimetry system [12] allows to obtain the SAR distributions not only rapidly and conveniently, but that the accuracy is practically determined by the accuracy of the probe used, with much smaller errors due to the remaining parts of the system.

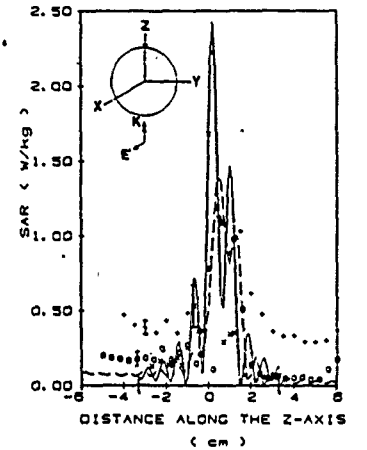

Fig. 4. Comparison of the calculated and measured SAR distributions along the z-axis for two saline-filled spheres $\epsilon' = 77.9$, $\sigma = 1.02$ S/m, $f = 2.45$ GHz, Incident Power Density = 1 mW/cm². Solid line indicates the calculated values, × × measured values with the Narda probe, Diameter = 6.6 cm, Diameter/λ_0 = 0.54, Sensitivity $B = 0.08 \pm 0.02$ $\mu V/(V^2/m^2)$. Dashed line indicates the calculated values, □□ measured values with the Narda probe, + + measured values with the EIT probe, Diameter = 12 cm, Diameter/λ_0 = 0.98, Sensitivity $B = 0.08 \pm 0.01$ $\mu V/(V^2/m^2)$ (Narda) and 0.10 ± 0.01 $\mu V/(V^2/m^2)$ (EIT). The vertical bars show the uncertainty of measurements, the double arrow indicates the direction of the incidence of the wave, and the single arrow shows the point of probe insertion.

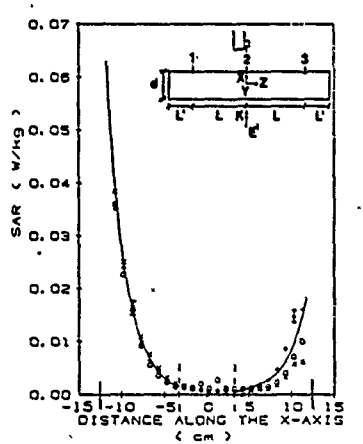

Fig. 5. Comparison of the calculated and measured SAR distribution across a circular cylinder filled with the average tissue phantom $\epsilon' = 38.9$, $\epsilon'' = 53.5$, TE Mode, $f = 350$ MHz, Incident Power Density = 1 mW/cm², $L = 0.62$ λ_0, $L' = 0.44$ λ_0, $d = 0.29$ λ_0, Probe Holaday, Sensitivity $B = 16 \pm 1$ $\mu V/(V^2/m^2)$. Solid line indicates the calculated values, + + measured values at 1, × × measured values at 2, □□ measured values at 3. The vertical bars show the uncertainty of measurements; the double arrow indicates the direction of incidence of the wave.

Lossy dielectric spheres of proper sizes are convenient for calibration of implantable electric-field probes in tissue phantoms. They are superior to cylinders and slabs, as they facilitate calibration with the same or even better accuracy than cylinders and slabs, and are smaller in size. The size is of particular importance at lower frequencies (below 1 GHz) where the slab size required becomes cumbersome to handle [13].

Acknowledgment

The technical assistance of G. Hartsgrove and D. Adamski is greatfully acknowledged.

References

[1] C. H. Durney, "Electromagnetic dosimetry for models of humans and animals: A review of theoretical and numerical techniques," *Proc. IEEE*, vol. 68, pp. 33–40, 1981.

[2] O. P. Gandhi, "State of the knowledge for electromagnetic absorbed dose in man and animals," *Proc. IEEE*, vol. 68, pp. 24–39, 1981.

[3] ——, "Biological effects and medical applications of RF electromagnetic fields," *IEEE Trans. Microwave Theory Tech.*, vol. MTT-30, pp. 1831–1847, 1982.

[4] A. Shapiro, R. Lutomirski, and H. Yura, "Induced fields and heating within a cranial structure irradiated by an electromagnetic plane wave," *IEEE Trans. Microwave Theory Tech.*, vol. MTT-19, pp. 187–196, 1972.

[5] S. M. Neuder, "Electromagnetic fields in biological media, Part II —The SCAT program, multilayered spheres, theory & applications," BRH Rockville, MD. Publication, Aug. 1979.

[6] H. Bassen, P. Herchenroeder, A Cheung, and S. Neuder, "Evaluation of implantable electric field probe within finite simulated tissue," *Radio Sci*, vol. 12, no. 6S, pp. 15–25, 1977.

[7] A. W. Guy, "Analyses of electromagnetic fields induced in biological tissues by thermographic studies on equivalent phantom models," *IEEE Trans. Microwave Theory Tech.*, vol. MTT-19, pp. 205–214, 1971.

[8] H. E. Bussey and J. H. Richmond, "Scattering by a lossy dielectric circular cylindrical multilayer, numerical values," *IEEE Trans. Antennas Propagat.*, vol. AP-23, pp. 723–725, Sept. 1975.

[9] R. Bansal, R. W. P. King, and T. T. Wu, "The measurement of the electric field inside a finite dielectric cylinder illuminated by a plane wave," *IEEE Trans. Microwave Theory Tech.*, vol. MTT-30, pp. 1282–1285, 1982.

[10] C. H. Durney *et al.*, *Radiofrequency Radiation Dosimetry Handbook*, Second Ed. 1978, pp. 48–61.

[11] A. Kraszewski, M. A. Stuchly, and S. S. Stuchly, "ANA calibration method for measurement of dielectric properties," *IEEE Trans. Instrum. Meas.*, vol. IM-32, no. 2, pp. 385–387, 1983.

[12] S. S. Stuchly, M. Barski, B. Tam, G. Harstgrove, and S. Symons, "A computer based scanning system for electromagnetic dosimetry," *Rev. Sci. Instr.*, vol. 54, no. 11, pp. 1547311550, 1983.

[13] M. A. Stuchly, A Kraszewski, and S. S. Stuchly, "Implantable electric field probe—Some performance characteristics," presented at the 5th Ann. Conf. of Bioelectromagnetic Society, Boulder, CO, June 12–17, 1983.

Andrzej Kraszewski was born in Poznan, Poland, on April 22, 1933. He received the M.Sc. degree in electrical engineering from the Technical University of Warsaw, Warsaw, Poland, in 1958, and the D.Sc. degree in technical sciences from the Polish Academy of Sciences, (PAN), Warsaw, in 1973.

Beginning in 1953, he was employed at the Telecommunication Institute, Warsaw, in the research and development of microwave components and systems. Beginning in 1963, he joined UNIPAN Scientific Instruments, a subsidiary of the Polish Academy of Sciences, as the Head of the Microwave Laboratory. Starting in 1972, he was Manager of the Microwave Department of WILMER Instruments and Measurements, a subsidiary of the Polish Academy of Sciences in Warsaw, where he co-developed microwave instruments for moisture-content measurements and control. Since November 1980, as a Visiting Professor at the University of Ottawa, Canada, he has been engaged in research of interactions between dielectrics and electromagnetic fields. He is the author of several books on microwave theory and techniques, has published more than 80 technical papers on the subject, and holds 18 patents. He received several professional awards, among them the State Prize in Science in 1980.

Dr. Kraszewski is a member of the International Microwave Power Institute, the Polish Electricians Association, and is a member of the Editorial Board of the *Journal of Microwave Power*.

Stanislaw S. Stuchly (M'70–SM'72) was born in Lwow, Poland, on November 20, 1931. He received the B.Sc. degree from the Technical University, Gliwice, Poland, and the M.Sc. degree from the Warsaw Technical University, both in electrical engineering, in 1953 and 1958, respectively, and the Ph.D. degree from the Polish Academy of Sciences, Warsaw, Poland, in 1968.

From 1953 to 1959, he was a Research Engineer in the Industrial Institute for Telecommunications, Warsaw, Poland. From 1959 to 1963, he was with the Warsaw Technical University. In 1963, he joined UNIPAN—Scientific Instruments, subsidiary of the Polish Academy of Sciences. From 1970 to 1976, he was with the University of Manitoba, Winnipeg, Canada. Since 1977, he has been with the University of Ottawa, Canada, where he is presently a Professor of Electrical Engineering.

Maria A. Stuchly (M'71–SM'76) received the M.S. and Ph.D. degrees in electrical engineering from Warsaw Technical University and Polish Academy of Sciences in 1962 and 1970, respectively.

From 1962 to 1970, she was employed as a Senior R & D Engineer in a subsidiary of the Polish Academy of Sciences in Warsaw, Poland. Between 1970 and 1976, she was engaged in research in the field of microwave instrumentation and measurements, and microwave power applications at the Departments of Electrical Engineering and Food Science at the University of Manitoba. Since 1976, she has been with the Non-Ionizing Radiation Section, Radiation Protection Bureau, Health and Welfare Canada, where she is responsible for the development of microwave radiation protection standards and carries out research in the field of biological effects of microwave radiation. She is also nonresident Professor of electric engineering at the University of Ottawa.

Dr. Stuchly is a member of the Board of Directors of the Bioelectromagnetics Society and a member of IEEE Technical Committee of Man and Radiation.

Gary H. Wong, photo and biography not available at time of publication.